Development of Novel Image Enhancement Methods for Bio-medical Images

A Thesis

Submitted in partial fulfilment of the requirements for the award of the degree of

Doctor of Philosophy

In

Department of Electronics & Communication Engineering

Submitted by:

KARISHMA RAO

(Reg no: 901906008)

Under the Supervision of

Dr. Manu Bansal
Assistant Professor, ECED
TIET, Patiala

Dr. Gagandeep Kaur
Associate Professor, EIED
TIET, Patiala

Electronics and Communication Engineering Department
Thapar Institute of Engineering and Technology, Patiala, 147004

April 2022

Certificate

I, **Karishma Rao**, hereby certify that the research work presented in this thesis entitled "**Development of Novel Image Enhancement Methods for Bio-medical Images**" being submitted by Karishma Rao **Registration No. 901906008** in the Department of Electronics and Communication Engineering, Thapar Institute of Engineering and Technology, Patiala, India for the fulfilment of the requirements for the award of the degree of "**Doctor of Philosophy**." It is an authentic record of bonafide research work carried out under the guidance and supervision of **Dr. Manu Bansal, Assistant Professor, Electronics & Communication Engineering Department (ECED), and Dr. Gagandeep Kaur, Associate Professor, Electrical & Instrumentation Engineering Department (EIED), Thapar Institute of Engineering & Technology (TIET), Patiala, Punjab, INDIA.**

The matter presented in this thesis has not been submitted either in part or full to any other university or institute for the award of any other degree.

Date: 4/10/23

Karishma Rao
(Reg no: 901906008)

It is certified that the above statement made by the student is correct to the best of my knowledge and belief

Dr. Manu Bansal

Assistant Professor, ECED
TIET, Patiala

Date: 4/10/23

Dr. Gagandeep Kaur

Associate Professor, EIED
TIET, Patiala

Date: 4/10/23

Acknowledgement

First of all, I would like to express my heartfelt gratitude to Almighty God for providing me with strength, courage, good health, and the ability to learn and understand during the full period of my Ph.D. studies. This work could never have happened without the grace, guidance, and blessings of God.

I am obliged to Dr. Padmakumar Nair, Director, Thapar Institute of Engineering & Technology for facilitating the research aspirants to pursue their research interests in this esteemed institute as the institute is well equipped with all the necessities of research scholars.

I am very thankful to Dr. Alpana Agarwal, Professor and Head, Department of Electronics & Communication Engineering, Thapar Institute of Engineering & Technology, Patiala for continuous support during the period of research work.

I would like to express my special thanks to my research supervisors, Dr. Manu Bansal, Assistant Professor, Department of Electronics and Communication Engineering, and Dr. Gagandeep Kaur, Associate Professor, Department of Electrical and Instrumentation Engineering, Thapar Institute of Engineering and Technology, Patiala, Punjab, for providing me an opportunity to carry out research in the said area and providing invaluable assistance even during the pandemic times and always.

Words are inadequate in paying regards to my parents. I would like to thank my mother whose heavenly blessings supported me spiritually throughout my life. I am forever grateful to my father whose foresight and values paved the way for a privileged education and helped me to do better each day.

I express my sincere thanks to the members of my doctoral research committee Dr. Sanjay Kumar, Associate Professor, Department of Electronics and Communication Engineering, Thapar Institute of Engineering & Technology; Dr. Vinay Kumar, Associate Professor, Department of Electronics and Communication Engineering, Thapar Institute of Engineering & Technology; and Dr. Rajiv Kumar, Associate Professor, Department of Computer science Engineering, Thapar Institute of Engineering & Technology for providing necessary facilities and valuable suggestions throughout this research work and in the submission of this manuscript.

I am deeply obliged to Dr. Mohit Aggarwal, Dr. Mayank Rai and Dr. Sanjay Kumar PhD Coordinators of the Department of Electronics and Communication Engineering, Thapar Institute of Engineering & Technology for their constructive discussions and valuable suggestions during the meetings for evaluation of my research work by the research committee. I am also thankful to all other faculty members of the department for their support. I extend my warm thanks to all teaching and non-teaching staff, Department of Electronics and Communication Engineering, Thapar Institute of Engineering & Technology for their day-to-day co-operation

Karishma Rao

DEDICATED

TO

MY PARENTS

ABSTRACT

Image enhancement is a critical image processing approach that emphasizes critical information in an image and minimizes or eliminates some secondary information in improving the identification quality. The purpose is to make the objective images more application-specific than the original images. The primary goal of image enhancement is to improve the interpretability and visual quality of images, aiming to enhance the perception of information contained within the pictures for human viewers. Additionally, it can serve as a valuable pre-processing step for machine learning algorithms. The concept of image enhancement has been extensively employed in various fields of study, including biology, computer vision, remote sensing, and medical imaging.

Physicians often utilize medical images for illness diagnosis, disease monitoring, and therapy planning. Medical imaging methods can produce detailed human body images in vivo. Organs and tissue are shown structurally and functionally via the pictures obtained. This information may be utilized to aid in diagnosing and treating patients. Among all radiology examinations, the computed tomography (CT) scan is the most popular and frequently utilized by medical professionals since it is less expensive and reveals comprehensive structures of inside body components. Histopathology is another critical tool for physicians to determine the causes and consequences of all illnesses and disorders. The fundus image is the most often acquired image for diagnosing different eye diseases. This thesis's most often used medical images are CT scans, digital histopathology images, and retinal fundus images. CT, Histopathology, and Fundus pictures all exhibit a variety of image abnormalities, including low contrast, noise, blur, and distorted features, which vary according to the kind of medical imaging modality used.

Medical image enhancement is a key technique for improving diagnostic images for illness diagnosis, disease monitoring, and treatment planning. Although existing image enhancement methods are useful for a variety of application areas, the effects are often inappropriate for medical images due to the presence of multiple defects, color distortion, noise amplification, under or over enhancement, brightness degradation, and information distortion. In order to address these shortcomings, this dissertation

proposes a variety of medical image enhancement algorithms for CT scans, digital histopathology images, and retinal fundus images.

The first algorithm is based on optimal morphological transforms for improving the noise and contrast of CT images in the wavelet domain. Initially, the optimal morphology transform (OMT) technique is employed to increase the contrast of the original CT image, and then the discrete wavelet transform (DWT) method is utilized to partition the original CT image and the OMT transformed image into four separate portions. For increased contrast while preserving image brightness, the singular value decomposition (SVD) technique is utilized on LL sub-band output alone, while the Edge Map (EM) method is applied on the HH sub-band of the original CT image to denoise it. The proposed method outperforms the other six enhancement approaches. The experimental findings indicated that the suggested approach is capable of properly enhancing CT images while preserving their inherent features. The proposed approach outperforms existing methods such as S-curve [85], AGC-DWT [69], AGC-WHD [65], GAGC-DWT [61], EBCHE [50], and TCHE-DWT [51] in terms of EME, CII, Michelson contrast ratio and Weber contrast ratio, peak signal to noise ratio (PSNR), and entropy of the enhanced images. The proposed technique is appropriate for enhancing CT images and may be used to help pathologists or physicians in making the correct diagnosis.

The second algorithm effectively enhances non-contrast CT images with dual tree complex wavelet transform (DT-CWT) and adaptable morphology. This new approach for effectively enhancing non-contrast CT images is introduced, which employs a dual tree complex wavelet transform (DT-CWT) technique and adaptable morphology for efficient high-frequency sub-bands denoising and low-frequency sub-bands enhancement. Experiments on structured CT scan images were conducted to evaluate the proposed procedure's success on quantitative and subjective tests. Furthermore, experiments on CT image databases explicitly show that the proposed methodology outperforms other conventional enhancement techniques to improve and maintain fine information devoid of noise. The suggested algorithm produces greater brightness preserved CT images with higher contrast and lower noise levels, with all regions becoming visible and prominent. The suggested approach is appropriate for CT image enhancement and may be used to help pathologists or physicians precisely diagnose the disease.

The third algorithm seeks to improve the color histopathology image contrast based on

retinex theory and local contrast adjustment. To begin, a novel multiscale retinex with adaptive weighting is presented to enhance the contrast of a color histopathological image in the HSV color model, and then the image's local details are strengthened using a new weighted Contrast Limited Adaptive Histogram Equalization (CLAHE) methodology applied to the luminosity component in the L*a*b* color model. Experiments using histopathology images have been used to assess the proposed procedure's success on both quantitative and subjective measures. Additionally, experiments conducted using histopathology image databases reveal strongly that the proposed methodology outperforms existing standard enhancement strategies in terms of overall contrast improvement and fine detail preservation. The proposed technique generates brightness preserved, better contrast natural histopathological images with no image artifacts, with all areas being apparent and noticeable. The proposed methodology is appropriate for histopathology image enhancement and may be utilized to support pathologists or doctors in makingaccurate diagnoses.

The fourth algorithm is an effective image enhancement method for improving the luminosity and contrast of color retinal fundus images. The purpose of this algorithm is to provide an efficient technique for color retinal fundus image enhancement that is based on luminance and contrast improvement. To begin, the luminosity of the color retinal image is improved using a novel just noticeable difference (JND)-based adaptive gamma correction method, followed by multiple layers of CLAHE in the L*a*b* color mode to enhance retinal image contrast. Experiments using benchmark test retinal images are utilized to evaluate the proposed method's performance on qualitative and quantitative metrics. Furthermore, findings from experiments on retinal image databases demonstrate vividly that the proposed approach surpasses other conventional enhancement approaches. The proposed approach produces natural-looking fundus images with increased contrast in which all areas are visible and distinct. The proposed technique is suitable for color retinal image enhancement, which can be used to help ophthalmologists or clinicians inaccurately diagnose disease.

Each of the novel methods is presented, described thoroughly, and applied to a set of medical images from a publicly available database to measure its effectiveness qualitatively and quantitatively in terms of various performance parameters, such as signal-to-noise ratio, discrete entropy, edge preservation index, contrast ratio, and enhancement ratio. There are significant quantitative and qualitative findings that show improvements when compared to the reference enhancement methods. These results

indicate that the newly developed algorithms represent a valuable contribution to advancement in this field.

CONTENTS

List of Figures

List of Tables

List of Abbreviations

Abbreviation	Full Name
DWT	Discrete Wavelet Transform
SVD	Singular Value Decomposition
DT-CWT	Dual Tree Complex Wavelet Transform
DCT	Discrete Cosine Transform
JND	Just Noticeable Difference
et al	And Others
PSO	Particle Swarm Optimization
A	Adaptable Parameter
B	Shrinking Factor
Λ	Adjustable Parameter
Θ	Gradient
PCA	Principal Component Analysis
CT	Computed Tomography
MRI	Magnetic Resonance Imaging
DHI	Digital Histopathology Image
FI	Fundus Images
CDF	Cumulative Density Function
PDF	Probability Density Function
BBHE	Brightness Preserving Bi-Histogram Equalization
AMBE	Absolute Mean Brightness Error
DSHE	Dualistic Sub-Image Histogram Equalization
RDSHE	Recursive Dualistic Sub-Image Histogram Equalization
MMBBHE	Minimizing The Absolute Mean Brightness Error
BPLHE	Bi-Histogram Equalization With A Plateau Limit
DHE	Dynamic Histogram Equalization
BPDHE	Brightness Preserving Dynamic Histogram Equalization
BPDFHE	Brightness-Preserving Dynamic Fuzzy Histogram Equalization
AHE	Adaptive Histogram Equalization
TCLAHE	Traditional Contrast Limited Histogram Equalization
DCT	Discrete Cosine Transformation
EBCHE	Exposure- Based Contrast Limited Bi-Histogram Equalization
AGGCWD	Adaptive Gamma Correction With Weighted Distribution
HSV	Hue, Saturation, And Value

NGC	Normalized Gamma Correction
PSO	Particle Swarm Optimization
SVD	Singular Value Decomposition
DWT	Discrete Wavelet Transforms
HE	Histogram Equalization
GAGC	Globally Adaptive Gamma Correction
LH	Low-High
LL	Low-Low
HH	High-High
HL	High Low
TCHE	Triple Clipped Histogram
GSF	Gaussian Surround Function
SSR	Single-Scale Retinex
MSR	Multiscale Retinex
RBLA	Retinex Based Luminance Adaptation
JNT	Just Notable Transform
GCRIE	Gamma Error In Image Enhancement
NSCT	Non-Sampled Contourlet Transform
NLM	Nonlocal Means
NSST	Non-Subsampled Shearlet Transform
HCM	Heat Conduction Matrix
HCMBE	Heat Conduction Matrix-Based Image Enhancement
CNN	Convolutional Neural Network
DCCN	Deep Convolutional Neural Network
RDC UNET	Residual Dense Connection Based Unet Architecture
PSO	Particle Swarm Optimization
EM	Edge Map
IDWT	Inverse Discrete Wavelet Transform
AIC	Average Information Content
MSRAW	Multiscale Retinex With Adaptive Weighting
WCLAHE	Weighted Contrast Limited Adaptive Histogram Equalization
CII	Contrast Improvement Index
MC	Michelson Contrast
WC	Weber Contrast
EME	Measures Of Enhancement

EPI	Edge Preservation Index
UIQI	Universal Image Quality Index
PSNR	Peak Signal To Noise Ratio

CHAPTER 1
INTRODUCTION

1.1. Medical Imaging Overview

Medical imaging involves employing a range of imaging techniques and technologies within the medical field to visualize the internal structures and functions of the human body. To help doctors detect and cure illnesses, medical imaging can peer through the body's tough outer layers and reveal what is going on inside. In vivo (in the body) photographs of a human being's anatomy can be obtained with medical imaging techniques [1-3]. The resulting images display the structural and functional characteristics of organs and tissue. A patient's diagnosis and treatment could benefit from this data. Diagnostics, disease monitoring, and treatment plans all benefit greatly from the use of medical imagery by doctors.

Figure 1.1 illustrates the various ways in which medical images, such as those used for pathology, radiography, and diagnosis inspection, might be sorted.

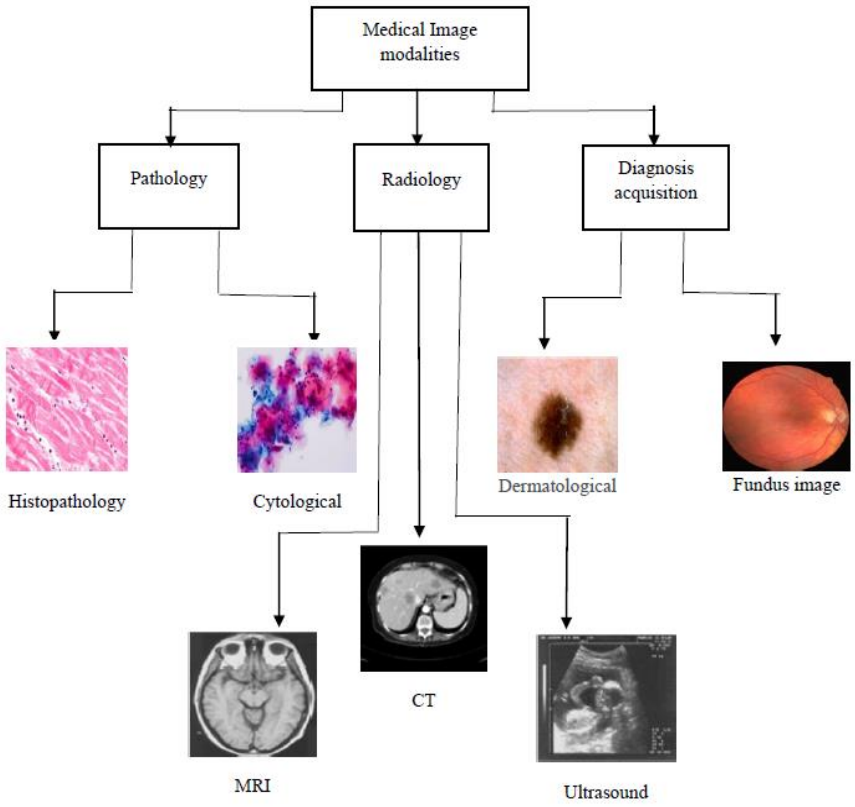

Figure 1.1: Different medical images under several categories.

1.1.1. Pathology

Pictures of human tissue taken under the microscope are called pathology [5-6]. Pathology is the study of disease and injury, including their causes and effects. The term "pathology" describes the study of disease in its broadest sense, which includes a wide range of biological disciplines and medical sub-fields. The term "general pathology" is often used in a narrower sense when discussing modern medical therapy, although referring to a wide range of distinct but related clinical disciplines that detect disease primarily through the study of tissue, cell, and body fluid samples. Figure 1.2 depicts the abnormal process. It is possible to classify the pathology into the following subtypes:

Figure 1.2: A pathologist at the pathology lab examines a tissue sample [5].

1.1.1.1. Histopathology

Under a microscope, histopathologists look for signs of disease in tissues in order to find possible causes of illness. The study of a biopsy or surgical specimen by a pathologist after it has been processed and histological sections have been placed onto glass slides is known as histopathology. [5]. This is in contrast to cytopathology methods, which use isolated cells or tissue fragments. Tissues are first examined on a histological level after they have been subjected to surgical intervention, a biopsy, or an autopsy. After removal from the organism, the tissue is placed in a fixative to prevent further degradation. Figure 1.3 displays various histopathological images.

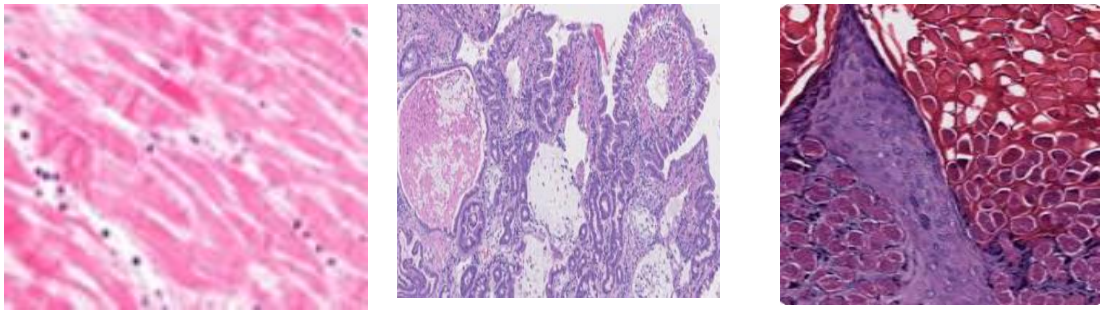

(a) (b) (c)

Figure 1.3: Various histopathology medical images [5]

1.1.1.2. Cytopathology

The field of cytopathology [5] is a subset of pathology that focuses on the cellular level in the study and classification of disease. Its primary application is in cancer diagnosis, but it has a wide series of additional uses, including the detection of lesions and the analysis of diseases affecting normally sterile bodily cavities. Figure 1.4 depicts various cytopathology pictures.

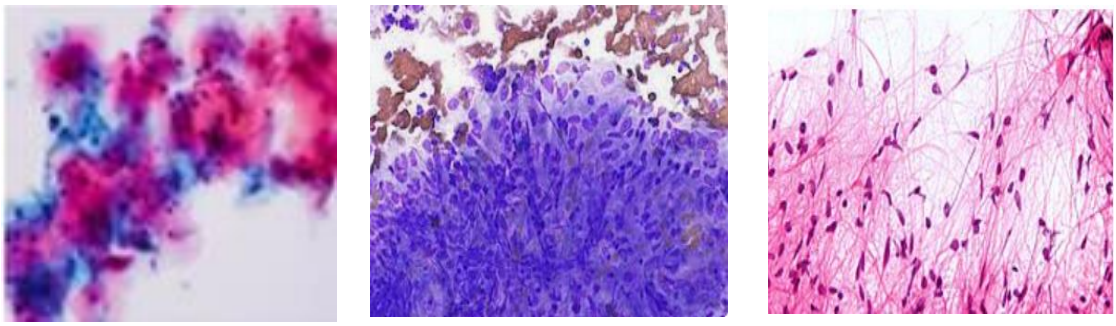

(a) (b) (c)

Figure 1.4: Various cytopathology medical images [5]

1.1.1.3. Anatomical Pathology

Physical, microscopic [5], chemical, immunological, and molecular analysis of tissues, organs, and entire bodies are the focus of anatomical pathology, a medical specialty dedicated to the diagnosis of disease.

1.1.1.4. Forensic Pathology

Post-mortem examination of a body or its remnants is the cornerstone of forensic pathology, which seeks to determine the cause of death. To verify the identity of a deceased person, a coroner or medical examiner is typically called upon to perform an autopsy during the course of a criminal inquiry.

1.1.1.5. Neuropathology

Neuropathology, the learning of illnesses of the nervous system, typically requires either tissue samples taken during surgery or, in extremely rare cases, whole brains obtained during autopsies [6]. Neuropathology encompasses the fields of anatomical pathology, clinical neurology, and neurosurgery. If an illness of the neurological system is assumed and a judgement cannot be made using less invasive means, a biopsy of nerve tissue is collected from the brain to help in the analysis. The neuropathology picture is depicted in figure 1.5.

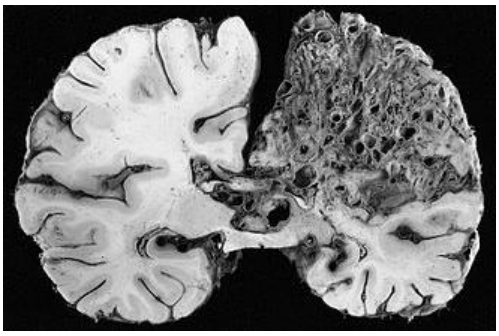

Figure 1.5: Neuropathology medical image [6]

1.1.2. Radiology

The field of study known as "radiology" [4] is concerned with the analysis of diagnostic images obtained by irradiating human bodies from the outside. As a subspecialty of internal medicine, radiology makes use of diagnostic imaging to pinpoint disease and guide treatment in both humans and animals. Computed tomography (CT), fluoroscopy, nuclear medicine, magnetic resonance imaging (MRI), ultrasonography, and positron emission tomography are only few of the imaging modalities that fall under the umbrella of "radiology," which also includes modalities that do not require electromagnetic radiation. Figure 1.6 depicts the stages of a radiologic procedure. The field of radiology can be subdivided into the following:

Figure 1.6: Radiology imaging process [4]

1.1.2.1. Magnetic Resonance Imaging

MRI uses strong magnetic rays to align atomic nuclei within the body's tissues. The nucleus's rotational axis is then perturbed with a radio signal, and the radio frequency signal produced by the nuclei as they revert to their initial states is monitored. [8] Tiny coil antennas are placed in close proximity to the target area to pick up radio signals. MRI has the convenience of providing images in several oblique planes, such as the axial, coronal, sagittal, and others. Magnetic resonance imaging (MRI) [6] is a diagnostic imaging technology used in radioscopy to create images of anatomical and functional structures using magnetism. MRI scanners create images of internal organs by combining radio waves with powerful magnetic fields and magnetic field gradients. Figure 1.7 represents various MRI pictures of different body parts.

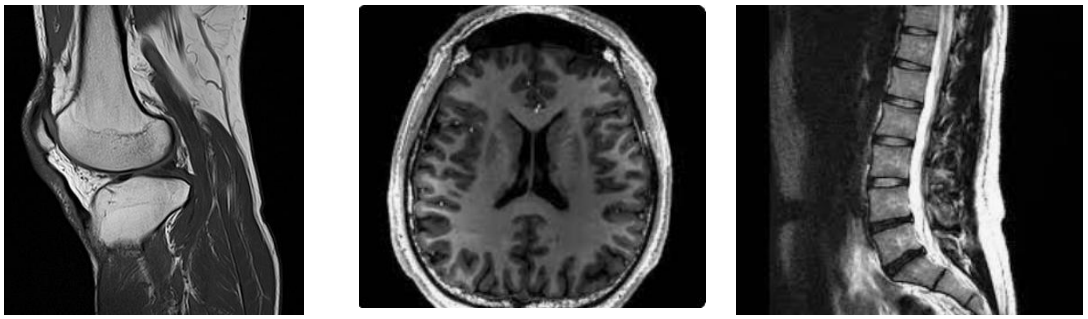

(a) (b) (c)

Figure 1.7: (a) Knee MRI medical image, (b) Brain MRI medical image, (c) Spine MRI medical image [8]

1.1.2.2. Computed Tomography

CT imaging creates pictures of the body using a combination of x-rays and computing power. [7] The CT scan creates a digital cross-sectional image by rotating a patient while an X-ray tube and detector in a ring-shaped device look on from opposite sides. CT scan data is acquired in the axial plane, and the computer reconstruction process starts with coronal and sagittal images. In order to better define anatomical structures, CT is often used in conjunction with radiocontrast medications. CT scans can detect more modest variations in X-ray attenuation than radiographs can. The patient is subjected to higher levels of ionising radiation exposure with a CT scan compared to a radiograph. Figure 1.8 shows the various CT pictures.

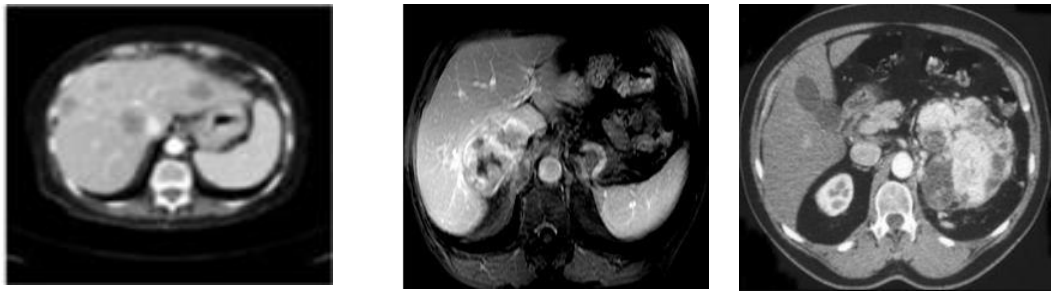

(a) (b) (c)

Figure 1.8: (a) Stomach CT medical image, (b) Adrenal CT medical image, (c) Kidney CT medical image [7]

1.1.2.3. Ultrasound

When used for medical purposes, ultrasound allows for real-time visualisation of anatomical structures within the body's soft tissues. Although ultrasound does not employ ionising radiation, the images' accuracy depends largely on the ultrasound technician's expertise and the patient's size. Diagnostic ultrasonography is a non-invasive imaging procedure used for diagnosis [5]. The sound waves that ultrasonic probes emit, also known as transducers, are above the human hearing threshold. Today's transducers, however, often function at much higher frequencies. Most ultrasonic diagnostic tools are applied topically, usually to the skin. Image quality can be enhanced, however, by inserting probes into the body via the digestive tract, the vagina, or the blood vessels. The use of ultrasonography during surgery is also possible by putting a sterile probe into the area undergoing treatment. The various ultrasound images is presented in figure 1.9.

(a) (b) (c)

Figure 1.9: (a) Stomach ultrasound medical image, (b) Kidney ultrasound medical image, (c) Liver ultrasound medical image [5]

1.1.3. Diagnostic Inspection Acquisition

Diagnostic inspection acquisition imaging [3] is a visual depiction of the medical

images that can be gathered during the inspection part of the test. Images are typically captured using specialised medical equipment, such as fundus cameras for digital retinal fundus imaging or generic cameras for dermatological photography.

The term "monocular indirect ophthalmoscopy" refers to the method through which specialised fundus cameras create images of the retina. Both a sophisticated microscope and a high-speed camera are integrated into this setup. Creating dermatological photos requires a strong lighting system and a high-quality magnifying lens. Dermatological photographs allow a more thorough evaluation of the skin's structures and patterns.

CT scans, which are less invasive and reveal more detailed structures of internal body parts, are the most common and widely used radiology tests. Histopathology is an important diagnostic tool that helps doctors understand the root causes of diseases. When it comes to identifying various eye illnesses, the fundus image is by far the most commonly acquired image. This work makes use of medical pictures such computed tomography scans, digital histopathology photos, and retinal fundus photographs.

Low contrast, noise, blur, and distorted features can appear in CT, Histopathology, and Fundus pictures, among others, and these anomalies are not uniform among medical imaging modalities. Let us take a look at their imaging workflow and the artefacts resulting from it.

1.2. Imaging Modalities

1.2.1. Computed Tomography Scan

Computed tomography (CT) scans [7] are X-ray images taken from diverse angles around the body that are analysed by a computer to provide a sequence of cross-sectional images of the body's major organs. Medical professionals rely heavily on CT scans to diagnose patients with cancer and other diseases, track the development of these conditions over time, and map out treatment strategies.

The purpose of a computed tomography (CT) scan [8] is to visualise the interior architecture of many parts of the body, including the head, neck, lungs, shoulders, cardiac, spine, abdomen, chest, and heart, in order to diagnose a medical condition and plan a course of treatment.

1.2.1.1. CT scan Image Formation

Unlike conventional X-ray machines, which use a stationary tube, CT scanners employ motorised X-ray sources that spin around the center hole of a donut-shaped assembly

called a gantry. A CT scan is performed by spinning an X-ray tube around a patient as they lie on a bed that gradually moves along the framework, allowing thin X-ray beams to pass through the body.

Special digital X-ray detectors, rather than film, are used on the CT scanner's opposite end. When an X-ray is taken, it is captured by a detector and sent to a computer. Each time the X-ray source rotates completely, the CT computer generates a new two-dimensional imaging slice of the patient. Slices of an image are normally between 1 and 10 millimeters in thickness, but this might vary based on the CT scanner being utilised. Once the entire slice has been completed and saved, the motorised bed is progressively placed into the gantry. Another slice of an X-ray image can be made by repeating the scanning procedure. Iterations of this procedure are taken till the required quantity of slices has been achieved. The computer can then offer the doctor a 3D representation of the patient, complete with bony structures, organs, and any abnormalities the doctor may be looking for. By rotating a 3D image in space or seeing slices in succession, the precise position of an issue can be pinpointed using this method. Figure 1.10 depicts a person through the CT scan creation procedure.

Figure 1.10: CT imaging process [8]

1.2.1.2. CT scan Quality Artifacts

Poor CT scan quality may result from a number of factors, such as noise in specific image regions, insufficient contrast, or artefacts of various kinds. External ambient noise, the patient's individual position during the scan, emergency scenarios,

insufficient illumination, and the technological limitations of imaging tools are all potential causes of these image anomalies. A CT scanner's thin slices, weak current, and lack of contrast can all contribute to audible noise.

- Non-contrast CT scan images are generally poor contrast, making it difficult for a physician to discriminate between several types of material within a single scan. Here we see CT scans with very little contrast. 1.11 can be obtained for several reasons, including the use of low-dose radiation during the examination, transmission, storage, external ambient noise, poor lighting circumstances, and technological limits of the imaging equipment.

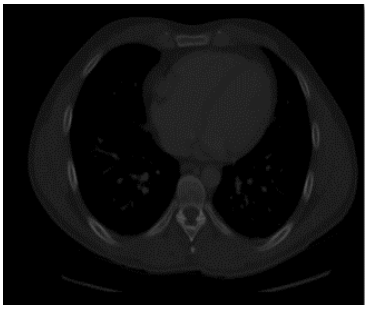

Figure 1.11: Low contrast CT image [8]

- CT scan is also affected by noise [10], which generally appears grainy, as seen in figure 1.12. Noise may emerge in CT for various reasons, including the CT scanner's minimal slice thickness, inadequate power supply, and insufficient contrast dosage.

Figure 1.12: Noisy CT scan [10]

To improve contrast, which can help make an image's target area stand out more clearly, patients are sometimes given dosages of contrast material orally or intravenously. However, some people (the elderly, young children, pregnant women, and people with renal disease) for whom using a contrast agent can be extremely risky or even fatal. It has also been shown that exposure to these compounds can have a number of unfavourable effects on the typical patient. Scanning a patient multiple times to increase

contrast and reduce noise on a CT scan poses a risk to the patient's organs due to the radiation used in the scanning process.

1.2.2. Digital Histopathology Image

After a doctor analyses tissue under a microscope, the DHI (Digital Histopathology Image) [16-17] is created by scanning equipment. In this case, the glass slides being examined under the microscope contain human tissue that was removed from a patient during a biopsy or surgical procedure. The liver, kidney, breast, and skin are just a few of the many body parts from which tissue can be taken. DHI aids in the diagnosis of diseases and cancer and provides important insight into their origins for medical professionals.

1.2.2.1. DHI Image Formation

Depending on the type of cancer being investigated, pathology samples can be collected from virtually everywhere in the body. Most fresh tissues are extremely sensitive and readily destroyed, making it difficult to study slices under the microscope. Therefore, when a biopsy specimen has been removed by a physician or surgeon, a specific procedure routine must be followed in order to preserve it for later pathology analysis [18], which can be read as follows:

- **Fixation**: In order to stabilise the tissue, prevent deterioration, and keep it in a "life-like" state, the biopsy is placed in a container containing formalin or other fluid for six to twelve hours.
- **Processing and embedding**: After being immersed in formalin, the tissue is put through a series of dehydrating and clarifying solvents before being cast in molten paraffin wax. Once the wax has cooled, a solid block will have formed, with the tissue embedded within it.
- **Sectioning**: Using a microtome, tiny slices of paraffin wax are cut from the block and mounted on microscope slides. Typically, a paraffin section will be between 3 and 5 micrometers thick, with the expectation that it will only contain a single layer of cells.
- **Staining**: Most tissue samples are translucent because they lack significant intrinsic pigment save for a few natural pigments like melanin. Contrast is improved with counter-stains that bind selectively to particular components,

allowing structural features of tissue slides to be seen under a microscope for inspection and diagnosis. The glass slides are then inspected by pathologists using transmission microscopy, a technique in which the specimen is illuminated from behind and the pathologists observe the light that is transferred through the sample without being absorbed or dispersed. Figure 1.13 depicts the process of digital pathology, in which whole-slide imaging technologies are used to scan specimens, followed by their storage in digital format on computers for later analysis and diagnosis.

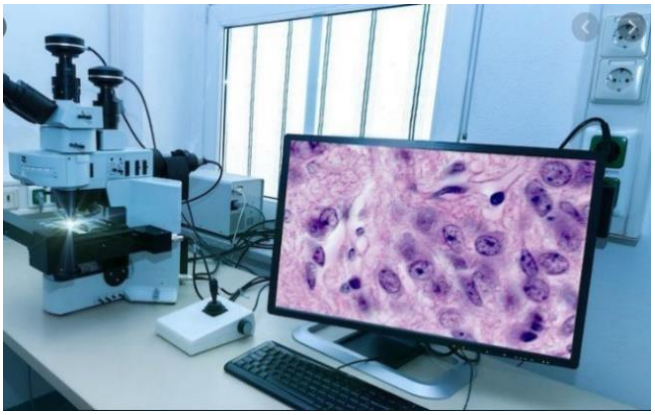

Figure 1.13: Digital histopathology imaging process [18]

1.2.2.2. DHI Quality Artifacts

Low contrast across parts of the histopathological picture, blurring, and other bad artefacts might emerge from DHI due to inadequate straining techniques [18]. Overstraining or understaining both nuclei and other surrounding tissues, over- or under-staining one of the components, inappropriate staining timing are common causes of these picture defects.

- DHI has a general lack of contrast between nuclei and other surrounding tissues [18]. As seen in figure 1.14(b), DHI is excessively dark, resulting in poor contrast between nuclei and surrounding tissues compared to the original DHI image shown in figure 1.14(a).

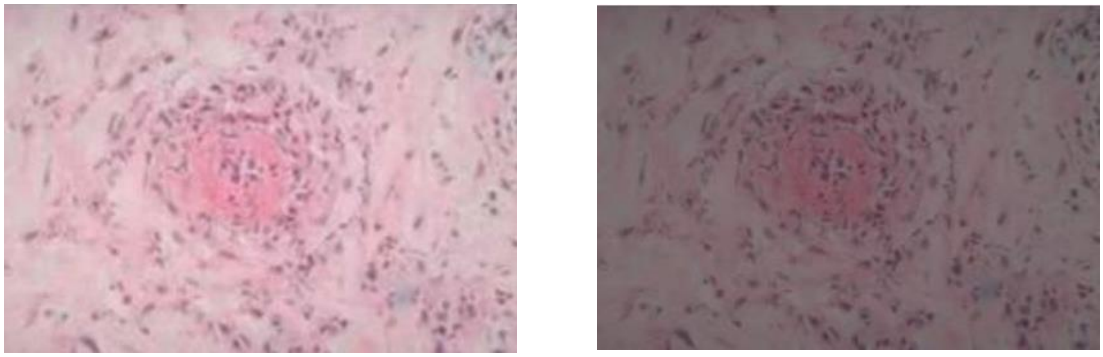

(a) (b)

Figure 1.14: (a) Original DHI image (b) Poor contrast DHI [18]

1.2.3. Fundus Image

The term "monocular indirect ophthalmoscopy" (FI) [24] refers to the process by which fundus images are created utilising specialised fundus cameras. The camera in question is a sophisticated microscope coupled with a high-speed shutter. The retina, macula, and optic disc are the primary targets of the fundus camera because they are located inside the eye. FI aids the doctor in diagnosing and monitoring the development of eye conditions such as diabetic retinopathy, AMD, macular edoema, and retinal detachment.

1.2.3.1. Fundus Image Formation

Fundus imaging refers to taking pictures of the backbone of the eye, often known as the fundus. Specialized fundus cameras, which incorporate a microscope with a flash-capable camera, are needed for the fundus photography process. In a fundus image, the retina, optic disc, and macula are most clearly depicted. Fundus photographic cameras are based on the assumption of monocular indirect ophthalmoscopy. A fundus camera is an instrument that inverts and magnifies images of the fundus. While standard lenses only allow for a field of view of 30–50 degrees at a magnification of 2.5x, a wide-angle lens may increase that by a factor of 5 to a whopping 140 degrees (with 2.5x magnification). Fundus cameras, like indirect ophthalmoscopes, use a variety of lenses for observing and lighting the eye. The light is first focussed by a set of lens system onto a doughnut-shaped space; from there, it travels via the camera's objective lens and finally strikes the retina via the cornea. During illumination, light is reflected from the retina and travels through a dark spot in the donut shape created by the light source.

This is because the two schemes use different paths for their respective light signals. Therefore, there are very few reflections in the final product. The low-magnification telescopic eyepiece continues to receive the image-forming rays. In order to prevent the flash from blinding the subject, the illumination system is interrupted the moment the shutter is released. At the same time, a mirror on the inside of the telescope focuses the reflected light onto the recording media. Light is captured by the mirror regardless of whether you're using a digital CCD or film. Due to the eye's tendency to acclimate when looking through a telescope, a parallel exit vergence is required for an in-focus input to be shaped on the recording medium, as shown in figure 1.15.

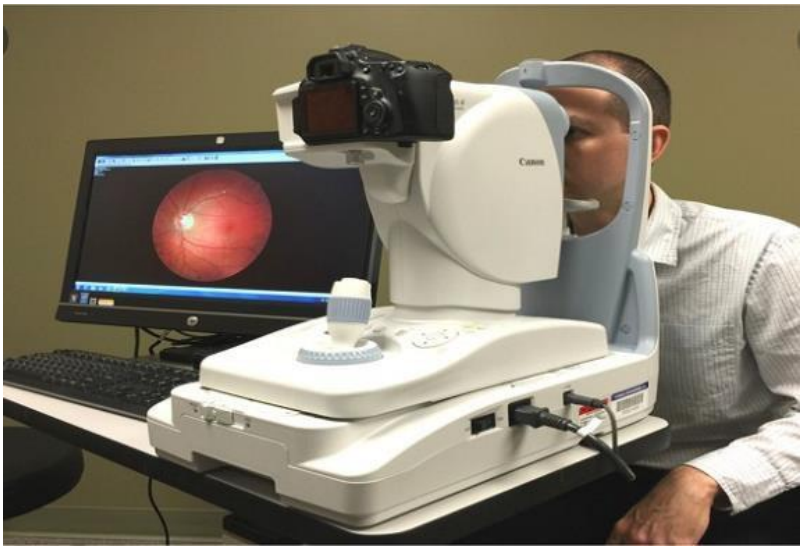

Figure 1.15: Fundus imaging process [24]

1.2.3.2. FI Quality Artifacts

Uneven lighting, low contrast, and noise make some fundus photos less than ideal. Fundus camera malfunction, inappropriate camera settings (e.g., inaccurate exposure or focal plane), lens contamination (e.g., dirt or scratch), and improper patient eye movement are all potential causes of this problem.

- Most retinal fundus photographs do not have consistent lighting [25], which means that some parts of the image are brighter than others. As seen in Figure 1.16(b), however, others have a low brightness and appear darker as compared to uniform illuminated fundus image shown in figure 1.16(a).

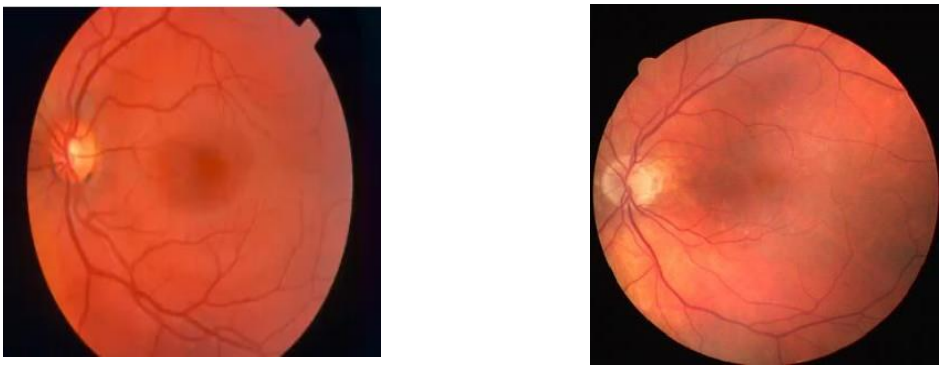

(a) (b)

Figure 1.16: (a) uniform illumination (b) Non-uniform illumination [25]

- The inappropriate placement of the fundus camera, a curved retina surface, dilation, refractive media, exudates, and head/eye movement can all contribute to a lack of contrast and noise [26], which is another major issue in FI. Figure 1.17 (b) displays the FI at low contrast levels as compared to original fundus image shown in figure 1.17(a).

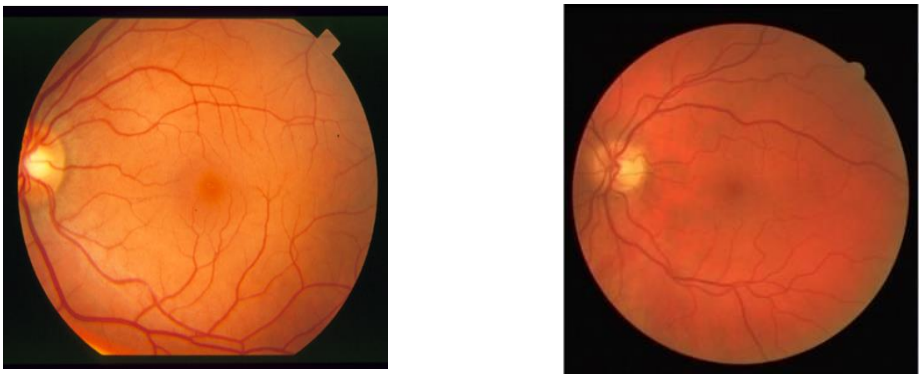

(a) (b)

Figure 1.17(a) highly contrast FI (b) Low contrast FI [26]

1.3. Need of the Present Work

Problems arise in subsequent procedures, including disease diagnosis, tumour categorization, and treatment planning, due to the aforementioned poor quality of medical imaging. Poor contrast, a high noise level, and blurring can make it difficult for doctors to distinguish between different organs, lesions, and cancers, increasing the risk of a misdiagnosis. Furthermore, inaccurate and undesired results from computer-aided illness segmentation and classification techniques are produced by low-quality medical images. Defects in medical images must be corrected for two reasons: first, so that doctors can provide an accurate diagnosis, and second, so that computer-assisted operations can be more efficient. To improve the contrast and signal-to-noise ratio of a

CT scan, the doctor will frequently inject the patient with a contrast substance orally. Repeat CT scans are often recommended when patients want the best possible diagnostic picture.

If we take digital histopathology as an example, in order to get a good one, the doctor has to undertake a lot of microscopic imaging sessions with different experimental setups until they have a good enough contrast between different things in the image. When employing Fundus imaging, patients may need to have their eyes examined multiple times, each time subjecting their retinas to more and more intense light in an effort to produce a sharper image. In addition, angiography is used to provide a clearer picture of certain crucial eye problems to the patient. Contrast dye is injected into the blood during an angiogram.

However, there are some people (the elderly, young children, pregnant women, and people with renal disease) for whom using a contrast agent can be extremely risky or even fatal. There is also evidence that these substances have a number of negative effects on the typical patient. Scans, especially those that use radiation to provide a mid-sectional image, can be harmful to a patient's internal organs. It is not always possible to improve image quality by collecting numerous human organs or skin samples. Depending on the experimental conditions, a histopathology technician may find it challenging and time-consuming to analyse microscopic photographs. Therefore, gathering the new and improved medical photos could be risky, perhaps harmful to the patient, and labour intensive for the doctor. Furthermore, computer-assisted procedures like segmentation and categorization of a particular disease may produce misleading results if the medical pictures used were of low quality [4-5]. To make medical image analysis easier, more compact, and less labor-intensive, we need to boost the overall quality of medical pictures, which necessitates a combination of new and enhanced computer-aided methodologies. To improve therapy and analysis, the current study requires the following medical imaging enhancements.

1.3.1. CT Image Enhancement

CT scan pictures are widely used by doctors for making diagnoses, tracking illness progression, and formulating treatment plans for a wide range of chronic conditions. Acquired CT pictures include poor quality, low contrast, and visual noise because of external air noise, unintentional patient placement, insufficient lighting, and technological restraints of the imaging equipment [1]. The CT image quality is

diminished by visual noise. Poor contrast and a high noise level might lead to a misdiagnosis since it is difficult for doctors to distinguish between different organs, lesions, and cancers. Computer-aided analysis, including segmenting anatomical structures like the heart, lungs, pancreas, etc., and diagnosing disorders, has become increasingly challenging due to low-quality CT images [4]. In order to better see the anatomical structures and detect the abnormalities, a method must be devised to enhance the visual condition of CT scans. This work details a technique for enhancing CT scan images by reducing noise and enhancing contrast, allowing for more precise disease diagnosis.

1.3.2. Histopathology Image Enhancement

Segmenting microscopic assemblies like nuclei and cells in tumour and non-tumor areas and then classifying image sections and full images are two of the most typical tasks in histopathology image processing. Hematopathology image analysis relies heavily on computer-based methods that can identify and isolate nuclei for further study. This process is necessary for obtaining, withdrawing, and rendering sub-cellular morphological data from digital slide images. Low-contrast, low-quality histopathology images can negatively affect the accuracy of diagnosis and the outcomes of computer-assisted procedures like segmentation and classification. Therefore, a method must be devised to enhance the visual eminence of histopathology images, allowing for improved visibility of microscopic structures and easier detection of abnormalities. In this study, a technique is introduced for increasing contrast in histopathology images, which aids in the reliable diagnosis of disease.

1.3.3. Retinal Fundus Image Enhancement

Retinal imaging is commonly used by ophthalmologists in the analysis of retinal diseases like diabetic retinopathy, refractive errors, amblyopia, and glaucoma [1]. However, due to eye disorders and poor imaging procedures [2], such as an incorrect camera setting, dirtiness or scratches in the lens, or opaque refractive medium, some retinal photographs are clinically unsatisfactory. Retinal pictures are degraded by non-uniform illumination and inadequate contrast, reducing their specificity and sensitivity for medical tests and potentially limiting ophthalmologists' skill to understand important eye characteristics or discriminate between different retinal diseases. Diabetic retinopathy, age-related macular deterioration, and choroidal

neovascularization are only a few of the retinal illnesses that might be difficult to categorise using computerised eye disease diagnostics due to inaccurate retinal images used to segment the retina's anatomical features. In order to better observe the functional structures and detect the anomaly, a method must be devised to enhance the pictorial quality of retinal images. In these findings, a technique is described for enhancing the brightness and contrast of retinal fundus images, which aids in the diagnosis of disease.

1.4. Summary

Low contrast, noise, blur, and distorted features are some of the image defects discussed in this section, along with their development and their prevalence in CT, Histopathology, and Fundus pictures. The significance of the current work is also discussed in this chapter. After this, a primer on image enhancement and a thorough analysis of the various techniques now in use will be discussed.

CHAPTER 2
LITERATURE REVIEW

2.1. Introduction to Image Enhancement

Image enhancement, a significant technique in image processing, consists of bringing attention to the most relevant aspects of a picture while diminishing or eliminating the less relevant ones in order to boost the reliability of identification. The objective is to enhance the original images such that they are more helpful in the specified setting. Image enhancement involves altering the luminance of individual pixels to boost the legibility of a picture for human eyes or the efficiency of feature extraction. It's no secret that the fields of biology, computer vision, remote sensing, and medical imaging all make use of the idea of image enhancement.

In order for clinicians to make accurate diagnosis, medical image enhancement is essential. The purpose of medical image enhancement is to increase the quality of a medical photograph by boosting its visual appeal in various ways, such as by raising the contrast and delivering more information in the image, and by removing undesirable aspects, such as blur and noise. There are a number of methods used to enhance images; some examples include de-noising algorithms, contrast enhancement, filtering, interpolation, and enhancement of non-uniform lighting. Numerous academic disciplines make considerable use of the idea of image enhancement, including biology, computer vision, remote sensing, and medical imaging. Enhanced medical images are necessary to help doctors make correct diagnoses. The goal of the medical image enhancement process is to improve the quality of a medical picture so that it can be more clearly viewed by a doctor or other healthcare provider. This is accomplished by, among other things, decreasing the amount of blur and noise in the image, boosting the contrast, and adding new information to the picture. De-noising algorithms, contrast enhancement, filtering, interpolation, and boosting of non-uniform lighting are just a few of the picture improvement techniques used. Several techniques for improving the contrast, noise reduction, and general image quality of medical images have been documented in the published literature. These techniques can be categorised in a wide variety of ways, including histogram-based methods, retinex-based methods, morphological methods, gamma-based methods, wavelet-based methods, contourlet transfer-based methods, filter-based methods, and deep learning-based methods.

2.1.1. Histographic Approaches Review

Traditional histogram equalisation (THE) [30] is a commonly utilised contrast enhancement method in both general and medical picture improvement. By making the core low contrast histogram flatter, each pixel is more likely to contain a value from the histogram, which in turn increases global contrast. The probability density function (PDF) is obtained by normalising the intensity histogram, and the CDF is the result of the PDF times the number of observations. An improvement to the low contrast image is achieved by using the CDF to build a transformation function that transfers each intensity value in the original image to the improved intensity.

Oversaturation has reduced the image's entropy and caused some loss of detail. The publication explains the BBHE technique, which is a form of bi-histogram equalisation that keeps the original image's luminance intact. In the first step, a mean estimate is calculated, and then the histogram for the low-contrast image is divided in half so that each half can be processed separately using THE. The probability density function is calculated by translating the intensity histogram into a normal distribution (PDF). Next this PDF is utilized to derive the CDF for each sub histogram. After the intensity histogram has been normalised, the PDF can be calculated. The cumulative density function (CDF) of each sub histogram is then determined using the PDF thus obtained. To produce the transformation function that maps each intensity in the low contrast image to the new enhanced intensity, we first compute the cumulative distribution function (CDF) for both small sub-histograms.

While the BBHE approach does a better job of preserving the Absolute Mean Brightness Error (AMBE) than the THE method, the latter retains more of the information that would otherwise be lost due to the loss of entropy in the image. Due to this drawback, dualistic sub-image HE (DSHE) [32] was developed. DSHE is the same as BBHE. The histogram is divided in half based on the image's median value. The probability distribution function (PDF) is calculated after the intensity histogram has been normalised. Next this PDF is utilised to derive the CDF for each sub histogram. In order to raise the contrast of a low-contrast image, we first calculate the cumulative distribution function (CDF) for both small sub-histograms, and then utilise it to create a transformation function that maps each original intensity to the improved intensity.

Using BBHE does not result in a sufficiently small mean brightness error. Iteratively The independent histogram equalisation (RMSHE) [34] is introduced as an extension

of the BBHE. The RMSHE method iteratively rifts the input histogram into numerous small histograms depending on the mean of the previously produced histogram, while the BBHE method rifts the histogram only once based on the mean value. This recursive method converges when the target average brightness is reached. An image with low contrast will have a histogram that is split into four smaller histograms. After normalising the intensity histograms, the program generates probability density functions (PDFs) for all four histograms and uses them to derive CDFs for each sub histogram. The cumulative distribution function (CDF) for both small sub-histograms is then used to build the transformation function. The new, improved image is obtained by mapping each intensity from the low-contrast original to the higher-quality intensity. The average brightness error cannot be sufficiently reduced by DSHE. As a natural progression from DSHE, the recursive dualistic sub-Image histogram equalisation (RDSHE) method was developed. Using the computed median value, the RDSHE method divides the input histogram in half, and then again in half using the sub histograms that were formed in the first step [35]. This recursive method converges when the target average brightness is reached. An image with low contrast will have a histogram that is split into four smaller histograms. After normalising the intensity histograms, it generates PDFs for all four histograms and computes CDFs for each sub histogram using the PDFs as inputs. The CDF for both small sub-histograms is calculated in advance, and this information is used to generate the transformation function that maps each intensity in the low contrast image to the new boosted intensity. The MMBEBHE, or minimum mean brightness error bi-histogram equalisation, was created by Chen et al. [33] as a refined version of the BBHE. For reducing the Absolute Mean Brightness Error, MMBEBHE has been demonstrated to be more effective than conventional histogram equalisation methods. The histograms of low contrast photos are split by MMBBHE according to the threshold value that results in the smallest absolute mean brightness error for the image (AMBE). The method first determines the AMBE for a range of threshold values and then selects the threshold value resulting in the lowest AMBE. Last but not least, it receipts the input histogram of low contrast and divides it by the threshold value, applying THE to each of the resulting short histograms. By transforming the intensity histogram into a normal distribution, it determines the probability density function (PDF). From there, the CDF of each individual sub-histogram may be calculated. The CDF for both small sub-histograms is calculated ahead of time, and this is used to build the transformation function. The new,

improved image is obtained by mapping each intensity from the low-contrast original to the higher-quality intensity.

The conventional histogram-based enhancement methods are complicated and time-consuming to calculate, and the primary strategies have issues with over-enhancing. In a variant of BBHE called Bi-Histogram Equalization with a Plateau Limit (BPLHE) [37], the input histogram is split into two smaller histograms with respect to the calculated mean value. Next, the limit of the plateau is used to determine where to split these two little histograms. The value at the plateau is the geometric mean of the sub histograms multiplied by the geometric mean of THE. By transforming the intensity histogram into a normal distribution, it determines the probability density function (PDF). From there, the CDF of each individual sub-histogram may be calculated. The CDF for both small sub-histograms is calculated in advance, and this information is used to generate the transformation function that maps each intensity in the low contrast image to the new boosted intensity.

An alternative to traditional HE methods that avoids over-enhancing and saturation is fast image contrast enhancement based on weighted threshold histogram equalisation (FWTHE) [38]. Specifically, it alters the normal PDF into the threshold PDF with weighting. Through the use of the tailored power-law function, the original PDF is scaled between the upper and lower bounds. A fresh CDF derived from the PDF after being thresholded is used to calculate the enhanced image.

Over-amplification in the case of THE is most commonly caused by spikes, and Poddar et al. [39] presented a non-parametric histogram equalisation solution that first changes the histogram to remove spikes. Changing the histogram requires a number of operations, such as weighting, smoothing, and clipping with a threshold value. The original image is then normalised by creating a new transformation function based on an already-obtained, more recent histogram. At last, an adaptive Power-law gamma alteration is applied to the image.

After extracting only the values of the histogram that are six pixels apart, as proposed by Rao et al. [40], the low contrast picture histogram is then transformed [29] into four equally divided tiny histograms based on the preceding histogram's central value, thus solving the problem of spikes. Finally, the average of these four smaller sub-histograms is used to derive the plateau value for these mini-histograms, and clipped them based on this value. Then, a bilateral filter is utilized to the equalised histograms to generate the final, high-entropy enhanced image after applying THE separately to these clipped

histograms, which includes calculating the probability density function (PDF) [41, 42] and cumulative distribution function (CDF).

Wadud et al. [42] proposed a new dynamic histogram equalisation (DHE) method to control the stretching of intensity levels to achieve sufficient enhancement and to mitigate the over enhancement caused by the higher frequency portion of the unenhanced image histogram being prioritised over the lower frequency portion. DHE divides the entire histogram into n smaller histograms, each of which is then mapped with the transformation function until the smaller histograms are no longer dominated. Then, similar to THE, a transformation mapping function is produced for each little histogram, resulting in a unique final image. Mean brightness from DHE cannot be maintained at an adequate level.

Brightness preserving dynamic histogram equalisation (BPDHE) was first introduced by Ibrahim et al. [43] and consists of several stages. The histogram is first blurred using a Gaussian blur with parameters (1*9) and (sigma, 1.0762). Using local maxima as a dividing line, the smoothed histogram is subdivided into multiple smaller histograms. The next step is to apply a spanning function tailored to the amount of grey levels present in each sub-histogram to each individual histogram. The last step is to apply THE's mapping function to each individual mini histogram.

D. Sheet et al. [44] proposed brightness-preserving dynamic fuzzy histogram equalisation to deal with the issue of unwanted noise amplification and enhancement (BPDFHE). Starting with the input image, the fuzzy histogram is built by approximating the image's grey level with a fuzzy number, thus creating a smoothed histogram free of spikes due to similar grey levels. To rift the input histogram into numerous small histograms, the local maxima are computed in a manner analogous to that of DHE. Two recurrent local maxima form a valley that serves as a separating line. Finally, the enhancement is implemented via a spanning function using the equalisation mapping function.

The problems mentioned above can be tackled with the use of a novel adaptive histogram equalisation (AHE) technique, as proposed by Zimmerman et al. [45]. The AHE method uses the CDF of the block histogram to derive a transformation function that is then used to apply THE to the image by creating non-overlapping rectangular portions. The final AHE image is formed by combining the enhanced regions using a bi-linear interpolation method. In general, AHE has the potential to amplify ambient noise [46].

To improve upon the conventional CLAHE method, Siddiqi et al. [47] applied two local histogram equalisers with different distributions in series. Initial input into CLAHE is a low contrast CT scan with a uniform distribution, and the resulting image is sent back into CLAHE with a Rayleigh distribution.

With the use of the tried-and-true contrast limiting histogram equalisation technique, Saleh et al. [48] improved the green channel of a low contrast retinal image (TCLAHE). Instead of applying THE to the entire image, it is separated into tiny, non-overlapping windows. To stop the creation of induced borders, bilinear interpolation is used to mix the neighbouring blocks. Blocks were 88 pixels in size, while histograms had 128 bins. The naturalness of photographs was improved with the use of a logarithmic law-based histogram correction approach, as proposed by Bhandari et al. [49]. Before equalising the histogram to get the mapping function, the histogram was modified by addition and the logarithmic rule. Discrete cosine transformation was used to improve the local data (DCT).

By using an exposure-based contrast limited bi-histogram equalisation (EBCHE) procedure, Subramani et al. [50] enhanced the aesthetic quality of medical pictures. To begin, the exposure value is used to classify the entering image's histogram. Then, a new dynamic range is applied after clipping. The histogram is clipped to prevent over-enhancement while still yielding a somewhat improved medical image.

A genetic algorithm, histogram sub-division, and a revised probability density function are the three main components of a recently proposed method for increasing the clarity of medical imaging offered by Kumar et al. [52]. (PDF). This method has the highest visual quality of any enhancement technique, but it is also the most computationally intensive because it relies on finding appropriate settings.

2.1.2. Gamma-Based Approaches Review

Adaptive gamma correction with weighted distribution was made possible by Huang et al [53] unique hybrid enhancement methodology, which blends THE and gamma correction techniques (AGGCWD). Before calculating the weighted PDF, the regular PDF is multiplied by the adjusted value. The input image is then subjected to gamma correction, with the gamma value being produced by extrapolating the cumulative distribution function (CDF) from the previously determined probability density function (PDF).

Zhou et al. [54] devised a novel two-stage method for improving colour retinal images.

After converting the image to the HSV model and gamma correcting the luminance channel, the picture is brightened (V). To prevent colour shifts, the gain matrix is calculated by splitting the V channel before and after gamma correction. The red, green, and blue channels are multiplied by this matrix to ensure that they are all improved by the same amount. After the exposure has been corrected, the image is transformed to LAB, and contrast is increased using the TCLAHE method.

To make up for image information loss without sacrificing naturalness, Gupta et al. [55] proposed a quantile-based fundus image contrast augmentation strategy. There are two unique optimization approaches that make up the entire method. The V channel of the input image is first enhanced by AGGCWD, and then the gain matrix is calculated by dividing the improved V channel by the original V channel. To preserve colour accuracy, the resulting gain matrix is multiplied independently by each of the RGB channels. To further boost the contrast, a quantile-based histogram equalisation method is applied.

To improve the quality of old CT scans, Ameen et al. [56] improved a histogram-based contrast enhancement method. To begin, we applied our proprietary normalised gamma correction (NGC) technique to damaged CT images in an effort to boost their contrast. The NGC function performs gamma correction and then normalises the value to a range from 0 to 1. It used traditional TCLAHE to improve local details, which involves dividing the image into tiny blocks, clipping the part of the block histogram that is above the threshold, and then rearranging the clipped pixels.

Subermani et al. [116] created a histogram equalization-based weighted multi-exposure image contrast enhancement technique. Separation between the input image's low- and high-exposure regions is achieved with this technique. Sub-image exposure data is utilised to cut the input histogram into sub-histograms, where excessive amplification is limited. Only then is histogram equalisation used. Each sub-histogram must then be integrated and equalised to maintain the original image's natural appearance and fine features. As an added bonus, the dual gamma correction enhances the contrast in low-light regions. Based on the objective function, which can be either discrete entropy or mean square error, a metaheuristic stud krill herd optimization algorithm is performed. When it comes to improving fundus images with varying levels of illumination and contrast, V. Sathananthavathi et al. [117] developed a new approach using particle swarm optimization (PSO).

As part of the proposed method for HSV colour space, contrast and gamma correction

are applied to the LAB colour space. By maximising the contrast, the PSO algorithm aids in the augmentation procedure..

2.1.3. Wavelet-Based Approaches Review

Using singular value decomposition (SVD) and discrete wavelet transforms, Demirel et al. [57, 58] came up with a new method for improving contrast (DWT). At first, the standard HE method is used to boost the contrast of a low-quality input image. The low- and high-frequency elements of the input and enhanced images are separated into four frequency bands using discrete wavelet transform (DWT). After that, the SVD method is used to decompose the lower frequency sub-bands of both images, and then the correlation coefficient is computed by employing the singular matrices so obtained. And last, a new, lower frequency sub-band is generated using the correlation coefficient, leading to an enhanced final image. Mid-tone photographs cannot benefit from this method's increased contrast. Therefore, the majority of the input picture's mid-intensity details are preserved.

To solve this problem, atta et al. [59] introduced a novel correction factor for computing the singular matrix, which helps boost low-frequency details in the input image. The unaltered and HE-enhanced images' weighted sum singular matrices serve as the basis for the new correction factor. While this method does boost contrast generally, it leads to over-enhancement, which in turn causes an error in the maximum brightness.

For the first time, Sahnoun et al. [60] combined wavelet and histogram transformations into a single method. The process is divided into two phases, the first of which involves employing the atta approach to adjust approximation components at lower frequencies. The second step involves further processing of the enhanced lower frequency sub-band by modifying the PDF of the improved image and then creating a CDF from the updated PDF. The image's histogram is then stretched with the use of this CDF as a correction factor. With this method, the average brightness is preserved even as the signal-to-noise ratio is kept low.

The system for MRIs was introduced by Sahnoun et al. [61], who proposed a method centred on two contrast enhancement approaches. At first, it improved the images in the low-frequency sub-bands by employing SVD-based approaches. After the DWT low-frequency sub-band image was created, the globally adaptive gamma correction (GAGC-DWT) method was utilised to further boost contrast.

Previously unexplored methods for brightening low-light photographs were developed

by Kallel et al. [62]. It starts by employing the traditional DWT approach to break down the input and HE image into different frequency components, and then it amplifies the lower frequency components by adding a new correction factor to the singular matrix of SVD. Using a combination of singular and orthogonal matrices, we are able to obtain the new correction factor. The resulting image is then enhanced independently using a refined gamma transformation algorithm based on whether it was determined to be of low or moderate contrast during the CT scan.

In order to stretch the intensities of approximation sub-bands, Koh et al. [63] devised a method for decomposing an input image into approximation components like low-low (LL) and detailed components like low-high (LH), high-low (HL), and high-high (HH) (LL). Inverse discrete wavelet transform (DWT) is used to generate an output picture, which is then further enhanced using the adaptive gamma correction with weighted distribution (AGGCWD) method.

Li et al. [64] were the first to develop a groundbreaking technique for improving CT scans. The first step of the wavelet method is to break down the input and HE-processed images into their individual frequency components. After that, a passive blur filter and a median filter were applied to the image to enhance the high frequency details. For both the unprocessed and HE-enhanced versions of the image, it determined an average of the low-frequency components. It improves the spatial representation of the lower frequency components by first applying a new correction factor to the singular matrix of the SVD.

For better fundamental features, brightness preservation, and contrast in clinical photographs, Kumar et al. [51] proposed an enhanced triple clipped histogram system based on the DWT (TCHE-DWT) and easy fusion methodology. The method's superior effectiveness comes at the expense of increased computational complexity and time, however, when compared to histogram-based approaches.

2.1.4. Retinex-Based Approaches Review

Improved retinex-based non-contrast CT image enhancement was proposed by Ameen et al. [72]. By bringing together the deformed picture with the commonly utilised gaussian surround function (GSF) [38], and then subtracting the convolved image from the original, this method improves the quality of the GSF. Specifically, it took advantage of GSF's tuning parameter, which may be used to alter an image's luminance and chrominance. To better control maximum brightness at larger parameter values, it

used a different, modified sigmoid gaussian surround function.

Through the use of a retinex-based enhancement strategy, V'azquez et al. [73] were able to improve the Artery/Vein classification. After the original illumination was removed, the reflectance of the image was calculated using the single-scale retinex (SSR) model. Gaussian convolution of the image yields light. The Multiscale Retinex (MSR), which is just a weighted sum of the outputs of the several SSRs, is computed to get the final enhanced image.

The segmentation of retinal vessels was provided with an augmentation method by Memari et al. [74]. The method begins by removing noise from the retinal image by isolating the green channel from the full red, green, and blue (RGB) spectrum. Finally, the TCLAHE method is applied to highlight the contrast between the vessels and their environment. Morphological opening is then used to further minimise the noise introduced by TCLAHE. Finally, a retinex method based on bilateral filters is proposed to deal with the uneven lighting. This technique computes the reflectance image by comparing the logarithms of the input picture to the picture produced after applying a bilateral filter on the TCLAHE picture.

Retinex-based luminance adaptation (RBLA) [17], proposed by Fu et al. [75], is a method for enhancing images' perceived contrast. Through the application of the luminance just noticeable difference (JND), the method calculated an illumination weakening factor that was then employed in MSR to enhance finer details. Adaptive gamma correction combined with the weighted allocation was finally used to improve contrast. While this technique does well for dimly lit photographs, it does not function as well when trying to highlight the image's local vital information. The dynamic range reduction and tone reproduction properties [17] of approaches based on Retinex are useful for improving contrast everywhere over the world.

Correcting the gamma error in picture enhancement is the focus of a novel approach proposed by Bhadria et al. [118], which makes use of Gaussian and guided filtering techniques (GCRIE). At first, multiscale Gaussian sifting is used to capture the irregular components of the lighting, and then guided filtering is used to refine these components. Reflectance is determined using a nonlinear logarithm function and the visual contrast measure.

Wang et al. [119] suggest a method for improving colour images with low lighting by combining the Gabor filter and the Retinex theory. The approach first extracts the luminance I component from the original image in the HSI colour space, and then uses

MSRCR (the Retinex algorithm for colour restoration) to improve it. However, SSR (Single Scale Retinex Algorithm) in the RGB colour space based on the Gabor filter is used to improve the original image's edge and texture details. The final improved image is obtained by combining and weighting the two source photos.

2.1.5. Morphology-Based Approaches Review

To better the CT images, Bai et al. [76] suggested using a modified top-hat transform. Top-hat transform, which uses the same shape structuring elements but with increasing sizes, is initially used to remove bright and light multi-scale regions. The final bright and dark parts of the image are then derived using multi-scale information between the nearest scales. The final step in obtaining an improved image involves adjusting the contrast between them. This method amplifies additional noise in a CT picture and does not improve all local details.

To increase the differentiation between blood vessels and the backdrop, Khan et al. [77] presented a novel contrast enhancement method. To begin, the colour fundus image's green channel is removed to increase vascular contrast. After that, the extracted green channel is locally improved using TCLAHE. To avoid noise from being amplified, the tile histogram is clipped with a clip limit between 0 and 0.01. In the end, a two-stage modified top-hat transform is created to further boost the local vessel intensities: Output TCLAHE picture closes, then opens with operator.

2.1.6. Transferred-Based Approaches Review

Feng et al. [79] suggested a new transfer-based strategy for improving retinal images. The process has two primary phases. The initial process involves removing the green channel from the colour image (RGB retinal image) and creating a grey scale image. After a first augmentation using histogram stretching, the greyscale image is further improved using the contourlet transform. The incoming image is Laplacian-pyramid-divided into a number of frequency sub-bands in the contourlet transform, with each of these sub-bands being realised independently by a number of directional filter banks. To get a better fundus image, this technique employs three Laplacian Pyramids and eight direction filters.

Following the low contrast input image being treated by the NSCT to convert the image into low-frequency coefficients and various high-frequency coefficients, Liu et al. [80] suggested a non-sampled contourlet transform (NSCT) with unsharp masking [49]. The

high-frequency coefficients are then denoised using an adaptive threshold method. To increase the contrast, the coefficients of the low-frequency components are stretched. To finish off the process, unsharp masking is used to the finalised image to bring out the edges and details. This inverse conversion is accomplished to obtain the improved image.

NSCT with TCLAHE was proposed by Liu et al. [81]. To begin, the input raw image is processed with CLAHE to increase the global contrast. Second, the NSCT is using the CLAHE enhanced image to separate the low-frequency component from the various high-frequency components of the original enhanced image. To improve the low-frequency part, a linear contrast stretch is performed, while the adaptive threshold is employed to reduce the high-frequency noise. Finally, the unsharp masking is used to sharpen the edges and the inverse NSCT transform is performed to produce the enhanced image from the coefficients of low-frequency and high-frequency sections.

Goyal et al. [120] introduced an NSST-based nonlocal means (NLM) technique for picture denoising, which is computationally simple (non-subsampled shearlet transform). At first, NSST is used to break down the original picture into different, progressively finer layers. Low-frequency coefficients (coarse layer) and high-frequency coefficients (four sets) are generated at two distinct stages of decomposition in NSST (fine layers). Therefore, the NLM algorithm is applied to the lower levels (which are more refined) but not the higher layers. In order to keep the image's silhouette sharp while simultaneously lowering noise in the finer layers, the NL-Means algorithm does the following.

2.1.7. Filter-Based Approaches Review

Image contrast was improved with the help of a novel approach proposed by Polesal et al. [82]. In this method, an adaptive filter was utilised instead of the standard practise of using a fixed Laplacian filter for unsharp masking. As a result of the adaptive filter's fine-tuning, contrast enhancement works very well in the detail regions while having less effect on the smooth ones. In order to denoise and improve the contrast of damaged fundus pictures, Sonali et al. [83] presented a hybrid model. The colour fundus images are first segmented into R, G, and B channels so that various denoising filters can be applied to each one separately. These filters include the median, wiener, mean, and gaussian. Once it was done, the regular CLAHE method was used for each individual channel. The enhanced colour fundus image is created by combining the red, green, and

blue channels. Several different types of denoising filters, including the median, wiener, mean, and gaussian filter, have been employed in this research.

Fundus images are notoriously difficult to work with due to uneven and inadequate lighting. However, Saha et al. [84] presented an innovative approach to address these issues. The fundus image's luminance is best described by the value channel after the input colour image has been transformed to an HSV channel whose H channel describes the hue, S channel the saturation, and V channel the value. The integral luminance (V) image is then used to determine the background image by averaging its intensity over a sizable window. Pixel-by-pixel, a threshold value of 0.0015 is used to compare the average image to the brightness image. Using the difference image as a starting point, we compute the background by blurring it with a Gaussian distribution. By subtracting the source picture from the background, we are left with the corrected, lit version of the image. After deducting the source image from the backdrop, the lit rectified image is revealed.

Gray-scale S-curve transformation (S-curve) for medical pictures was first used by Gandhamal et al. [85]. The translation from one pixel to the next results in a curve like a sigmoid. In this case, we can improve the image's contrast by widening the gap between its darkest and brightest pixels. This method prevents artefacts from appearing in the final medical image while also reinforcing the image's margins and boosting the image's contrast. A unique heat conduction matrix-based image enhancement (HCMBE) method was introduced for colour images by Ferzan et al. [86]. The HSI model's produced intensity channel pixels are modified by the heat conduction matrix's elements (HCM). However, the final image produced using this method may have inaccurate colours.

2.1.8. Neural Network-Based Approaches Review

Convolutional neural networks (CNNs) are a relatively new type of neural network that has proven to be quite useful for improving images. In order to de-noise and super-resolve the CT image, Chia et al. [87] created a uniform deep convolutional neural network (DCNN) architecture. There are two parts to the framework: To begin, it is proposed to estimate the background noise using a dense-inception network. Second, for noise-free high-resolution image reconstruction, a modified residual-dense network with joint loss is proposed. Reconstructing image edges and details is much easier using this method, however there are still limitations due to things like computing cost,

network architecture, input manner, and the need to generate training data. To solve this problem, Lyu et al. [121] present a novel network that combines the nonsubsampled shearlet transform (NSST) with a wide convolutional neural network. The method employed a unified model that could handle varying degrees of noise as well as additive gaussian noise with spatial correlations. By combining the two networks, denoising performance can be enhanced without incurring excessive computational expense. More texture is obtained and gridding is avoided thanks to NSST and inverse NSST.
Raj et al. [122] developed a residual dense connection based UNet structure to improve retinal fundus images (RDC-UNet). This paper proposes techniques to generate the five most prevalent distortions. Boosting the quality of an image is a global and local task, and the UNet captures both types of information in an efficient manner by making use of residual dense connections. Synthetically degraded fundus images were used to train the RDC-UNet, which was then applied to each of the five distortions individually..

2.2. Research Gaps Identified

This section highlights the major research gaps linked with image enhancement approaches based on a comprehensive review of several research papers.

1. First, while histogram-based image enhancement approaches do a better job of bringing out contrast, they also introduce noise, over-brightness, a washed-out appearance, and the loss of small and crucial detail regions.
2. At any given clip limit, the local enhancement in the enhanced images produced by the CLAHE approach is always insufficient. It provides moderate local enhancement at low clip limits but severe enhancement and colour distortion when the limit is increased.
3. Most modern medical image enhancement procedures are very involved since they determine the CLAHE method's clip limit based on an experimental investigation of a wide variety of clinical images.
4. When used to medical photos, the current crop of gamma correction-based luminous enhancement methods can distort areas of high grey value because they use improper gamma value settings for significant pixel intensities. Furthermore, the mean brightness of the original image is degraded, and important details of the medical image are completely obscured, by using these methods.
5. Directional selectivity in fixed directions is poor in wavelet transform methods like DT-CWT and DWT. Thus, it yields subpar denoising results and is inadequate

for describing the finer points of the medical picture.

6. Standard multiscale retinex (MSR) provides an artificial image in which the overall brightness is lost and increases noise concentrated inside a large dark patch. As a result, it is not useful for medical pictures with complex backdrops, lots of greyscale, or lots of dark areas.
7. In medical photos, noise, high-frequency image intensities, and a dark background make it difficult for the Standard Top hat transform approach to improve contrast.
8. Present image enhancing methods fare well in some performance matrices but poorly in others. Therefore, they are not universally applicable to rating scales.
9. Nine out of ten image enhancement techniques distort the edges and pump up the noise even as they boost contrast.

2.3. Objectives of the Proposed Work

The following research objectives are formed based on the above-mentioned gaps for medical image enhancement.

1. Identify and analyze existing state-of-art image enhancement techniques.
2. To develop a new integrated image enhancement method that can deal with both noise removal and poor contrast problem of Non-contrast CT scan.
3. To develop and implement a novel contrast enhancement method for the poor-quality histopathology
4. To propose a new image enhancement technique to provide both nonuniform illumination correction and contrast enhancement of low-grade retinal fundus images.

2.4. Research Questions

The following research questions are formulated based on the above-mentioned gaps for medical image enhancement.

1. How can the image quality of non-contrast CT scan images be improved to address noise removal and poor contrast issues?
2. What is an efficient and effective method for enhancing contrast in poor-quality histopathology images without introducing noise or over-brightness?
3. How can low-grade retinal fundus images be enhanced to address nonuniform illumination and improve overall contrast without distorting important eye structures or increasing noise?

2.5. Organization of the Thesis

In this first chapter, we will get an introduction to the field of medical imaging and its history. The visual artefacts unique to each type of medical image modality are also included. The thesis also lays out why the study is necessary and what its goals will be. A literature review of picture enhancing techniques is offered in Chapter 2. Histogram-based methods, retinex-based methods, morphological approaches, gamma-based methods, wavelet-based methods, contourlet transfer-based methods, filter-based methods, and deep learning are all examples of such techniques.

Chapter 3 presents a fresh strategy for enhancing the noise and contrast of CT images in the wavelet domain, one that relies on optimal morphological transforms. First, we use the optimised morphology transform approach, which finds the best possible value for the parameter in the base morphology transformation equation, to transform the low-quality CT picture. Particle swarm optimization (PSO) is used to find the best possible setting for the parameter. The proposed method then used the discrete wavelet transform (DWT) to split the input and processed CT image into high- and low-frequency bands. A correction factor is applied using SVD to alter the low-frequency bands. A denoising technique based on edge maps (EM) is applied on the HH of the input image. The result is improved CT scans with reshaped low- and high-frequency bands. The inverse discrete wavelet transform (IDWT) is then used to process the adjusted sub-bands and the remaining untreated higher frequency sub-bands, resulting in an improved CT image. The suggested scheme is evaluated both qualitatively and quantitatively through tests on CT images taken from a publically available catalogue.

In Chapter 4, we see how dual tree complex wavelet transform (DT-CWT) and flexible morphology can be used to improve the quality of non-contrast CT scans. First, a CT image is fed into the DT-CWT system, dividing it into low- and high-frequency sub-bands. When applied to high pass sub-bands, denoising utilising the wavelet-related shearlet transform approach improves high-frequency sub-images. The low pass sub-bands are enhanced via DCT-based local augmentation and an adaptive morphology top hat transform. Improved CT images can be generated by recombining the increased low and high-frequency semi-components using inverse DT-CWT. A large set of CT images from a publically available database is used for experiments and validations to qualitatively and quantitatively evaluate the effectiveness of the proposed method.

To improve the contrast of colour histopathology images, chapter 5 explains a new method based on retinex theory and local contrast modification. After processing the V

channel in the HSV colour space, a multiscale retinex with adaptive weighting (MSRAW) is proposed, which combines the outputs of several single scale retinexes (SSRs) in such a way that the weight corresponding to each SSR scale is determined adaptively from the value channel image, depending on the strengths and weaknesses of the various SSR outputs. Next, by merging the two CLAHE outputs corresponding to the large and lower clip limits, the novel weighted contrast limited adaptive histogram equalisation (WCLAHE) technique improves local contrast in the luminosity channel of the L*a*b* colour space, thereby increasing local histopathological details. We compare the offered approach to standard practises, both aesthetically and numerically. The suggested method outdoes all other standard methodologies and produces higher-quality histopathology imageries, which is notably valuable for analysis, as evidenced by visual and quantitative findings on a variety of test images.
Enhancing the brightness and contrast of colour retinal fundus pictures is covered in detail in Chapter 6. A colour retinal fundus image is first converted to the HSV (Hue, Saturation, and Value) colour model, which isolates the luminance channel (V) from the other colour elements hue (H) and saturation (S). After that, a novel JND-based adaptive gamma correction algorithm is used on the luminosity channel (V) to enhance the brightness of fundus images. Later, a novel contrast enhancement method using multiple layers of contrast limited adaptive histogram equalization (CLAHE) is used to boost contrast in the luminance component of the L*a*b* colorspace. While maintaining the average brightness, maintaining an original appearance, and optimising entropy, these two methods significantly boost the total luminance and contrast in retinal images. The efficiency of the suggested approach is evaluated by extensive experimental analysis of a wide variety of fundus images.

2.6.Tool Used

MATLAB is used due to its following advantages:

Advantage: To put it simply, it is a programming language for doing numerical computations that is interpreted. One may quickly create images and visualise the results of numerical operations. Data analysis, method development, model building, and application development are all simplified with the help of MATLAB. When compared to spreadsheets and other conventional programming languages, it has the advantage of being an interpreted language, making it ideal for numerical operations.

You can get to a solution just as fast as with the language, tools, and built-in math function, and it's capable of conducting numerical computations and displaying correct results.

2.7.Performance Parameters

In medical imaging, image quality evaluation is inextricably linked to image analysis and detection of diseases. The development of objective evaluation measures for determining the diagnostic accuracy of medical images is crucial. The most often employed metrics for evaluating the accuracy of medical images are classified as Average Information Content (AIC), Contrast Improvement Index (CII), Peak Signal to Noise ratio (PSNR), Michelson Contrast (MC), Weber Contrast (WC), and Measures of enhancement (EME), Edge preservation Index (EPI), Universal Image Quality Index (UIQI)

2.7.1. Average Information Content or Entropy [22]

It is a metric that can be used to quantify the amount of information present in an enhanced picture. This term is donated as:

$$E = -\sum_{i=0}^{255} p_i \log_2(p_i) \tag{2.1}$$

Where p_i is the probability of a intensity value present in the enhanced picture and i denotes the whole set of intensity values.

2.7.2. Contrast improvement index

CII [23] is an objective indicator of image contrast enhancement that is denoted as:

$$CII = \frac{C_e}{C_i} \tag{2.2}$$

Where C_e and C_i are the enhanced and initial input image contrast values, respectively. *C* refers to contrast and is expressed as follows

$$C = \frac{max - min}{max + min} \tag{2.3}$$

Where max and min signify the maximum and minimum image intensity values, correspondingly, in a 3 × 3 non-overlapping regions. C is calculated in this manner for each non-overlapping window, and then the mean of all C values is calculated to obtain the final contrast value. A good CII score shows a substantial improvement in contrast

in an output image.

2.7.3. Peak signal to noise ratio (PSNR)

PSNR [23] is a measure used to assess the improved image's efficiency. It is the ratio of the signal's highest potential power to the power of the distorting noise. To begin, let's measure the Mean Squared Error (MSE) of the output result as follows:

$$MSE = \frac{\sum_{c=0}^{m-1}\sum_{v=0}^{n-1}|I_i(c,v) - I_e(c,v)|^2}{m * n} \tag{2.4}$$

Where m and n are the rows and columns of an image and PSNR is calculated as below:

$$PSNR = 20\log\frac{Max(I_e)}{\sqrt{MSE}} \tag{2.5}$$

2.7.4. Michelson contrast ratio

The Michelson contrast (MC) [23] ratio is described as follows:

$$MC = \frac{I_{high} - I_{low}}{I_{high} + I_{low}} \tag{2.6}$$

Where I_{high} and I_{low} denote to the picture's higher and lower intensity values in a 3 × 3 non-overlapping windows, respectively.

2.7.5. Weber contrast ratio

The Weber Contrast (WC) [50] ratio is denoted by the following:

$$WC = \frac{C_{high} - C_{low}}{C_{high}} \tag{2.7}$$

Where C_{high} and C_{low} represent the picture's higher and lower intensity values in a 3 × 3 non-overlapping windows, respectively.

2.7.6. Measure of enhancement

The enhancement measure (EME) [18] approximates the image's average contrast by splitting it into 3 × 3 nonoverlapping regions and calculating a factor dependent on the image's lower and higher gray values. The EME is measured in the following manner:

$$EME = 20\log\frac{I_{max}}{I_{min}} \tag{2.8}$$

Where I_{max} and I_{min} represents maximum and minimum of the picture within the small area.

2.7.7. Universal Image Quality Index (UIQI)

An evaluation of UIQI accounts for image distortion, loss of luminance, contrast distortion, and correlation [33]. As shown in equation [22], it can be calculated.

$$UIQI = \frac{4\sigma_{X,\bar{X}}\mu_X\mu_{\bar{X}}}{(\sigma_X^2 + \sigma_{\bar{X}}^2)(\mu_X^2 + \mu_{\bar{X}}^2)} \tag{2.9}$$

where $\sigma_{X,\bar{X}}$ denotes the covariance between X and $\bar{X}$. Additionally, μ_X^2 and $\mu_{\bar{X}}^2$ represent the mean values of X and $\bar{X}$, and σ_X^2 and $\sigma_{\bar{X}}^2$ represent the variances of X and X, respectively.

2.7.8. Edge Preservation Index (EPI)

EPI is a quality evaluation metric that is often used to determine the degree of edge retention after an image has been enhanced [23]. To avoid data loss, it is critical to enhance the picture while preserving the edges, particularly in medical image improvement. The best edge retention in the enhanced image occurs when EPI approaches 1. An EPI value greater than one indicates that the edges of the output image have been enhanced and strengthened, and can be expressed as follows:

$$EPI = \frac{\sum_{c=0}^{m-1}\sum_{v=0}^{n-1}|I_e(c,v+1) - I_e(c,v)|}{\sum_{c=0}^{m-1}\sum_{v=0}^{n-1}|I_i(c,v+1) - I_i(c,v)|} \tag{2.10}$$

where I_i is the input image, I_e is the enhanced image, and c and v denote the column and row counts in the image.

2.8.Summary

This section provides an overview of medical images as well as image formation and image abnormalities in CT, Histopathology, and Fundus images, such as low contrast, noise, blur, and distorted features. The current chapter also discusses the importance of the current work. The next chapter provides an introduction to image enhancement as well as a comprehensive review of existing enhancement methods in the literature.

CHAPTER 3

AN OPTIMIZED MORPHOLOGY TRANSFORM-BASED DIAGNOSTIC CT IMAGE ENHANCEMENT USING EDGE MAP

3.1. Introduction

Low-quality CT scans, or CT images with low contrast and high noise, might make it difficult to visually interpret affected areas. For better noise and contrast in CT images in the wavelet domain, a unique optimal morphological transform-based technique is proposed. First, an optimum morphology transform (OMT) is performed on the input CT picture using the optimal parameter in the underlying morphology transformation equation. Particle swarm optimization (PSO) is used to find the best possible value for this parameter. Then, Discrete Wavelet Transform (DWT) was used to decompose the input and transformed CT image into higher and lower sub-bands, as part of the suggested method. The correction factor is applied by SVD to the lower sub-bands, changing their frequencies. Denoising is performed using an edge map (EM)-based technique on the higher sub-band (HH) of the input image. By altering the lower and higher sub-band, CT pictures are improved. In the end, the inverse discrete wavelet transform (IDWT) is used to process the updated sub-bands and the remaining unprocessed higher frequency sub-bands, yielding an improved CT image. To qualitatively and quantitatively evaluate the efficacy of the suggested system, experiments and validations are undertaken on CT scans obtained from a publicly available database. The suggested method is shown to outperform state-of-the-art image enhancement techniques in terms of signal-to-noise ratio, discrete entropy, enhancement measurement, and contrast ratio, according to a large-scale quantitative analysis. The proposed method results in better quality CT scans, which is helpful for examining and diagnosing diseases.

While present and previously defined enhancement methods in chapter 2 are suitable for a wide range of application areas, the results are frequently undesirable for medical images due to numerous defects, noise augmentation, over enhancement, original mean brightness deterioration, and detail distortion. To address the drawbacks of the existing techniques, an effective method to improve the contrast and noise of a CT image while preserving its natural characteristics is proposed. The highlights of the proposed method are as follows:

- PSO has been defined in Section. 3.2 and is used in the proposed scheme for OMT-

based enhancement to increase the contrast of CT images while preserving their features.

- The method enhances CT images by splitting the original and transformed CT images from OMT into numerous sub-bands using DWT. It then enhances the LL sub-band using SVD by determining the suitable correction factor related to the OMT and applying it to the eigenvalues of the input and transformed images. The result is an improved CT image that preserves the mean brightness and fine features of the input.
- Using an EM-based approach, the proposed method denoised the high-frequency component obtained from DWT of the input CT image.

3.2.Methods Used in the Proposed Method

3.2.1. Particle Swarm Optimization (PSO)

PSO is a stochastic optimization method that takes its cues from the social behaviours of animals like birds and fish. PSO has fewer parameters and has very severe convergence scales [98] because it lacks a natural idea of selection. Compared to other optimization methods, such as genetic algorithms [100], ant colony optimization [101], and evolutionary algorithms [102], PSO excels in a number of ways. Also, a better solution can be found in less time. [103]. In this research, PSO is utilized as an optimization technique to determine the optimum rate of a specific parameter used in the image enhancement process, satisfying the objective function tailored for medical image enhancement.

The proposed medical image enhancement approach involves an optimal morphology transform (OMT) on the input CT picture, where the underlying morphology transformation equation depends on a parameter that requires optimization. PSO is employed to efficiently find the best value for this parameter, ensuring improved results for the subsequent steps of the image enhancement process.

Specifically, the PSO algorithm operates on a population of particles, where each particle represents a potential solution in the search space of the parameter for the OMT. The collective behavior of the particles is influenced by their individual best locations (local best) and the best global location explored by the swarm (global best). The PSO algorithm iteratively updates the velocity of each particle based on these best locations and its existing speed, which guides the particles towards promising regions in the

search space. During each iteration, the particles' positions are adjusted, and the OMT parameter values associated with these positions are evaluated based on a fitness function designed to optimize the medical image enhancement process. Through the iteration process, PSO efficiently explores the search space, progressively improving the value of the OMT parameter until convergence criteria are met. The combination of PSO with other image processing steps, such as Discrete Wavelet Transform (DWT) and denoising using an edge map (EM)-based technique, contributes to the overall enhancement of CT images, providing a valuable tool for medical professionals.

The typical PSO algorithm's stages for finding the optimum solution are as follows:

Step:1 Prepare the swarm arbitrarily in accordance with the solution search space, taking into account thecomputing cost or periods necessary to obtain the optimum contract in the event it happened. On D Dimensions, the particles in the search place have inconsistent locations and velocities. In PSO, the initial particle locations and velocities are either set to zero or given any value.

Step:2 For each particle in dimension D, a fitness function is defined.

Step:3 Allocate the extreme best location and analyse the existing best value to the maximum best value previously assigned.

Step:4 Discriminate between the particle's greatest accomplishment up to this point and the particle's best neighborhood.

Step:5 Enhance and rate the particle velocity to determine the existing best utilizing the equation stated before

$$v_i^{t+1} = w^t v_i^t + c_1 r_{1d}(\text{ pbest } t_i^t - X_i^t) + c_2 r_2 (gbest^t - X_i^t) \quad (3.1)$$

where X^t denotes the associated particle's location in the solution space, v^t denotes the particle's velocity

w^t denotes the velocity control coefficient, c_1 and c_2 denote the gain, r_1 and r_2 are simple random integers in the range [0,1], and $pbest$ is referred to as the local best place, while $gbest$ is referred to as the global best place among all of the particles.

Step:6 For the purpose of revising the particle location and rating the particle location in order to determine the existing best location

$$X_i^{t+1} = X_i^t + v_i^{t+1} \quad (3.2)$$

Step:7 If a criterion is fulfilled or converges (for example, usually good wellness or the largest number of cycles), then the circle is terminated.

3.2.2. Optimized Morphology Transform (OMT)

Mathematical morphology plays an important role in image processing [37,21], and it also corresponds to a specific division of mathematics. This method is comprised of several nonlinear filtering methods based on the subject's structural characteristics. In most cases, morphology operations require two inputs: the original image and its corresponding structuring component. The two main types of morphology operations are dilation and erosion. The procedures are then specified on the input image and a structuring element, indicated respectively by $I\ (x, y)$ and $B\ (s, t)$. Equations (3.3) and (3.4) define the fundamental morphological procedures' dilatation and erosion. Dilation amplifies the size of the image set while decreasing the extent of holes, which are regions of background pixels surrounded by foreground pixels. Conversely, erosion reduces the size of the image set while increasing the size of these holes in the image. As described in (3.5) and (3.6), the arrangement of dilation and erosion results in opening and closing procedures. The opening is erosion accompanied by dilation, which usually smooths the contours of an image. At the same time, the closing is dilation accompanied by erosion, which tends to fuse tiny cracks, remove minor holes, and fill small openings.

$$(I \oplus B) = \max_{s,t}\{I(x - s, y - t) + B(s, t)\} \tag{3.3}$$

$$(I \ominus B) = \max_{s,t}\{I(x + s, y + t) - B(s, t)\} \tag{3.4}$$

Where (x, y) and (s, t) are the coordinates of pixels in image I and structuring element B, respectively. Furthermore, there are two other operations related to dilation and erosion: opening and closing of the input $I\ (x, y)$ with $B\ (s, t)$, denoted by $I \circ B$ and $I \bullet B$ respectively.

$$I \circ B = (I \ominus B)B \tag{3.5}$$

$$I \cdot B = (I \oplus B) \ominus B \tag{3.6}$$

To extract the bright regions, the top-hat transformation is performed. It is produced by

deducting the opening image from the original one, which is provided in (3.7). The bottom-hat transformation is used to remove dark regions from images. It is produced by deducting the original input from the image's closing, as illustrated in (3.8). Contrast improvement is performed by of addition bright regions to the source image and removing dark ones as donated in (3.9)

$$I_T = I - I \circ B \tag{3.7}$$

$$I_B = I \cdot B - I \tag{3.8}$$

$$I_E = I + I_T - I_B \tag{3.9}$$

In this work, parameter β is introduced into the above morphology transformation equation and determines the degree of contrast enhancement applied to the output image, as shown in (3.10).

$$I_E = I + \beta(I_T - I_B) \tag{3.10}$$

The range of the parameter β should be between 0 and 3, and exceeding that value results in over-enhancement of CT images. The proposed method applies the modified morphological transformation described above to the input low contrast CT image in order to rise the contrast while maintaining the details of the input image. The entropy of an image, which indicates the amount of detail and contrast in it, is given by equations (3.11) and (3.12).

$$\text{Entropy } (E) = -\sum_{i=0}^{255} p_i \log_2(p_i) \tag{3.11}$$

Where p_i is the probability of an intensity value present in the enhanced picture and i denotes the whole set of intensity values.

$$\text{Contrast}(C) = \frac{max - min}{max + min} \tag{3.12}$$

Where max and min signify the maximum and minimum image intensity values, correspondingly, in a 3 × 3 non-overlapping regions. C is calculated in this manner for each non-overlapping window, and then the mean of all C values is calculated to obtain the final contrast value.

PSO is used in the proposed method to obtain an improved image I_E provided in (3.10) for

the value of β that yields the maximum objective function corresponding to a disc-shaped structuring element with a radius 5. The proposed fitness function (J) is expressed as a function of the Entropy (E) and Contrast (C) value in the output CT enhanced image.

$$J = \frac{(E+C)}{2} \tag{3.1}$$

Maximizing the fitness function given by equation yields the optimally improved image. (3.13). In order to determine this optimal value, the suggested technique makes use of PSO to compute. To begin, the solution space for the input low contrast CT picture is seeded with a random 'P' number of particles. Therefore, the value of is different for every single X particle. The CT image's average entropy and contrast are also calculated using formulas. Each pixel's values for (3.11), (3.12), and (3.13), respectively, are maximum. The goal of the average maximisation method is to improve the contrast of a CT picture without losing any of the image's current details or edges. Pbest ranks a particle's location in relation to both itself and its neighbours in order to determine the particle's current best exploiting location. This cognitive component keeps track of a particle's information or status solely based on its own experience and ranks a particle's location in order to determine the particle's existing best exploiting location. After a particle has communicated with its neighbour and established its optimal location using equation (3.1), the next step is to establish its optimal location using equation (3.2). In this context, each individual particle attributes and, where necessary, disregarded its own prior experience. Subsequently, they update their memory based on the combined efforts of all particles, and the improved morphological transformation calculates the unique velocity of each particle using equation (3.10). Lastly, this process is iterated for each pixel value according to the fitness function defined in equation (3.13). The PSO's fitness function must be used to find the locations of Pbest and gbest. The improved particle pictures are calculated for each value of. Its ideal setting improves contrast in the input CT image without blurring the finer details or sharper edges.

3.2.3. Discrete Wavelet Transform (DWT)

DWT decomposes the input signal into several sub bands. As a result, low

frequency sub bands have a lower temporal resolution but a higher frequency resolution than high-frequency sub bands. The initial level DWT components may be calculated using the preceding level DWT components, as defined in equations. (3.14) and (3.15).

$$W_L(u,v) = \sum_m W_L(m, v-1)h(m-2u) \tag{3.14}$$

$$W_H(u,v) = \sum_m W_L(m, v-1)g(m-2u) \tag{3.15}$$

Where $W_L(u, v)$ denotes the u^{th} scaling coefficient and $W_H(u, v)$ denotes the u^{th} wavelet coefficient at the v^{th} stage, respectively. Then, $g(u)$ and $h(u)$ denote wavelet and scaling functions, respectively. To recreate the original signal, the DWT coefficients are up-sampled and processed through a novel set of high-pass and low-pass filters according to equation (3.16).

$$W_L(u,v) = \sum_k W_L(k, v+1)h'(u-2k) + \sum_l W_H(l, v+1)g'(u-2l)\ W_L(u,v) \tag{3.16}$$

where $h'(u)$ and $g'(u)$ are the mother wavelet's low-pass and high-pass synthetic filters, respectively.

3.2.4. Singular Value Decomposition (SVD)

In the SVD method [57], the real matrix M is broken into the product of three matrices using equation(3.17).

$$M = UDV^T \tag{3.17}$$

Where U and V are orthogonal matrices and T is the transpose operator. D is recognized as the matrix of a diagonal value containing the intensity value of the input image, allowing for the use of the SVD method for image contrast enhancement. The improvement factor for a given image is the ratio between the largest diagonal value of the generated standardized matrix with a variance of one, a zero mean, and the largest diagonal value of the actual matrix, as calculated using equation (3.18).

$$\xi = \frac{maxD_{N(u=0,var=1)}}{\max(D)} \tag{3.18}$$

Where $D_{N(u=0,var=1)}$ is the diagonal value matrix for the synthetic intensity matrix. Using equation. (3.19), these components may be used to create an equalized image $Mequalized$.

$$M_{\text{equalized}} = U(\xi D)V^T \tag{3.19}$$

3.2.5. Edge Map (EM)

Edge Detection is a term that refers to the process of determining the borders between several pieces in an image I . It functions by finding boundaries at the pixel level within a local neighborhood. Numerous edge detection operators, including Sobel, Robert, Prewitt, and Canny, have been are present [107]. In the proposed study, the Sobel operator is used to detect edges. In contrast to computationally expensive edge detection methods, the Sobel operator offers a more effective implementation on the hardware side. Typically, the Sobel edge detector is used to create two-dimensional edge maps. The row and column masks for the Sobel detector, Mrs, Mcs, and Gr, Gc, are as follows:

$$M_{rs} = \begin{pmatrix} -1 & 0 & 1 \\ -2 & 0 & 2 \\ -1 & 0 & 1 \end{pmatrix} \tag{3.20}$$

$$M_{cs} = \begin{pmatrix} 1 & 2 & 1 \\ 0 & 0 & 0 \\ -1 & -2 & 1 \end{pmatrix} \tag{3.21}$$

$$G_r = M_{rs} * I \tag{3.22}$$

$$G_c = M_{cs} * I \tag{3.23}$$

Where I is the input image, $*$ is the convolution operator. G_r and G_c are two images that include horizontal and vertical derivative estimates at each position, and θ is a one-dimensional convolution function. For each point, the gradient G, also known as the EM, is represented as:

$$G = G_r^2 + G_c^2 \tag{3.24}$$

The direction of the gradient θ is specified by

$$\theta = \arctan\left(\frac{G_T}{G_c}\right) \tag{3.25}$$

3.3.Proposed Method of Enhancing CT Images Using an Optimized Morphology Transform and Edge Map

The proposed approach [123] is composed of many sections that produce the enhanced CT image. These sections are as follows. To begin, I_T is computed using the OMT technique on the low-contrast input CT image I. DWT is used to isolate the huge information included in the LL sub band from edge information contained to the other sub-band images (i.e., LH, HL and HH) and preserves the edge data by operating enhancement in the lower region as shown in Fig. 3.1. DWT decomposes both images into LL, LH, HL, and HH for I and LL_T, LH_T, HL_T, and HH_T for I_T. LL and LL_T sub-bands are respectively the approximation components of the input and improved image. LH, HL, HH sub-bands and LH_T, HL_T, HH_T signify the detailed components of the input and improved image respectively.

To begin, the SVD technique is applied to the lower frequency components of the LL and LLT sub-bands to generate ULL, DLL, VLL, and $ULLT$, $DLLT$, $VLLT$ respectively. The standard deviation of DLL, obtained from the LL sub-band, and the standard deviation of $DLLT$, decomposed from the LLT sub-band is calculated to compute the correction factor ε and then modified diagonal matrix D_M is computed as shown as below.

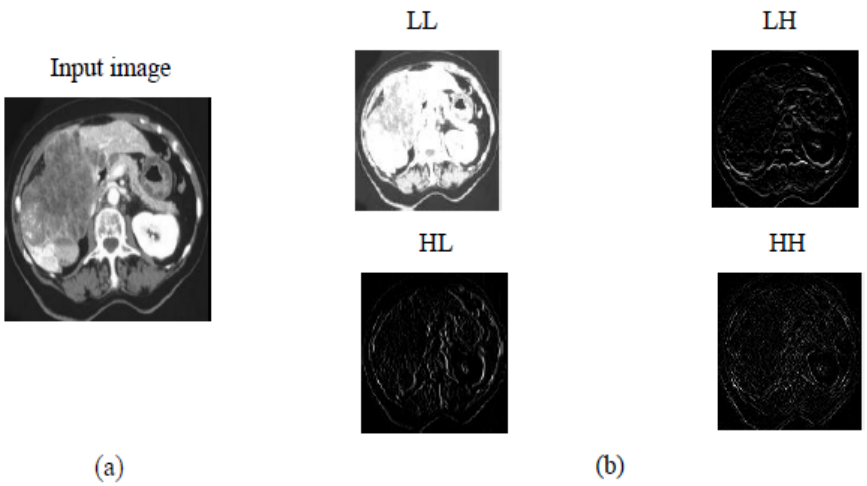

Figure: 3.1. (a) The original input image, (b) Sub-band outputs LL, LH, HL, and HH.

$$\varepsilon = \left(\frac{\text{std}(D_{LL}^{T})}{\text{std}(\text{D}_{LL})}\right) \tag{3.26}$$

$$\text{D}_{M} = \alpha * (\varepsilon) * \text{D}_{LL} + (1 - \alpha) * \left(\frac{1}{\varepsilon}\right) * D_{LL}^{T} \tag{3.27}$$

In the above equation, the parameter α is an experimentally adaptable parameter that allows for more freedom in adjusting the contrast of input images. The value of α may range between 0.05 and 0.95, depending on the image that was used as input.
The modified approximation coefficient is computed in two ways and donated as LL_{M1} and LL_{M2}

$$LL_{M1} = U_{LL}\text{D}_{M}V_{LL} \tag{3.28}$$

$$LL_{M2} = U_{LL}^{T}\text{D}_{M}(V_{LL}^{T})^{T} \tag{3.29}$$

Final modified approximation coefficient LL_{M} is derived in equation (3.30) by taking the fusion of above derived modified approximation coefficients

$$LL_{M} = \frac{LL_{M1} + LL_{M2}}{2} \tag{3.30}$$

The HH sub-band is the most densely packed of the four sub-bands, containing the majority of the coefficients corresponding to the noise contained in the input CT image. Since noise is often classified as having a high-frequency component HH, denoising is solely applied to this component. In addition to noise, the HH sub-band includes coefficients that match the diagonal edges that are present in the original image. Denoising on HH may result in an unwanted loss of edge detail. Because of this, denoising is limited to the modified HH sub-band, which is produced by eliminating the HH sub-band coefficients that correspond to edges from the original HH sub-band. For the first step, the Sobel detector [106] is used to generate an $EM$of an input CT image. The EM is then resized to fit the dimension of the HH sub band. The resized EM (EM_{r}) is created by down sampling the EM by two along both rows and columns of the EM. Since an actual edge is seldom a single pixel thick, an EM is dilated to get a more

accurate depiction of the actual edge thickness. As shown in equation (3.31), the stretched EM (EM_{rs}) is produced by dilating the EM by a structuring element B of disc-shaped with a radius 3 and can be written as

$$EM_{rs} = (EM \oplus B) \tag{3.31}$$

The inverted edge-map EM_{rdi} is obtained from above stretched EM, as shown in equation (3.32).

$$EMrsi = 1 - EMrs \tag{3.32}$$

Zeros represent edge positions in the spatial domain in the re-sized inverted stretched edge-map. In contrast, non-edge positions are signified by ones in the original edge-map. By using the Hadamard product of HH sub band component and the reversed resized EM, as shown in equation (3.33), this inversion aids in the direct elimination of edge components from the HH sub-band

$$HHne = HH \circ EMrds \tag{3.33}$$

HH_{ne} solely includes the noise contained in the input CT image, and signifies the HH sub-band component relating to non-edge area regions existing in the image. The resulting HH_{ne} sub-band is denoised using soft thresholding in order to get the denoised HH sub-band, which has been donated as HH_{dne}. To recover the edge information contained in the HH sub-band HH_{dne} is added to the EM_r to get the final denoised HH sub-band HH_d, which can be expressed as

$$HH_d = HH_{dne} + EM_r \tag{3.34}$$

With the IDWT concentrated on the improved LL and HH sub bands and the added intact LH, HL sub bands, a better CT image was created. A breakdown of the suggested method's individual steps is shown in Fig. 3.2. Fig. 3.3 depicts the suggested approach's intermediate stages in order to highlight the individual steps that make up the larger algorithm. The suggested approach is described in great length in Algorithm 1, which provides a summary of those phases.

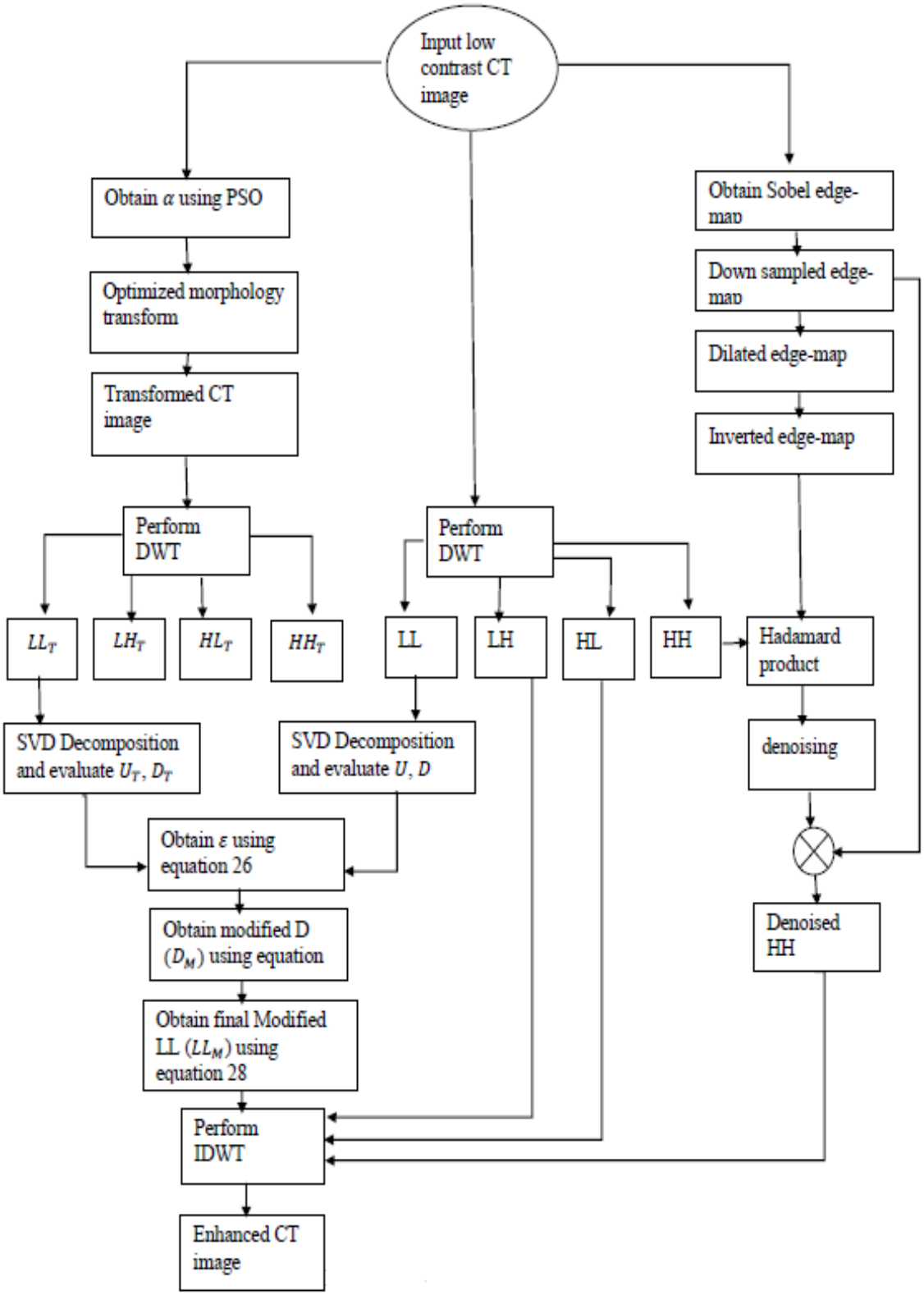

Figure: 3.2. Block diagram of the proposed technique of enhancing CT images using an optimized morphology transform and edge map

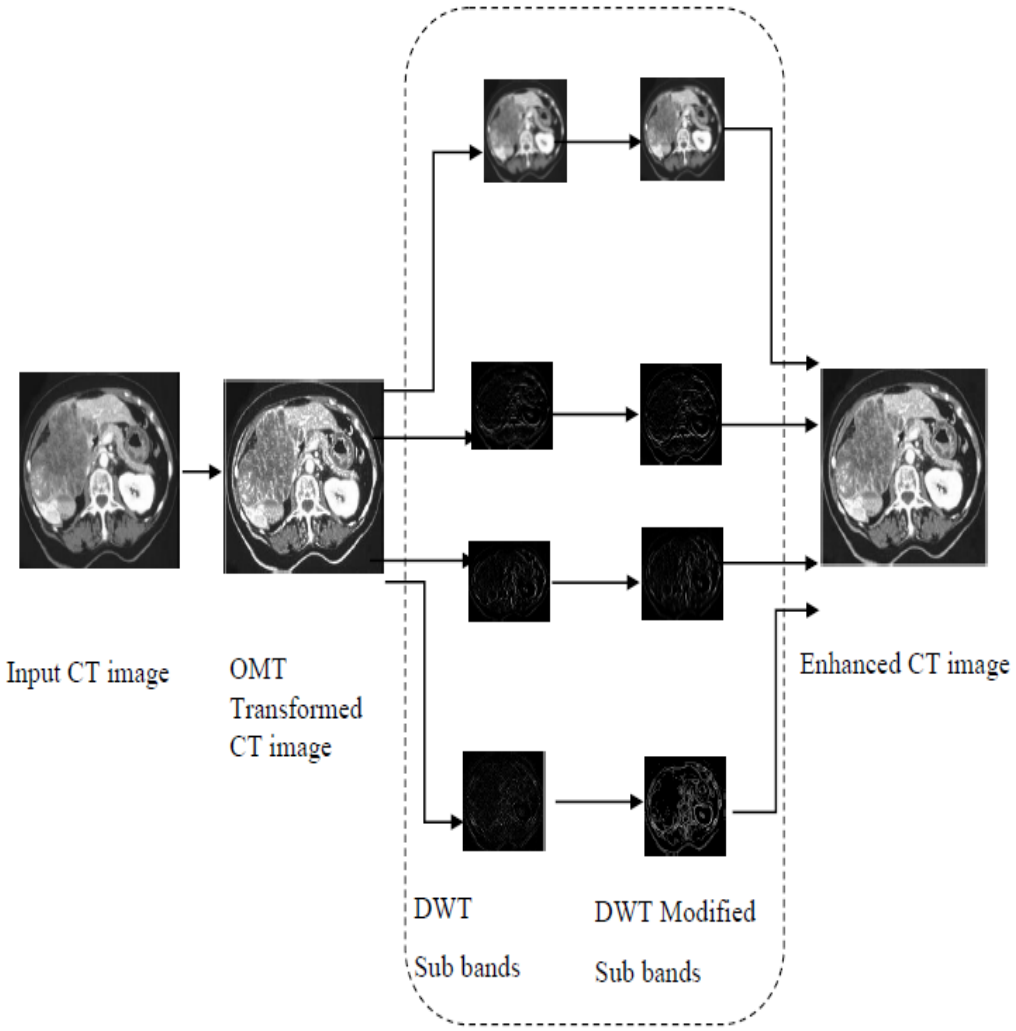

Figure: 3.3. The Middle phases of the proposed method

Algorithm 1: An optimized morphology transform-based diagnostic CT image enhancement Using EM

1. Input: Low contrast CT image (I).
2. Obtain the value of β for OMT enhancement method to improve the contrast of the original CTimage by maintaining the details of the original image, by equation. (3.10)
3. Apply DWT on input CT and transformed CT image to get sub-bands i.e. LL, LH, HL, and HH and LL_T,LH_T, HL_T, HH_T respectively.
4. Operate SVD on the lower element of the original CT image and transformed CT image and calculatethe correction factor ε by equation. (3.26). The modified LL is attained using equations. (3.30).
5. Denoise the high-frequency component HH obtained from DWT of the input CT

image using an EM-based approach using equation. (3.34)

6. To get the enhanced CT image, IDWT is applied on the modified lower component, the denoised HH component, and other untreated input image components.
7. Output: enhanced CT image.

3.4.Datasets

Several open-source datasets' worth of CT scans are used to test and verify the effectiveness of the proposed technique. The first is a free and easily available database known as CTSius.com (http://www.ctsius.com). It is the largest CT screening database in the field of radiology. The radpod (http://www.radpod.org) dataset is also focused on radiology and contains many CT pictures from different case studies. These archives are kept in JPEG format and are all resized to 256x256 pixels before processing.

3.5. Results and Discussions

In order to evaluate the potential of the proposed system, this part conducts a battery of tests on one hundred CT images culled from various online resources. The suggested method is compared to six existing prevalent methods: the S-curve [85], AGC-DWT [69], AGC-WHD [65], GAGC-DWT [61], EBCHE [50], and TCHE-DWT [51]. There is subjectivity and objectivity to these comparisons. The same machine with an Intel Core i5 processor running at 3.1 GHz and 8 GB of RAM is used for both testing.

3.5.1. Qualitative (Subjective) Assessment

The visual interpretation of a state is the subject's evaluation of the state. The goal of eliciting a subjective response is to have the subject look directly at the output visuals. People with pictorial perception can analyse visual artefacts, information degradation, unrealistic appearance, and excessive augmentation with great detail and accuracy. Evaluation of the effectiveness of various image contrast enhancement procedures requires a reliable method of gauging the quality of the enhanced images.

The proposed method is visually contrasted to standard contrast-enhancement strategies for a variety of CT scans. Figure 3.4 displays the visual outcomes of suggested and existing approaches applied to the 'CT-1' image. Blocks occur within the image when using the local S-curve method because of the sigmoid function's tendency to distort fine details (see Fig. 3.4b). The metastases denoted by the red arrows in Fig. 3.4c and

3.4d are lost in the unduly boosted areas and very bright images produced by the image enhancement techniques (AGC-DWT and AGC-WHD). Figures 3.4e and 3.4g illustrate how the GAGC-DWT and TCHE-DWT methods amplified noise and allowed contrast to spiral out of control in most areas. Figure 3.4f demonstrates how the EBCHE technique results in slightly more contrasty photos. In Fig. 3.4h, you can see that the proposed method successfully increased contrast without modifying the CT liver image, and that liver metastases are properly highlighted.

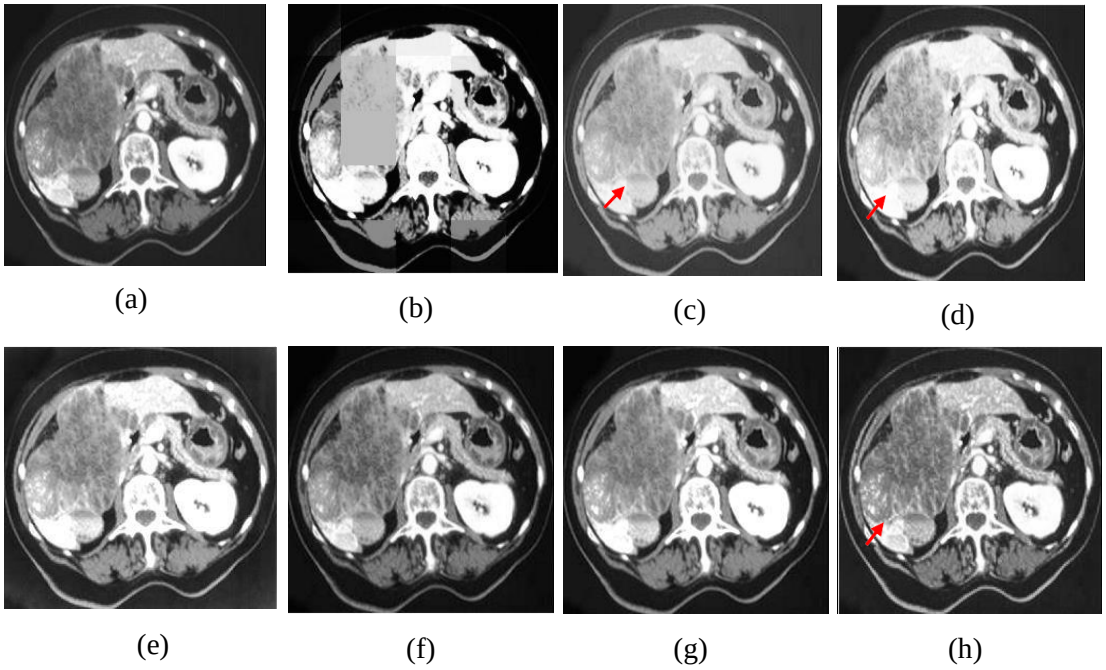

Figure: 3.4 Input "CT-1" image and it's associated enhanced images (a) Input image, (b) S-curve, (c) AGC-DWT, (d) AGC- WHD, (e) GAGC-DWT, (f) EBCHE, (g) TCHE-DWT, (h) Proposed technique

Figure 3.5 displays the 'CT-2' picture alongside the contrast-enhanced results achieved by employing the suggested method and the other six established methods. However, as can be seen in Fig. 3.5e, the image's fine details were lost due to the technique's over-amplification of the contrast. Both AGC-DWT and AGC-WHD methods over-enhanced the CT images, as seen in Fig. 3.5c and 3.5d, obscuring less important details. As seen by the red arrow in Fig. 3.5f, scars inside honeycomb-like tumours are darker and less distinguishable due to the inability of the EBCHE method to increase contrast, and

The noise level is quite high using this method. Figure 3.5b demonstrates how the S-curve method causes undesired artefacts in the final, enhanced photos. Fig. 3.5g

demonstrates that the TCHE-DWT method increased the contrast of the images while decreasing the average brightness. Once again, as is shown in Fig. 3.5h, the CT scan images of the pancreas produce much better visual results when the suggested steps are followed. Good visual contrast was also achieved by adequately amplifying the numerous thin-walled cysts seen within the tumour regions.

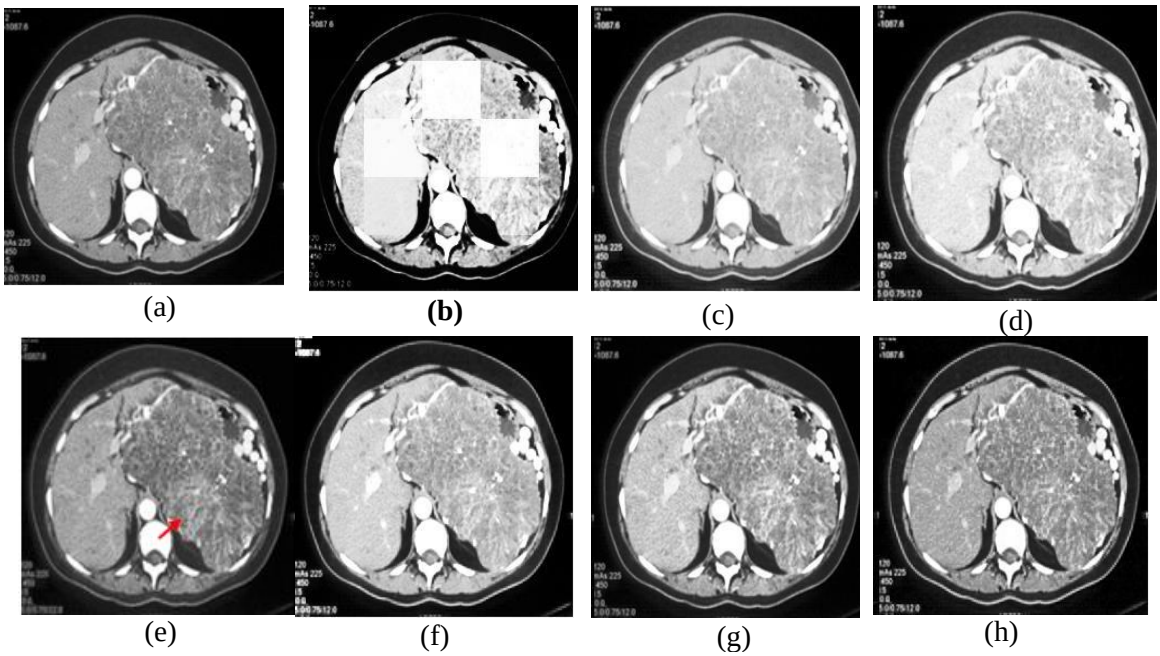

Figure: 3.5 Input "CT-2" image and it's associated enhanced images (a) Input image, (b) S-curve, (c) AGC-DWT, (d) AGC-WHD, (e) GAGC-DWT, (f) EBCHE, (g) TCHE-DWT, (h) Proposed technique

It can see the improvements made to the 'CT-3' image using both proposed and established methods in Fig. 3.6. Visual intensity differences between items in the CT picture were eliminated by using the AGC-DWT, AGC-WHD, or GAGC-DWT methods (Fig. 3.6c, 3.6d, and 3.6e), all of which significantly outperformed the mean brightness of the original CT image. As is typical, EBCHE fails to improve contrast in nearly all of the image in Fig. 3.6f. The accuracy of the image in Fig. 3.6b is compromised since the S-Curve approach produces output images with blocking and saturation distortions. Visual inspection of Fig. 3.6g demonstrates that the TCHE-DWT technique yields a superior image. However, as the red arrow indicates, there are certain instances of over-enhancement, especially in the area of details. When compared to the other six methods currently in use, the suggested algorithm achieves better results in terms of contrast optimization, brightness preservation, and realism. As may be seen in

Fig. 3.6h, as a result, most things disappear into the scenery..

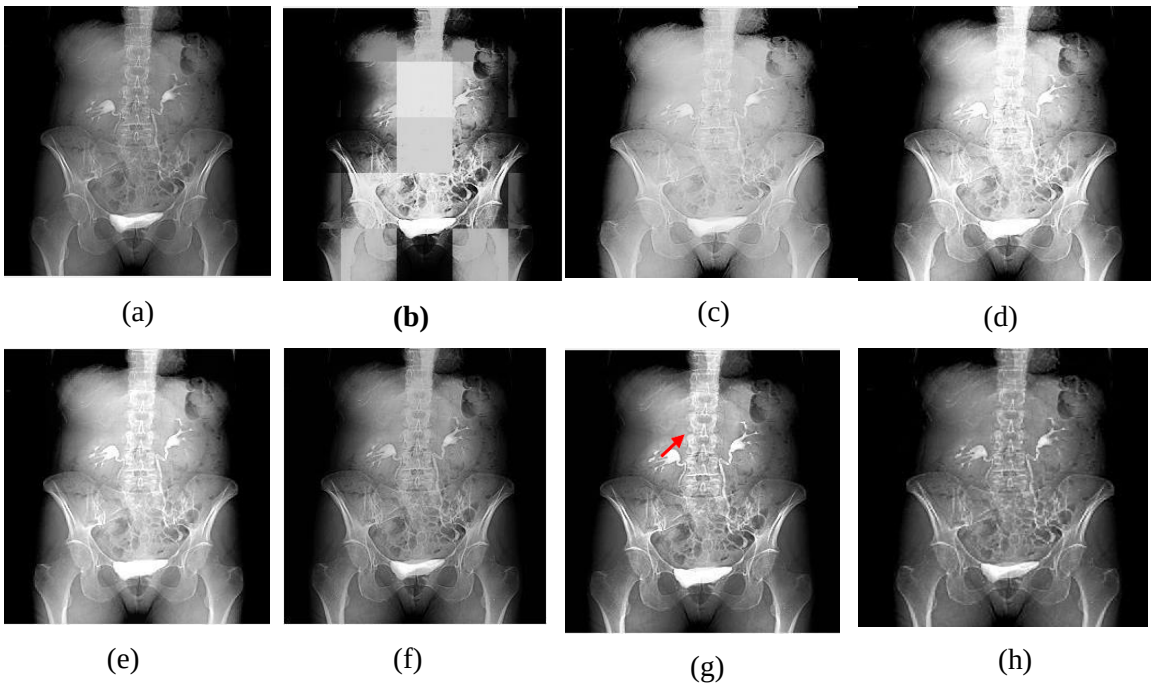

(a) **(b)** (c) (d)

(e) (f) (g) (h)

Figure: 3.6 Input "CT-3" image and it's associated enhanced images (a) Input image, (b) S-curve, (c) AGC-DWT, (d)AGC-WHD, (e) GAGC-DWT, (f) EBCHE, (g) TCHE-DWT, (h) Proposed technique

The results of both the proposed and standard methods for enhancing 'CT-4' images are displayed in Fig.3.7. In Fig. 3.7b, you can see how the S-Curve technique degrades the image quality by introducing blocking and intensity saturation artefacts into the final product. The visual intensity mismatch between distinct items in the CT image was eliminated using the AGC-DWT, AGC-WHD, and GAGC-DWT approaches (Fig. 3.7c, 3.7d, and 3.7e), all of which greatly outshone the mean brightness of the original CT image. Therefore, the improved outputs produced by these techniques are insufficient. The typical occurrence of EBCHE darkness throughout the entire scene is depicted in Fig. 3.7f. Visual inspection of Fig. 3.7g reveals that the TCHE-DWT method yields a superior image, despite the fact that some areas, particularly the details, are over-enhanced. By maximising contrast while keeping brightness and realism, the suggested algorithm outperforms the other six current algorithms. Figure 3.7h illustrates how this causes most items to blend into the scenery.

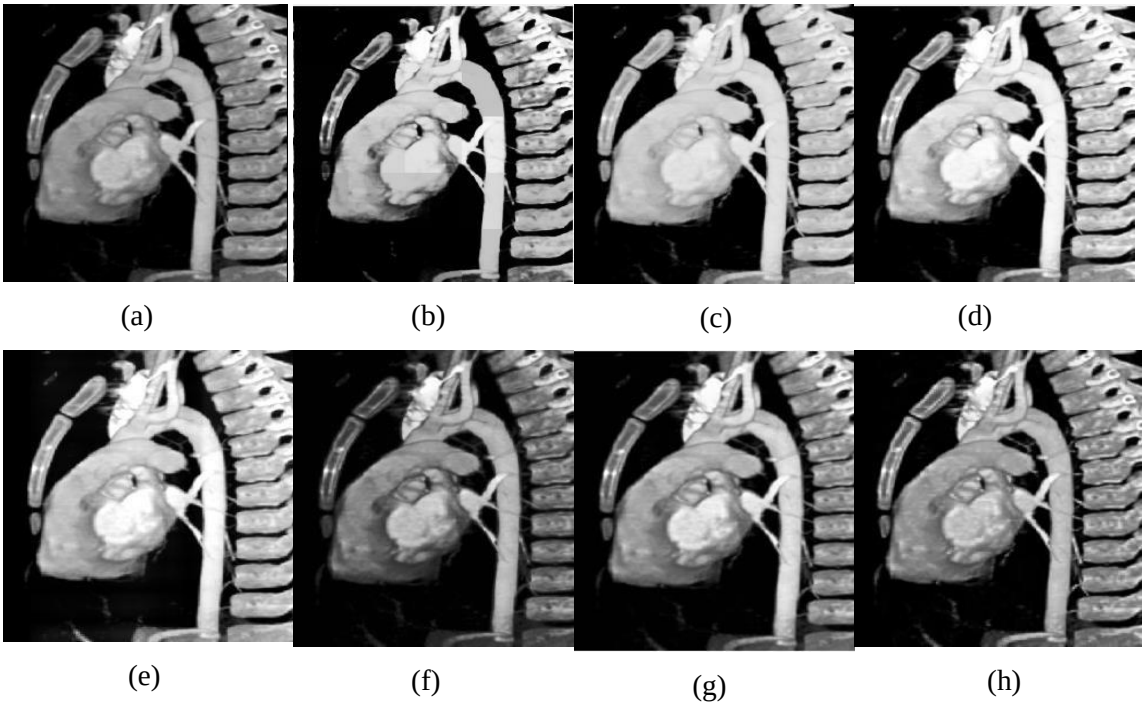

Figure: 3.7 Input "CT-4" image and it's associated enhanced images (a) Input image, (b) S-curve, (c) AGC-DWT, (d) AGC-WHD, (e) GAGC-DWT, (f) EBCHE, (g) TCHE-DWT, (h) Proposed technique

In Fig. 3.8, we see the original 'CT-5' image, as well as contrast-enhanced versions of the image generated with the proposed method, and the six other existing methods. Both AGC-DWT and GAGC-DWT greatly skewed the adrenal masses, as demonstrated by the red arrows in Fig. 3.8c and 3.8e, and had undesirable aesthetic impacts overall. As the red arrows in Fig. 3.8b illustrate, the S-Curve method yielded darker results in several regions, indicating a lack of data. Some important features of the processed image were lost even though the AGC-WHD and TCHE-DWT (Fig. 3.8d and 3.8g) attempted to boost contrast while keeping the brightness at a respectable level. In Fig. 3.8f, EBCHE caused a decrease in the visibility of fine details and a general dimming of the image because of an incorrect exposure value setting. The suggested method improves and readily detects the crucial minute properties of the CT picture, as displayed in Fig. 3.8g. The proposed technique additionally maintains the original image's brightness-sensitive qualities in the final product.

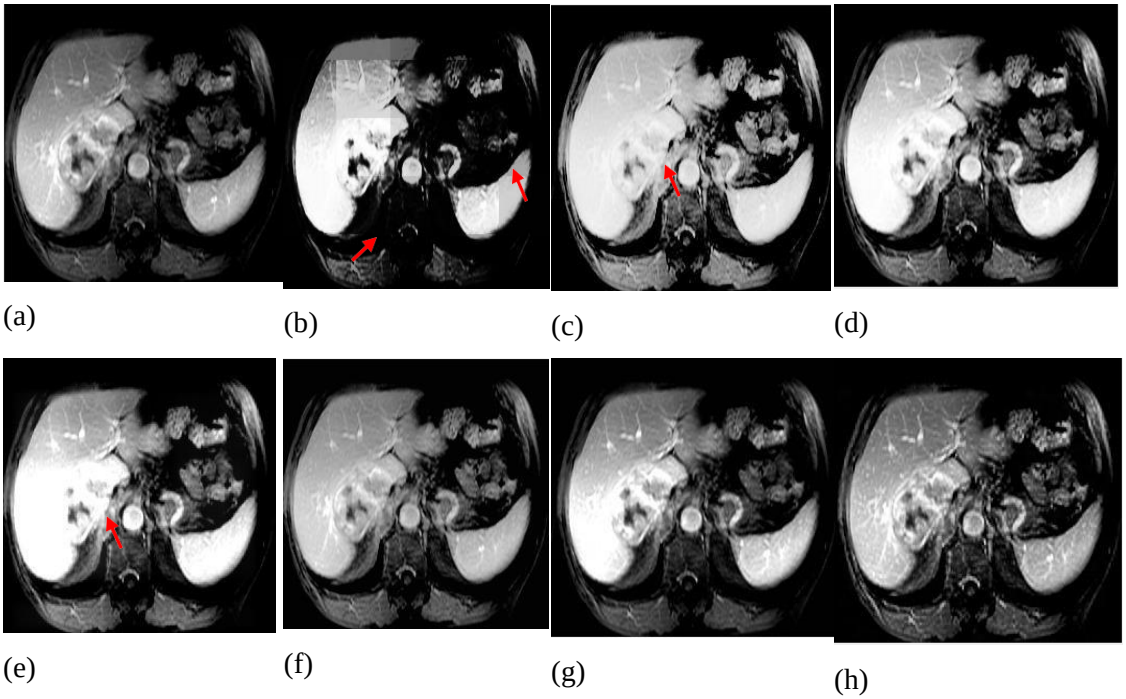

Figure: 3.8. Input "CT-5" image and it's associated enhanced images (a) Input image, (b) S-curve, (c) AGC-DWT, (d) AGC-WHD, (e) GAGC-DWT, (f) EBCHE, (g) TCHE-DWT, (h) Proposed technique

The 'CT-6' image with increased contrast is shown in Fig. 3.9. Figures 3.9c, 3.9d, and 3.9e reveal that the AGC-DWT, AGC-WHD, and GAGC-DWT methods all resulted in insufficient texture details and excessive augmentation, especially in solid renal masses (red arrows). Neither the S-curve technique nor the contrast enhancement method were able to provide an adequately high level of contrast, as evidenced in Fig. 3.9b by the darkening of most areas in the kidney image and the loss of clarity denoted by the red arrows. Output photos from these methods are similar to the original, as illustrated in Fig. 3.9f, which shows that the EBCHE system's output images demonstrate a minor contrast increase. Even though the mean brightness was maintained by the TCHE-DWT approach (Fig. 3.9g), the local texture information associated with solid lesions was distorted. Fig. 3.9g demonstrates that the suggested technique has the ability to provide aesthetically pleasing CT kidney images with enhanced mean brightness retention and visibility of fine details.

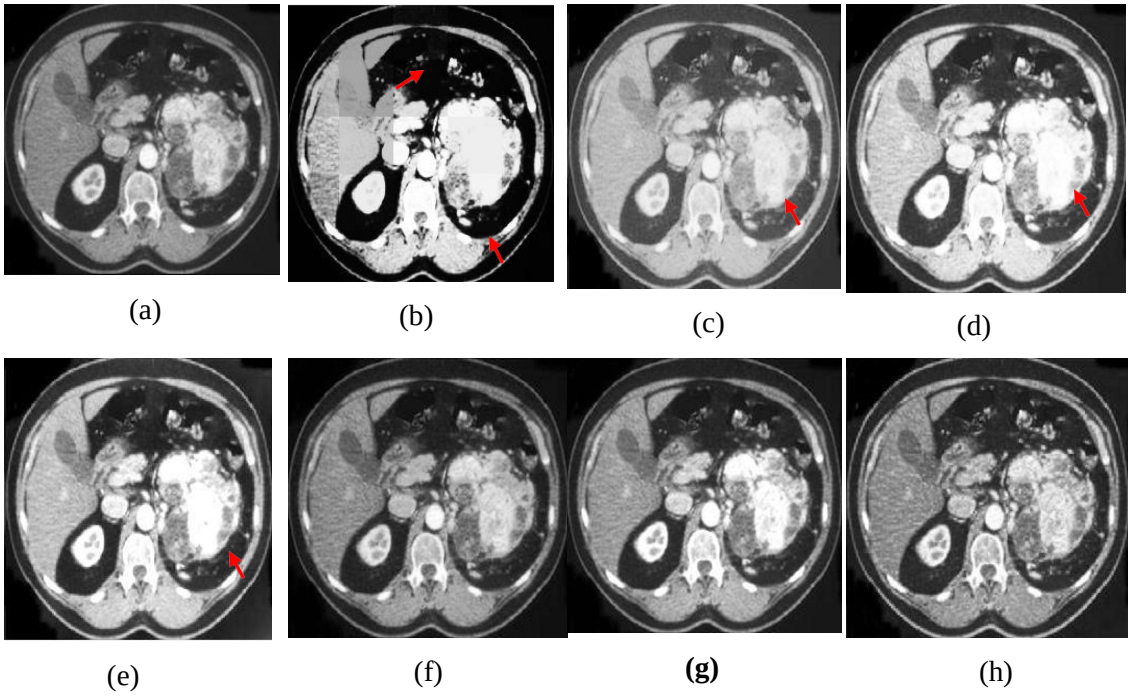

Figure: 3.9 Input "CT-7" image and it's associated enhanced images (a) Input image, (b) S-curve, (c) AGC-DWT, (d) AGC- WHD, (e) GAGC-DWT, (f) EBCHE, (g) TCHE-DWT, (h) Proposed technique

3.5.2. Quantitative (Objective) Assessment

Assessing picture quality has direct implications for medical diagnosis, which is why this process is so crucial to medical imaging. The diagnostic efficacy of medical imaging can't be established without the creation of reliable measures. As a result, the PSNR, AIC, CII, MC, EME, and WC are the metrics relied upon most frequently when assessing the precision of medical images.

The entropy values of various enhancement strategies are tabulated in Table 3.1. Image information is quantified using a measure called entropy. Many details can be extracted from an image with a high entropy. A high entropy value is sought through contrast enhancement methods to bring out the minute details in a diagnostic image and enable a precise diagnosis. Due to information being lost during the over-enhancement process, the S-curve approach has a low entropy value. The proposed method is found to generate significantly more entropy than state-of-the-art alternatives for all tested CT images. In contrast to existing contrast enhancement methods, this one successfully maintains the integrity of the original data.

Table 3.1 Evaluation of entropy

Image Name / Methods	Original	S-curve	AGC-DWT	AGC-WHD	GAGC-DWT	EBCHE	TCHE-DWT	Proposed scheme
CT-1	7.08	6.30	7.08	6.71	7.07	7.00	7.12	7.28
CT-2	7.02	5.93	6.78	6.77	6.92	6.86	7.05	7.17
CT-3	6.06	6.04	6.04	6.06	6.22	5.96	6.20	6.26
CT-4	6.32	6.05	6.15	6.13	7.01	6.19	6.51	6.59
CT-5	6.05	5.40	6.08	5.77	6.22	5.92	6.05	6.33
CT-6	7.37	6.81	7.47	7.08	7.38	7.27	7.45	7.51
CT-7	7.28	6.58	7.43	7.07	7.27	7.16	7.40	7.50
CT-8	7.25	7.22	7.25	7.10	7.53	7.16	7.33	7.55

The proposed solution provides the highest PSNR when compared to the other available options, as shown in Table 3.2. With a high PSNR, the suggested method reduces noise in the final image and increases the likelihood of producing an artifact-free final product. The PSNR of the suggested method is greater than that of all previously established contrast augmentation techniques. When the PSNR is high, the image has higher definition. A high PSNR value is achieved using the proposed method, leading to a visually pleasant image with improved contrast.

Table 3.2 Evaluation of PSNR

Image name/Methods	S-curve	AGC-DWT	AGC-WHD	GAGC-DWT	EBCHE	TCHE-DWT	Proposed scheme
CT-1	15.83	16.74	16.59	18.87	27.08	24.20	28.33
CT-2	13.99	16.05	14.63	17.37	26.86	22.80	27.86
CT-3	15.21	13.36	13.56	14.69	27.55	20.90	29.52
CT-4	18.93	15.96	15.89	15.85	23.94	25.89	28.31
CT-5	18.82	14.38	15.63	15.60	23.30	23.26	29.73
CT-6	15.90	16.69	14.87	16.67	30.58	24.45	27.66
CT-7	18.26	15.24	13.90	16.41	23.79	27.04	27.88
CT-8	15.62	16.48	14.35	16.97	25.24	24.47	29.81

Table 3.3 displays the CII values achieved by several picture enhancement methods, making it clear that the suggested method achieves a higher CII value. In every case, the suggested technique improves contrast while keeping crucial details of the CT picture intact. The CII value of the suggested method is proven to be greater than that

of any other contrast improvement method currently in use. The diagnostic value of the output CT image is increased as a result of the proposed method, which increases image contrast, structural data, and fine details.

Table 3.3 Evaluation of CII

Image name/Methods	S-curve	AGC-DWT	AGC-WHD	GAGC-DWT	EBCHE	TCHE-DWT	Proposed scheme
CT-1	1.61	0.85	1.31	1.03	1.10	1.32	1.40
CT-2	0.74	0.88	0.99	1.08	0.56	0.87	1.16
CT-3	1.77	0.98	1.11	0.96	1.06	1.29	1.46
CT-4	1.01	0.95	1.04	0.78	1.03	0.92	1.27
CT-5	1.06	0.99	1.04	0.89	0.76	0.92	1.24
CT-6	1.34	0.79	1.34	1.30	1.24	1.14	1.51
CT-7	0.92	0.97	1.13	1.17	0.93	0.89	1.27
CT-8	1.40	1	1.14	1.10	1.26	1.18	1.44

When compared to currently available approaches, as shown in Table 3.4, the suggested approach yields an EME value that falls smack in the middle of the spectrum. When it comes to enhancing the final image while eliminating unwanted artefacts, the recommended approach with a moderate EME value is the way to go. The proposed method yields an EME value that falls somewhere in the middle when compared to the other remaining contrast enhancement strategies.

Table 3.4 Evaluation of EME

Image name/Methods	S-curve	AGC-DWT	AGC-WHD	GAGC-DWT	EBCHE	TCHE-DWT	Proposed scheme
CT-1	38.57	12.83	17.84	18.89	27.41	24.39	21.52
CT-2	35.64	12.53	14.89	16.18	25.46	29.26	20.24
CT-3	16.53	4.89	8.67	10.26	19.82	20.45	10.08
CT-4	35.77	8.78	11.14	25.80	43.33	41.78	10.22
CT-5	22.19	5.21	7.32	20.65	40.64	34.34	8.04
CT-6	41.70	13.29	17.80	18.99	25.31	23.48	21.84
CT-7	39.78	13.33	16.99	19.42	21.91	22.56	22.93
CT-8	30.33	8.63	12.16	13.10	30.38	15.30	14.84

Over-enhancement occurs with extremely high EME values and has been demonstrated to be insufficient for medical analysis. The low value of EME indicates that there will be no major development in the concealed features of an image. The EME values for the suggested method fall about in the middle of the acceptable range for such assessments of performance.

Results from one hundred CT scans are summarised in Table 3.5, where the average of both the proposed and traditional approaches is presented. As was previously indicated, the proposed method yields better results on average for entropy, PSNR, EME, and CII than do alternative improvement techniques. The proposed method has better average values for entropy, PSNR, EME, and CII than prior enhancement methods. As indicated in the equations, the suggested approach is also evaluated by collecting Michelson contrast (MC) and Weber contrast (WC). (2.6)– (2.7). (2.7). Stronger differentiation is indicated by larger values for both WC and MC. The proposed method achieves the highest Michelson and Weber contrast ratios (0.41/0.37) of any similar enhancement method. The results show that the proposed method is accurate and successful for managing various CT diagnostic pictures, with improved contrast and preservation of subtle structures.

Table 3.5 Average measures values for 100 CT images

Methods/Measures	Entropy	PSNR	CII	MC	WC	EME
S-curve	6.55	16.25	1.40	0.36	0.29	39.13
AGC-DWT	6.94	16.52	0.92	0.28	0.20	12.12
AGC-WHD	6.68	14.59	1.28	0.34	0.25	16.33
GAGC-DWT	7.02	17.02	1.22	0.33	0.24	18.21
EBCHE	6.84	26.92	1.52	0.41	0.29	33.68
TCHE-DWT	7.15	26.01	1.34	0.38	0.26	24.88
Proposed scheme	7.21	27.66	1.64	0.42	0.42	18.16

3.6. Summary

The aim of this research is to suggest a novel method for effectively enhancing low-quality CT images. After the original CT image has been enhanced with the optimal morphological transform (OMT) methodology, it is then partitioned into four parts using the discrete wavelet transform (DWT) method. While the EM approach is used

to denoise the original CT picture's HH sub-band, the SVD technique is used on the LL sub-band output alone to boost contrast while maintaining image brightness. Compared to six other methods of improvement, the one we offer performs better by a wide margin. The results of the experiments showed that the proposed method can effectively enhance CT pictures without altering their original characteristics. When compared to other approaches like S-curve, AGC-DWT, AGC-WHD, GAGC-DWT, EBCHE, and TCHE-DWT, the suggested method produces superior results in terms of EME, CII, Michelson contrast ratio and Weber contrast ratio, PSNR, and entropy of the enhanced pictures. This method can be used to improve CT pictures, which can then be utilised to aid in a proper diagnosis by a pathologist or doctor.

CHAPTER 4
AN EFFECTIVE CT MEDICAL IMAGE ENHANCEMENT SYSTEM BASED ON DT-CWT AND ADAPTABLE MORPHOLOGY

4.1. Introduction

Medical diagnostic imaging plays a pivotal role in modern healthcare, enabling accurate and timely identification of various conditions and diseases. As technology continues to advance, the demand for high-quality imaging that preserves crucial details and natural features becomes increasingly paramount. Particularly in the realm of non-contrast CT imaging, obtaining clear and informative images is essential for precise diagnosis and subsequent analysis. To meet this demand and enhance the diagnostic accuracy of medical images, numerous methods have been proposed in the past. However, achieving a balance between improving image quality and preserving inherent characteristics remains a challenging task. In this study, effective enhancement of non-contrast CT images is proposed using dual tree complex wavelet transform (DT-CWT) and flexible morphology. The DT-CWT system begins by splitting the input CT image into low and high frequency sub-bands. When applied to high pass sub-bands, denoising utilising the wavelet-related shearlet transform approach improves high-frequency sub-images. To generate superior low-frequency sub-images, a DCT-based local enhancement is employed in conjunction with an adaptive morphological top hat transform technique for low pass sub-bands. Inverse DT-CWT can be used to recombine the improved low- and high-frequency semi-components to create the improved CT image. A large set of CT images from a publically available database is used for experiments and validations to qualitatively and quantitatively evaluate the effectiveness of the proposed method. Measurements of signal-to-noise ratio, discrete entropy, contrast ratio, and enhancement all show that the suggested method surpasses the state-of-the-art alternatives. Unlike existing and previously disclosed contrast enhancement approaches, as discussed in Chapter 2, the proposed method effectively addresses the specific flaws encountered in medical images. These flaws include noise amplification, under or over enhancement, brightness deterioration, and information distortion. Notable features of the suggested approach are as follows:

- The proposed method begins by utilizing the DT-CWT to decompose the input

image into low and high frequency components. After that, a unified strategy employing the NSST method is used to deal with the high frequency component of the image and the modified morphological top hat transform method is used to deal with the low frequency component.

- Boosting the contrast efficiency of the CT image by a combination of the modified morphology top-hat transform and DCT-based local enhancement. In contrast, the noise in the image is greatly diminished by the NSST solution.
- By reducing noise without altering fine features, keeping average brightness, keeping a natural appearance, and maximising entropy for poor contrast CT images, the aforementioned methods significantly enhance contrast.

4.2. Proposed Technique of CT Image Enhancement Based on DT-CWT and Adaptable Morphology

Figure 4.1 is a diagrammatic representation of the suggested method [124]. The DT-CWT procedure begins with the incorporation of the collected CT images. Based on the DT-CWT procedure, the input CT image is subdivided into eight distinct frequency bands: six high-frequency (approximation) sub-bands and two low-frequency (detail) sub-bands for each scale. Denoising is performed using the wavelet-related shearlet transform method, which produces high-frequency sub-images that have been denoised for high pass sub-bands. To improve the low-frequency bands, an adaptive morphological top hat transform method is utilised, then the DCT-based local improvement is applied. The final enhanced CT image is derived by applying the inverse DT-CWT algorithm to the generated sub-images. Each stage is described in further depth below.

4.2.1. DT-CWT for the CT Image

To create Hilbert transform pairs within each sub-band, Kingsbury presented the dual-tree complex wavelet transform (DT-CWT) in [16]. DT-CWT is almost shift-invariant, and it also enhances directionality, making it well-suited for capturing and preserving directional features in various image processing applications.

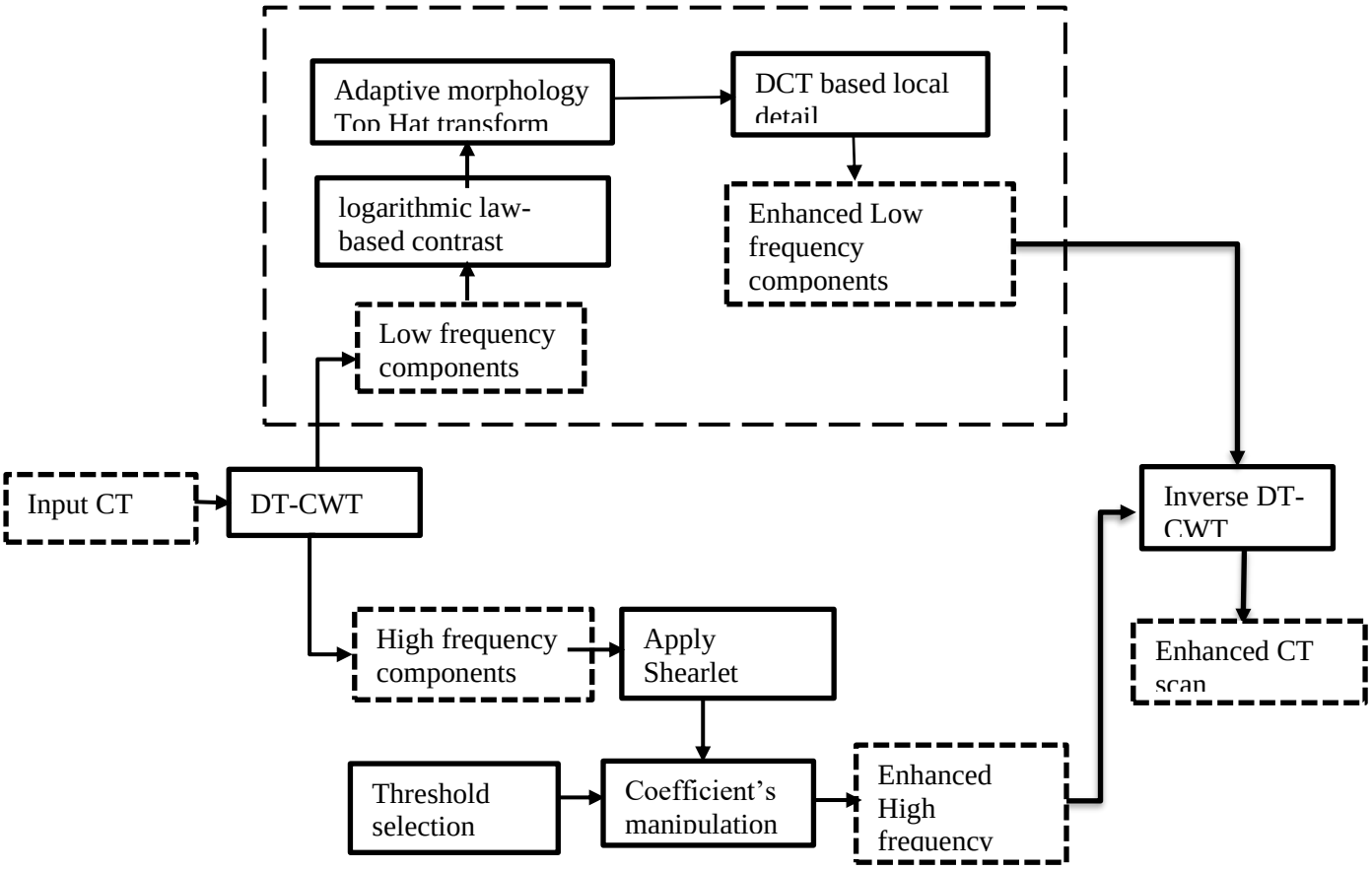

Figure 4.1: Block Diagram of CT image enhancement based on DT-CWT and adaptable morphology

As can be seen in Fig. 4.2, the DT-CWT [17] is used to perform a multi-scale decomposition of the input CT image, with six high-frequency sub-bands and two low-frequency sub-bands being generated at each scale. Tree A and Tree B are used in DT-CWT, with Tree A contributing the real wavelet coefficients and Tree B the imaginary ones; 2 denotes subsampling. Let's say the low pass/high pass filter couple h 0m (n), h 1m (n) represents the upper filter set, and let's say the low pass/high pass filter couple g 0m (n), g 1m (n) represents the lower bank set. The parameter 'm' denotes the specific stage of each low pass and high pass filter in the DT-CWT, influencing the scale of the decomposition.

DT-CWT algorithm decomposes an input into a complex shifting and stretched mother wavelet $\Psi(t)$ and a complex scaling factor $\varphi(t)$. The DT-CWT is a complex wavelet-based technique that is described as

$$\psi(t) = \psi_h(t) + j\psi_g(t) \quad (4.1)$$

Where $j = \sqrt{-1}$, $\psi_h(t)$ and $\psi_g(t)$ signify the real portion and imaginary portion of wavelets, and these are wavelet basis operators.

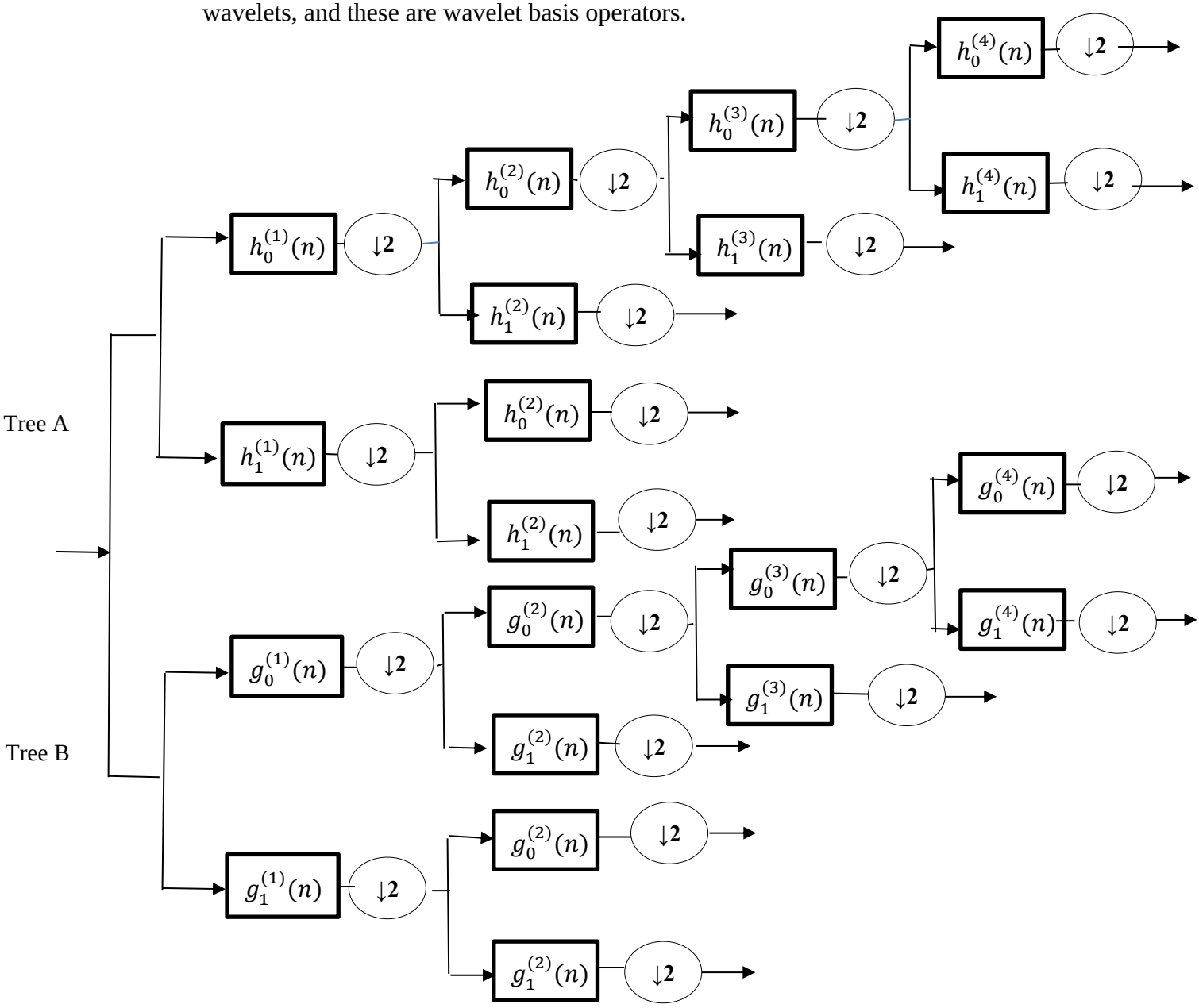

Figure 4.2: Illustration of 2D dual-tree complex wavelet transform (DT-CWT)

The DT-CWT employs analytical filters to complete the wavelet transformation. The DT-CWT employs two discrete wavelet transforms (DWTs); the primary DWT is used for the real portion of the transform, while the secondary DWT is used for the imaginary portion. To obtain approximately shift-invariant wavelets, the two low-pass filters ($h_0(n)$, $g_0(n)$) must satisfy a basic characteristic: one must have roughly half a sample delay of the other [15].

$$g_0(n) \approx h_0(n - 0.5) \tag{4.2}$$

In this case, the corresponding wavelets $\psi_h(t)$ and $\psi_g(t)$ form an approximation Hilbert pair, which can be seen as

$$\psi_g(t) \approx H\{\psi_h(t)\} \tag{4.3}$$

These dual-tree low pass filters can be used in all sections of the dual-tree Filter bank except the first. The first stage only requires a separate set of filters that should be offset by one sample. The filters of one tree (g_0, g_1) are identical to those of the other tree (h_0, h_1) but are offset by one sample.

$$g_0^{(1)}(n) \approx h_0^{(1)}(n - 1) \tag{4.4}$$

4.2.2. Shearlet based Enhancement for High-Frequency Sub-bands

Once the CT picture has been decomposed, the high-frequency subbands of the input CT image are manipulated to remove noise (centered on the 2D DT-CWT). Although DT-CWT overcomes the limitations of the conventional wavelet transform, it has weak directional selectivity for its fixed directions. Therefore, it cannot correctly represent the detailed information of the CT images. High directional selectivity is essential for separating different directions in CT images, which produces a better de-noising result for accurate diagnosis. The nonsubsampled shearlet transform is built on nonsubsampled Laplacian pyramid transforms and various combinations of shear filters, as stated by Easley et al. [108]. There is high direction selectivity, less redundancy, and improved shift-invariance in the NSST [109]. Here is a breakdown of the NSLP:

$$I_{m+1} = \left(HP_m \prod_{k=1}^{m-1} LP_k \right) f \tag{4.5}$$

Images are denoted by f, while the detail coefficients at scale m+1 are indicated by I (m+1). The low-pass (LP k) and high-pass (HP m) filters are indicated by the k and m values, respectively. In order to enhance directional selectivity, this paper employs the NSST on the high-frequency subbands of the input CT image. DT-CWT ability to partition data at several scales allows for the incorporation of high-frequency subbands into NSST, which provides the necessary directionality. After that, we get a set of scale and direction coefficients I (m,n) for each subband that is completely separate from the others. The NSST-derived coefficients I (m,n) are then denoised for each high-

frequency subband using soft thresholding [109]. For this reason, the standard deviation of the input CT picture is set as the adaptive threshold value, since the CT image noise is assumed to be Gaussian [110]. An enhanced high-frequency sub-image is derived by applying the inverse NSST to the improved coefficients $I_{m,n}$.

4.2.3. Adaptive Morphology-based Enhancement Technique for Low-Frequency Sub-bands

4.2.3.1. Mathematical Morphology

Mathematical morphology refers to a subfield of mathematics and is widely used in a variety of image processing applications [111]. It's an assortment of non-linear filtering techniques that focus on the structural qualities of the subject. These morphological techniques typically use the original image and a structuring component as their two inputs. Dilation and erosion are the two primary morphology operations used to characterise morphological changes. Let's pretend that M×N sized input picture F (x, y) is a given, and that S (u, v) stands for a structuring part.

The expansion by S (u, v) and contraction by F (x, y), denoted by $F \oplus S$ and $F\Theta S$, respectively.

$$F \oplus S = \max_{u,v}\big(F(x-u, y-v) + S(u,v)\big) \tag{4.6}$$

$$F\Theta S = \min_{u,v}\big(F(x+u, y+v) - S(u,v)\big) \tag{4.7}$$

Where (x, y) and (u, v) are the coordinates of pixels in image F and structuring element S, respectively**.** Related to dilation and erosion, two other main operations: opening and closing of input $F\ (x, y)$ with $S\ (u, v)$, denoted by $F \circ S$ and $F \bullet S$ respectively.

$$F \circ S = (F\Theta S) \oplus S \tag{4.8}$$

$$F \bullet S = (F \oplus S)\Theta S \tag{4.9}$$

Further, with the use of opening/closing procedures, the top hat transform of $F\ (x, y)$ with $S\ (u, v)$ are expressed as

$$T_w = F - F \circ S \tag{4.10}$$

$$T_B = F \bullet S - F \tag{4.11}$$

where T_w is known as traditional white top-hat transform, which is employed to obtain

bright regions of the image, and T_B donates the traditional black top hat transform, that is employed to obtain the dim areas of the image. Consequently, contrast enhancement related to the traditional top-hat transform can be achieved by addition of the previously obtained bright areas and deducting the obtained dim areas from the input as follows:

$$F_E = \mathrm{F} + \mathrm{Tw} - \mathrm{TB} \tag{4.12}$$

where F_E denotes the resultant enhanced picture. If you look at Fig. 4.3, you can see how the traditional top hat transformation is used to improve the contrast of CT scan images. Figure 4.3(a) illustrates the initial CT scan, Figure 4.3(b) depicts the white top-hat transform from Figure 4.3(a), Figure 4.3(c) depicts the black top-hat transform from Figure 4.3(a), and Figure 4.3(d) depicts the enhanced outcomes based on Figures 3(b) and 3(d). Fig. 4.3 displays the findings of an experimental analysis showing that the top-hat transform leads to over- amplification in bright regions, leading to full distortion of fine features in high-frequency pixel areas. Top hat also increases noise in the final CT scans because it boosts contrast by boosting bright pixels and reducing dark ones. Therefore, it does not provide adequate contrast improvement for CT images that contain noise, high-frequency image intensities, and a dark background. Over/under enhancement and noise concerns can be addressed and better enhancement results can be produced if we limit the amount of pixels added/subtracted in bright/dark locations during white/bottom-top hat analysis.

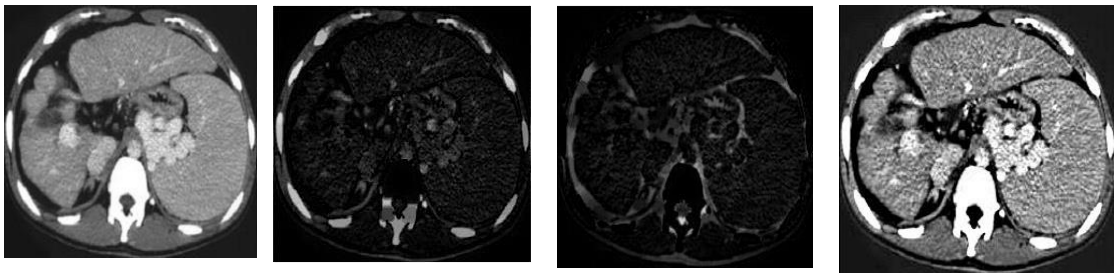

(a) (b) (c) (d)

Figure 4.3: (a) Original test CT image (b) White top-hat transform output image (c) Black top-hat transform output image (d) Enhancement output dependent on (b) and (c)

Instead of just adding or eliminating the bright/dark zone, a novel adaptive morphology top hat transform approach is proposed. To achieve this, an adaptive shrinkage factor is supplied, based on the Symmetric Naka- Rushton formula (SNRF), to limit the degree

to which pixels can be added or subtracted in the classical Top-hat transform.

4.2.3.2.Adaptive Morphology top-hat Transform

Even while the standard top hat transform boosts contrast by enhancing bright pixels and decreasing low-intensity pixels in dark regions, it distorts the information, especially in the bright zone, and raises the noise level. Adaptive morphology top-hat transform is a modification of the classical Top hat transform that introduces a shrinkage factor to control the amount of lightening or darkening of an image. The suggested adaptive morphology top-hat transform (AMTH) is formulated as such that it can be applied separately to each of the low-pass frequency sub-bands.:

$$F_{enh}(x,y) = I(x,y) + \left(\frac{1}{1+\lambda}\right) \times \left(\beta \times (T_W - T_B)\right) \quad (4.13)$$

Where λ is a adjustable parameter, β is the shrinkage factor, F_{enh} is the final image after adaptive top hat transforms are applied, I is the initial image, and h is the final image.
Figure 4.4 displays the output of the adaptive top hat transform for a range of values of β. The output image looks extremely similar to the input when is β tiny because fewer pixels are added or removed from bright/dark regions. For a greater value of β, more improvement is achieved when more pixels are added to, or subtracted from, the light and dark regions, respectively. If β is 1 and λ is 0, the algorithm is the traditional Top hat transform. By adaptively adjusting the shrinkage factor β, CT images can be improved by adding or removing pixels in certain areas. By using a smaller β value, the CT picture's low-intensity grey levels are transformed into Top-hat results that are equal to the original image, and the under enhancement that occurs in conventional Top-hat transformation can be eliminated in this area.
Using a lesser β value for produces a Top hat output that is equal to the original image, and the low-intensity grey levels in the CT image can be free of the under enhancement that is present in standard Top-hat transformation. To avoid over-enhancement and make sure the information is properly enhanced in bright CT image regions, a slightly bigger β is employed. In the proposed method, the value of λ, another tunable parameter, is set to 0 so that it does not affect the maximum value of the shrinkage factor. Therefore, the suggested system dynamically adjusts based on the need for improved CT images.

(a) (b) (c) (d) (e)

Figure 4.4**:** The adaptive top hat transform results with different βs (a) Original test CT image. (b) β = 0.2. (c) β = 0.4. (d) β = 0.8. (e) 1.0

4.2.3.3.SNRF based Adaptive Shrinking Factor

To implement brightness adjustment, Zhou used the Symmetric Naka-Rushton Formula (SNRF) [112]. To be more explicit, the Naka-Rushton-Fischer (SNRF) formula is obtained from the original Naka-Rushton equation by applying a symmetric transformation to the definition of underexposure and overexposure. This study proposes a symmetric Naka-Rushton-based adaptive shrinking factor to properly enhance CT images by adjusting the addition and subtraction of bright and dark regions based on the distribution profile of grey levels in the input CT image. Consequently, the SNRF-based adaptive shrinkage factor and the background intensity level are related as follows:

$$\beta(x,y) = \begin{cases} \dfrac{I(x,y)}{I(x,y) + H_{low}}(T + H_{low}) & 0 < I(x,y) \le T \\ 1 - \dfrac{1 - I(x,y)}{\big(1 - I(x,y)\big) + H_{high}}\big[(1 - T) + H_{high}\big] & T < I(x,y) \le 1 \end{cases} \quad (4.14)$$

Where β is the adaptive shrinking factor and $I(x, y)$ is the background luminance of the input image. For the β(x, y) computation, the original image is used as the background luminance. The parameter T denotes the pixel-by-pixel distinction between underexposure and overexposure.

According to the parameter T, pixels/areas may be categorized as underexposed or overexposed. Overexposed pixels/areas are those that exceed the T, while underexposed pixels/areas are those that are below the T. The other two parameters, H_{low} and H_{high}, regulate the amount of adaptation produced by SNRF.

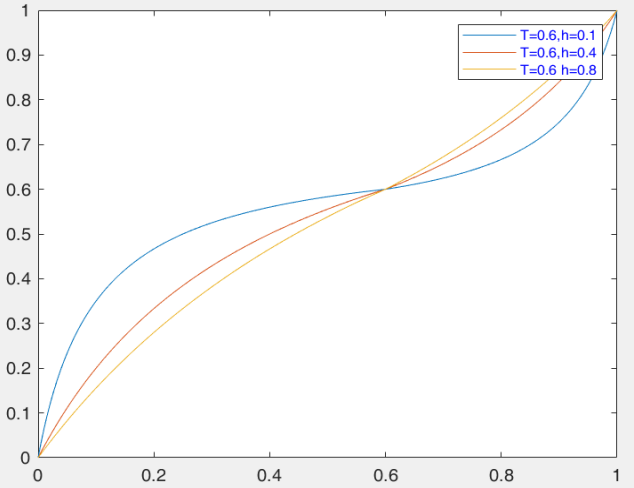

Figure 4.5: Behavior of β with different parameters.

Fig. 4.5 depicts the behavior of β with different parameters for background luminance. For the sake of simplicity, it is believed that H_{low} and H_{high} are identical and denoted as H in Fig. 4.5. T and H are set to 0.6 and 0.4 in Eq. (4.14) for experiments, respectively. For bright areas, a large β is produced, and this β slowly increases to add bright pixels adaptively for different high-frequency grey levels, avoiding over-enhancement in these areas. On the other hand, a small β is attained to reduce low-frequency grey level removal for dark areas, allowing the bottom hat under-enhancement to be improved. A new logarithmic law-based contrast stretching is used before the application of the adaptive morphology top hat transform for appropriate contrast enhancement in low grey level areas without excessive brightness of the CT image, and it is provided by

$$\mathrm{I_S(x,y)} = \frac{\big(1 - \ln\big(1 + \mathrm{I(x,y)}\big)\big) - (1 + \ln\,(1 + \mathrm{I(x,y)}))}{\mu \times (1 + \big(1 - \ln\big(1 + \mathrm{I(x,y)}\big)\big))} \qquad (4.15)$$

Where ln stands for logarithm, and $I_S(x, y)$ stands for contrast stretched image, while $I(x, y)$ stands for input image. Through adjusting the parameter μ, one can achieve various levels of enhancement. The parameters μ can range from 0 to 1. A lower value of parameter μ results in more enhancements in the output image

The value of the parameter μ should be related to the contrast of the image. Roughly, the contrast of the image is related to the min and max values of the image. In this paper, the value of μ is calculated as

$$\mu = \frac{\max\left(I(x,y)\right) - \min\left(I(x,y)\right)}{\max\left(I(x,y)\right) + \min\left(I(x,y)\right)} \tag{4.16}$$

4.2.4. Local Detail Enhancement

Although the adaptive morphology top hat transform did a good job of enhancing the CT images, the proposed method made much greater use of the relevant local information by scaling the coefficients directly in the DCT domain. As a result, enhanced low-frequency coefficients are DCT-applied. Smaller energy sections of the DCT coefficients are modified with [49] if they are within a certain bound; large energy parts, on the other hand, should be left unaltered to avoid any significant shifts in the DCT.

$$d(x,y)' = \begin{cases} d(x,y) & \text{if } |d(x,y)| > 0.01 * d(0,0) \\ \alpha * d(x,y) & \text{otherwise} \end{cases} \tag{4.17}$$

Where $D(0,0)$ represents the largest energy component, $d(x,y)'$ denotes the enhanced DCT coefficients, while $d(x,y)$ denotes the input image's dct coefficients.

The value of scaling element α can be chosen automatically in the following manner:

$$\alpha = 1 + \frac{1}{\pi} * \arctan\left(\sqrt{\frac{H\left(I_e(x,y)\right)}{H\left(I(x,y)\right)}}\right) \tag{4.18}$$

where $H(\cdot)$ is the image entropy, I_e is the AMTH transform obtained enhanced image, and I is the input image. Finally, the adjusted coefficients are subjected to the inverse DCT to recover the improved low-frequency sub- coefficients.

Fig 4.6 shows the intermediate steps of the proposed algorithm as part of the overall process for illustrating detailed steps involved in the process. The detailed steps for implementation of proposed algorithm are provided in Algorithm 1.

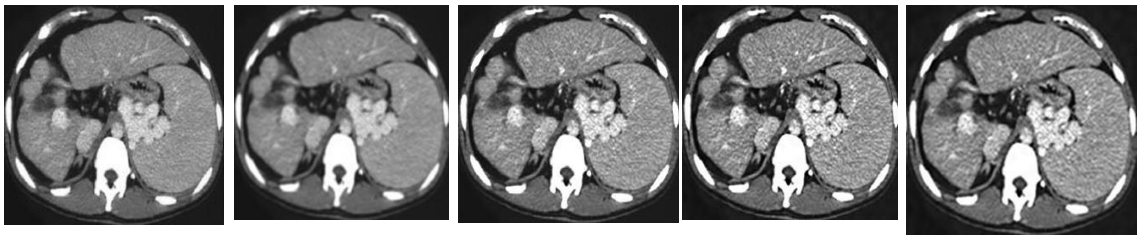

(a) (b) (c) (d) (e)

Figure 4.6: (a) Original test CT image. (b) Shearlet-based enhanced CT image (c) Adaptive morphology TopHat transform-based enhanced CT image (d) (d) DCT-based enhanced image (e) Final output enhanced CT image

Algorithm 1 Steps for the proposed CT image enhancement method.

Step 1: For the three scales $(j = 3)$, the low contrast input CT image $I(x, y)$ is decomposed using the DT- CWT method across six high-frequency sub-coefficients $(H(j + 1, m), m = 1, 2, \dots, 6)$ and two low- frequency sub- coefficients $(L(j + 1, 1), L(j + 1, 2))$.

Step 2: The two low-frequency sub-bands $(L(j + 1, 1), L(j + 1, 2))$ are further processed as defined in the previous section to produce the enhanced low-frequency sub-images.

(1) To begin, new logarithmic law-based contrast stretching is used to stretch the contrast of the input CT image's low-pass sub bands $(L(j + 1, 1), L(j + 1, 2))$ as mentioned in Eq. (4.15).

(2) Following that, the contrast stretched low-pass sub-bands $(L_s(j + 1,1), L_s(j + 1,2))$ are processed using a novel AMTH transform technique to obtain the enhanced low-frequency sub-images described in Eq. (4.13-4.14).

(3) These improved low-frequency sub-bands are then processed individually using DCT-based local information enhancement in accordance with Eq no (4.17-4.18).

Step 3: After DT-CWT decomposition, the high-pass sub-coefficients $(H(j + 1, m), m = 1,2, \dots, 6)$ are denoised using the NSST process [36].

(1) Determine the NSST for each of the six high-frequency sub- coefficients $(H(j + 1, m), m = 1, 2, \dots, 6)$. Then, for each sub-band, an independent collection of coefficients $I_{m,n}$ of the size, m, and direction n is obtained.

(2) These NSST-derived coefficients $I_{m,n}$ are then denoised using soft thresholding for

each high-frequency sub band.

(3) The enhanced high-frequency sub-images are obtained by applying the inverse NSST transform to the improved coefficients $I_{m,n}$.

Step 4: Finally, the inverse DT-CWT technique is applied to both the enhanced low-frequency and high- frequency sub-images to obtain the full enhanced CT picture $I'(x, y)$.

4.3.Datasets

In this section, we do numerous experiments on low contrast CT images from CTSius (http://www.ctisus.com) and radpod (http://www.radpod.org) to assess the robustness and effectiveness of the proposed method. These archives are kept in JPEG format and are all resized to 256x256 pixels before processing.

4.4. Results and Discussions

S-curve [85], AGC-DWT [69], AGC-WHD [65], GAGC-DWT [61], EBCHE [50], and TCHE-DWT [51] are some of the well-known methods compared to the proposed method. Both subjective and objective comparisons are provided. The same machine with an Intel Core i5 processor running at 3.1 GHz and 8 GB of RAM is used for both testing.

4.4.1. Qualitative (Subjective) Assessment

One's own impression of an image's condition is an example of subjective appraisal. Images generated as output are presented to the observer for a subjective rating. Visual perception allows for a close inspection of image artefacts, deterioration of details, unnatural look, and severe augmentation. The effectiveness of various picture contrast enhancement systems can be gauged, in large part, by means of visual quality checking. CT images of the liver, kidney, adrenal gland, heart, colon, gastrointestinal system, stomach, spleen, small bowel, and pancreas are used to visually compare the proposed method with existing contrast-enhancing methods (Figs. 4.7-4.14). In Fig. 4.7, we can observe the visual results of both new and old methods for analysing the 'CT-1' image. Figures 4.7c and 4.7d show how the AGC-DWT and AGC-WHD methods of image enhancement produce images with overly bright regions and excessively bright colours. The red arrows point to liver metastases, however they have been wiped out and are now invisible. As can be observed in Fig. 4.7b, the local S-curve technique drastically

distorts fine details because of the sigmoid function's characteristic, leading to blocks inside the image. As can be seen in Fig. 4.7e and 4.7g, the outputs of the GAGC-DWT and TCHE-DWT algorithms amplify noise and exhibit uncontrolled contrast in most of the areas. Figure 4.7f demonstrates how the EBCHE method only slightly enhances the contrast of the final photos. Liver metastases are correctly brought to light thanks to the proposed approach, which raised contrast precisely without altering any information in the CT-1 image (see Fig. 4.7h).

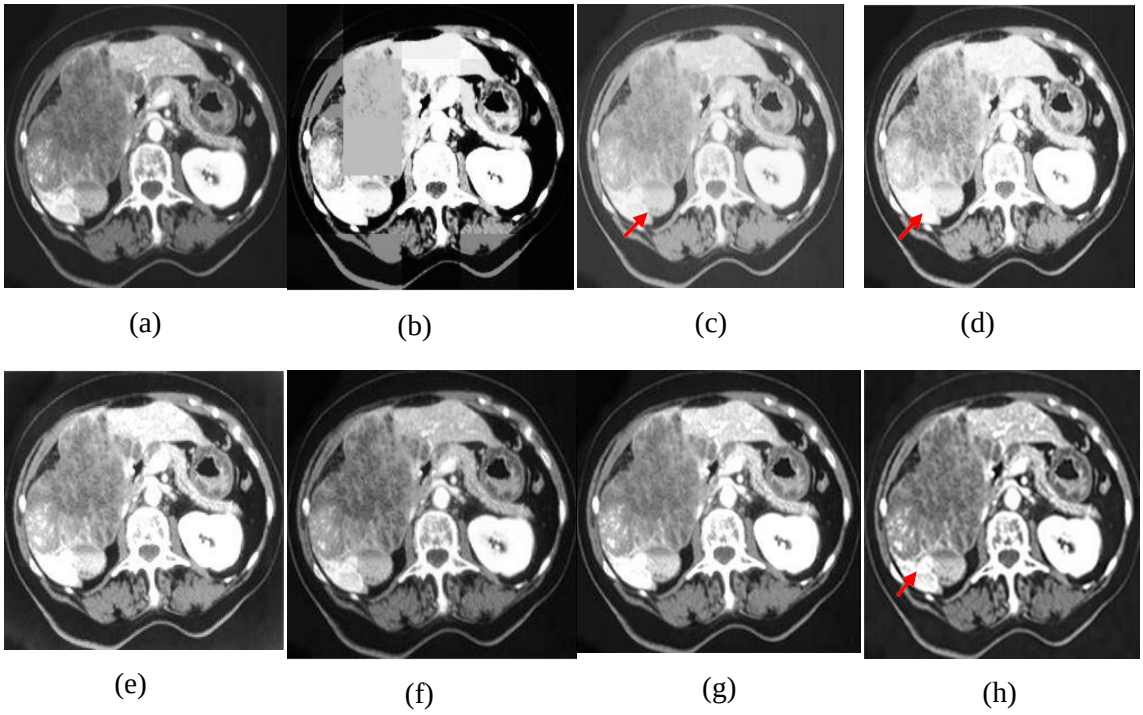

Figure 4.7: Experiment outcomes of the ‘CT-1’ Image (a) Original image, (b) S-curve, (c) AGC-DWT, (d) AGC WHD, (e) GAGC-DWT, (f) EBCHE, (g) TCHE-DWT, (h) Proposed scheme

Figure 4.8 displays the contrast-enhanced versions of the 'CT-2' image. The red arrows in Fig. 4.8b demonstrate how the S-curve approach did not successfully increase the contrast, leading to a darkening of the majority of the image's areas and a loss of detail in the kidneys. As shown by the red arrows in Fig. 4.8c, 4.8d, and 4.8e, the AGC-DWT, AGC-WHD, and GAGC-DWT approaches failed to adequately capture textural features and instead over-enhanced the images, notably in solid renal masses. TCHE-DWT (Fig. 4.8g) system-maintained influence over overall mean brightness preservation, but it distorts the local texture information correlated with solid lesions. Figure 4.8f shows that the EBCHE method only slightly improves the contrast of the

final images. Therefore, the final photographs produced by these methods are 100% faithful to the source material. As can be seen in Fig. 4.8g, the suggested method may produce CT-2 pictures that are more aesthetically pleasing due to improved mean brightness retention and the increased legibility of fine details.

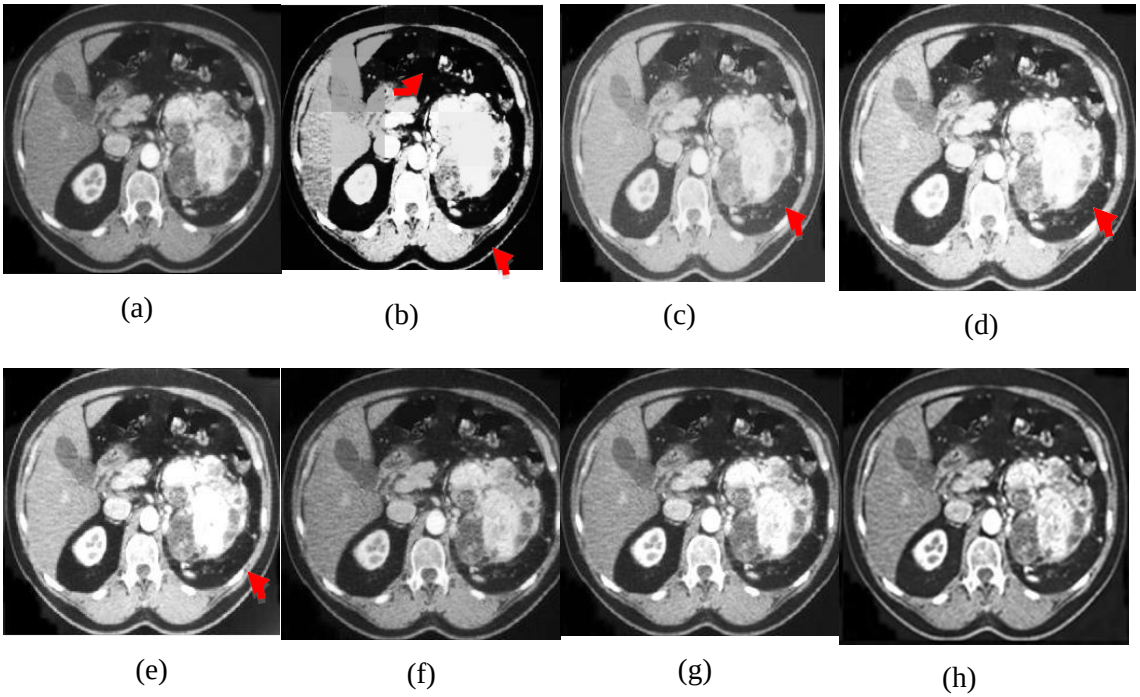

(a) (b) (c) (d)

(e) (f) (g) (h)

Figure 4.8: Experiment outcomes of the ‘CT-2’ Image (a) Original image, (b) S-curve, (c) AGC-DWT, (d) AGC-WHD, (e) GAGC-DWT, (f) EBCHE, (g) TCHE-DWT, (h) Proposed scheme

In Fig. 4.9, we can see the original 'CT-3' picture, as well as the contrast-enhanced versions created with the proposed process, and the other six current methods. As demonstrated by the red arrows in Fig. 4.9b, the S-Curve approach yielded darker results in several areas, suggesting data gaps. The AGC-DWT and GAGC-DWT methods greatly distorted the adrenal masses, as demonstrated by the red arrows in Fig. 4.9c and 4.9e, and their results are aesthetically unpleasing. Althoughthe AGC-WHD and TCHE-DWT (Fig. 4.9d and 4.9g) attempted to increase the contrast with sufficient brightness, the processed image's critical features were impacted. In Fig. 4.9f, the deterioration in brightness and the decrease in visibility of fine details are both attributable to EBCHE's improper exposure settings. As can be observed in Fig. 4.9g, the proposed method improves and easily identifies the crucial tiny features of CT-3. Furthermore, the proposed method results in the protection of contrast-sensitive aspects of the adrenal output photograph.

Results of proposed and traditional methods for improving the 'CT-4' image are

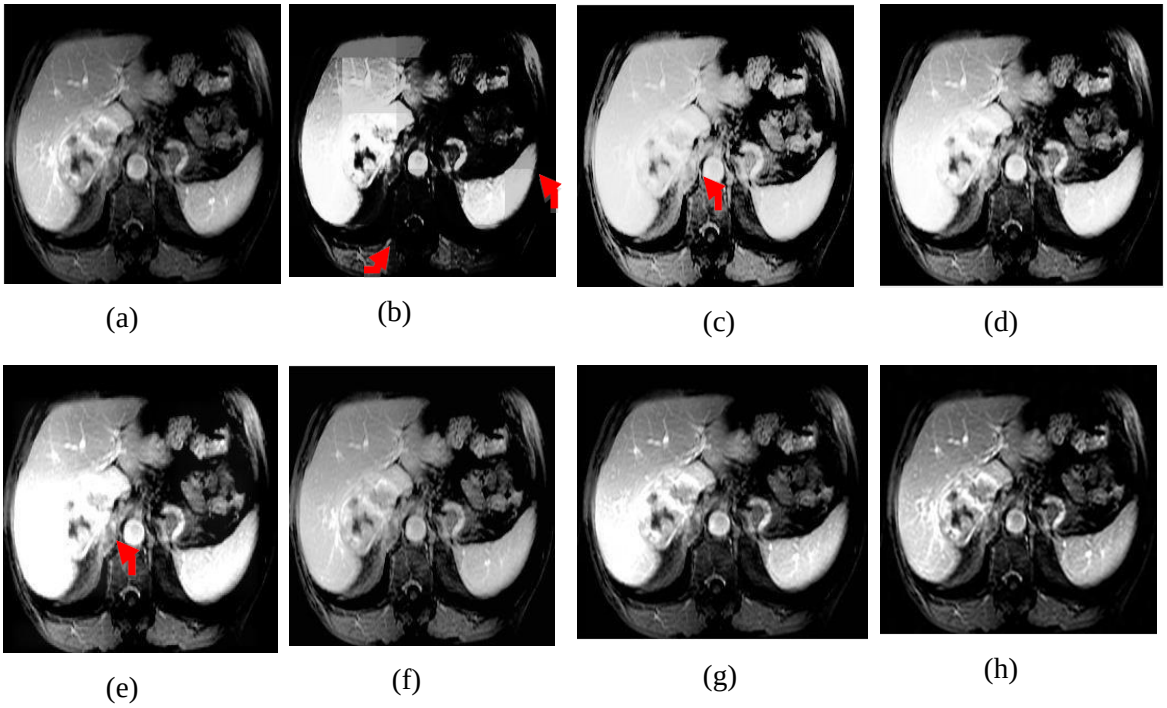

(a) (b) (c) (d)

(e) (f) (g) (h)

Figure 4.9: Experiment outcomes of the ‘CT-3’ Image (a) Original image, (b) S-curve, (c) AGC-DWT, (d) AGC-WHD, (e) GAGC-DWT, (f) EBCHE, (g) TCHE-DWT, (h) Proposed scheme

depicted in Fig. 4.10. In Fig. 4.10c, 4.10d, and 4.10e, it can be seen that the AGC-DWT, AGC-WHD, and GAGC-DWT approaches greatly outshone the average brightness of the original CT picture, effectively removing the glaring intensity disparity between various objects inside the CT image. Therefore, the improved outputs produced by these techniques are insufficient. As can be seen in Fig. 4.10b, the output images from the S-Curve technique suffer from blocking and intensity saturation artefacts, which compromise image quality. As expected, EBCHE is unable to significantly increase contrast in nearly all parts of the scene in Fig. 4.10f. The TCHE-DWT method results in a higher-quality image, as can be shown in Fig. 4.10g. However, as seen by the red arrow, some areas, notably the arteries, are artificially emphasised. The suggested algorithm outperforms the current six approaches by increasing contrast, keeping brightness, and keeping a natural look. Consequently, as illustrated in Fig. 4.10g, most items cannot be distinguished from the backdrop.

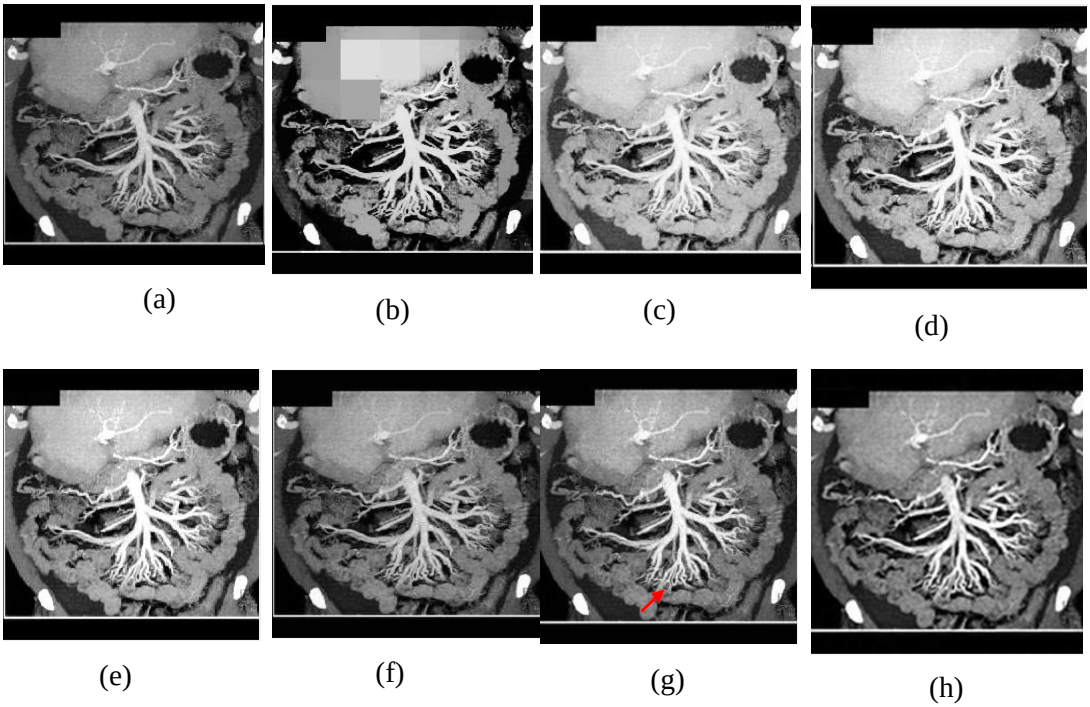

Figure 4.10: Experiment outcomes of the ‘CT-4’ Image (a) Original image, (b) S-curve, (c) AGC-DWT, (d) AGC-WHD, (e) GAGC-DWT, (f) EBCHE, (g) TCHE-DWT, (h) Proposed scheme

Figure 4.11 displays the 'CT -5' image, together with the results of the suggested method and the other six methods already in use to improve contrast. Fig. 4.11c and d demonstrate how the AGC-DWT and AGC-WHD techniques artificially enhanced the CT images, masking inconsequential details. As can be observed in Fig. 4.11e, the finer elements of the image were lost despite the GAGC-DWT method's best efforts to boost the contrast. Scars inside honeycomb-like tumours are more darkened and not better detected due to the inability of the EBCHE approach to boost contrast (red arrow in Fig. 4.11f). There's a lot of background noise in this technique. As can be observed in Fig. 4.11g, the contrast of the images was improved by the TCHE-DWT method, but the average brightness was lost. The improved photos contain distracting artefacts due to the S-curve method, as shown in Fig. 4.11b. As can be seen in Fig. 4.11h, CT scan pictures of the pancreas also benefit visually from the suggested methods. Also, the various tiny thin- walled cysts inside the tumor regions were enhanced correctly, resulting in an excellent visual comparison asshown in Fig. 4.11g.

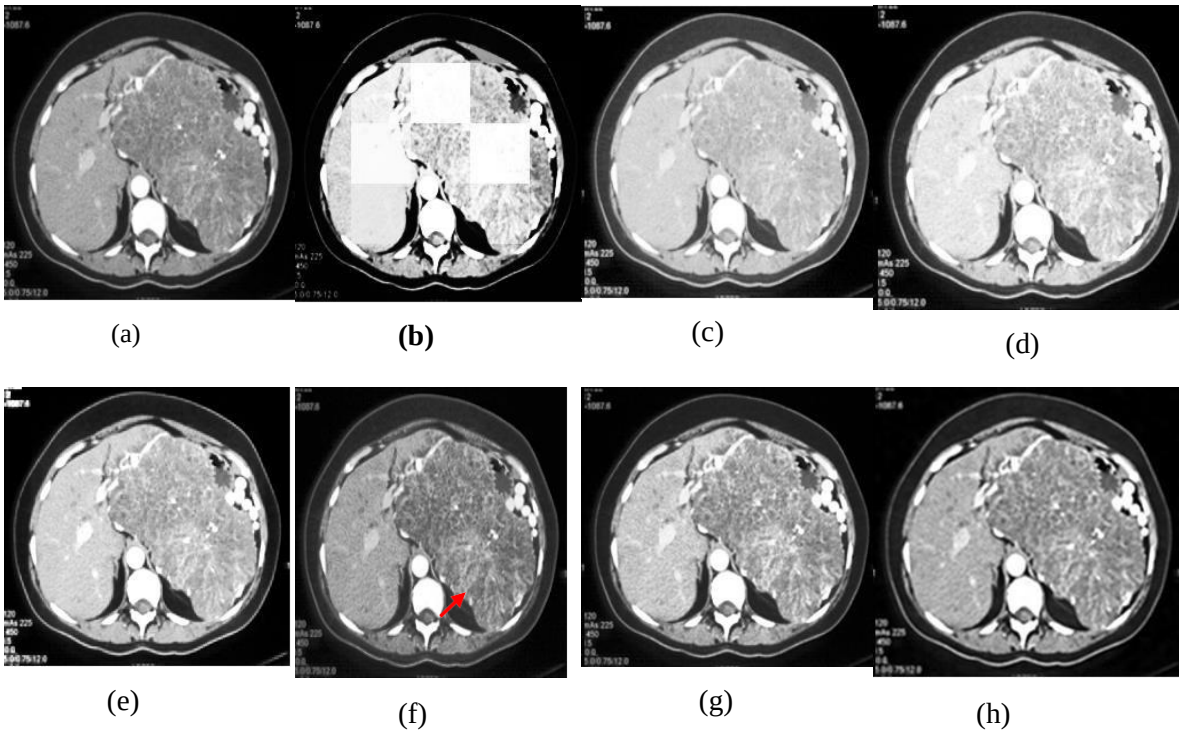

(a) **(b)** (c) (d)

(e) (f) (g) (h)

Figure 4.11**:** Experiment outcomes of the 'CT-6' Image (a) Original image, (b) S-curve, (c) AGC-DWT, (d) AGC-WHD, (e) GAGC-DWT, (f) EBCHE, (g) TCHE-DWT, (h) Proposed scheme

Figures 4.14 through 4.16 show the enhanced appearance of pictures in the CT-6, CT-7, and CT-8 scans, respectively. Visual inspection of the results from all three experiments indicates that the proposed enhancement procedure is the best method for boosting the contrast of CT photos without introducing any undesired defects, information distortion, brightness degradation, damage, noise enhancement, or unnatural appearance, as opposed to the other methods currently in use. From a visual comparison of the three outputs, it is clear that the suggested method successfully improves image clarity by suppressing unwanted noise without adding any jarring artefacts. Successful diagnosis is ensured by the preservation of fine details in the CT picture and the preservation of the image's average brightness.

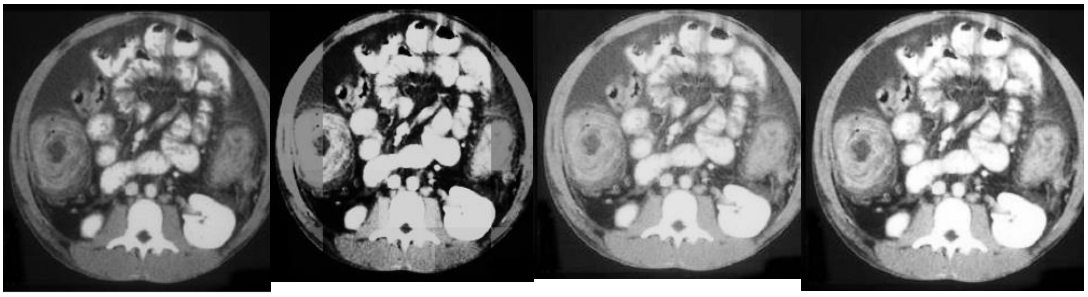

(a) (b) (c) (d)

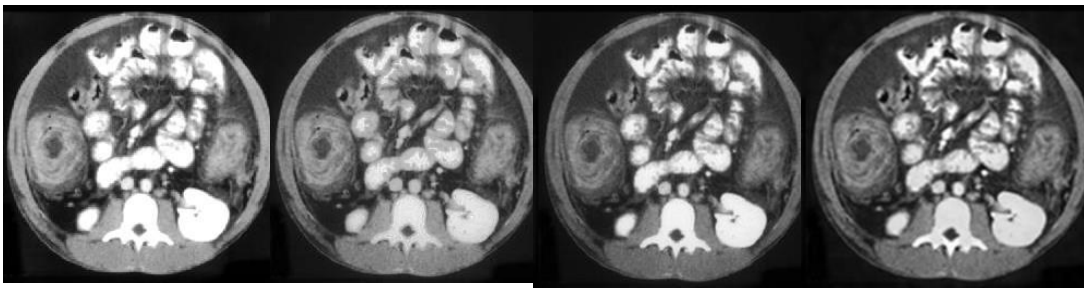

(e) (f) (g) (h)

Figure: 4.12 Experiment outcomes of the ‘CT-5’ Image (a) Original image, (b) S-curve, (c) AGC-DWT, (d) AGC-WHD, (e) GAGC-DWT, (f) EBCHE, (g) TCHE-DWT, (h) Proposed scheme

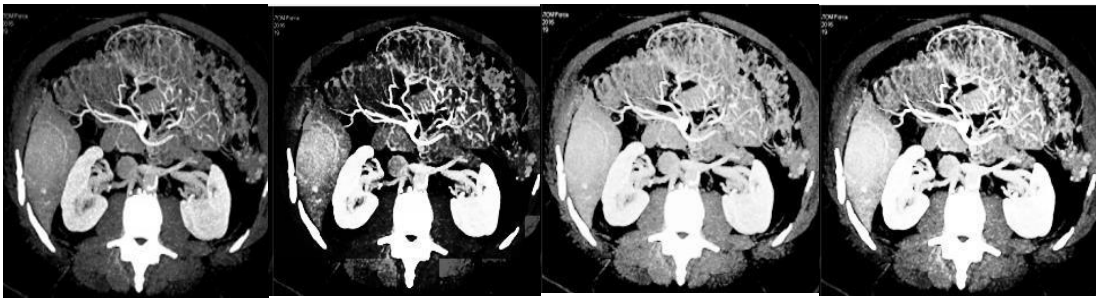

(a) (b) (c) (d)

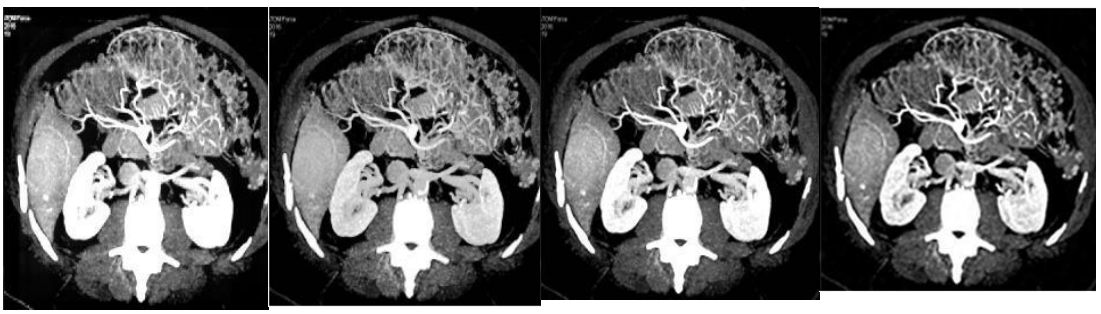

(e) (f) (g) (h)

Figure 4.13: Experiment outcomes of the ‘CT-7’ Image (a) Original image, (b) S-curve, (c)AGC-DWT, (d) AGC-WHD, (e) GAGC-DWT, (f) EBCHE, (g) TCHE-DWT, (h) Proposed scheme

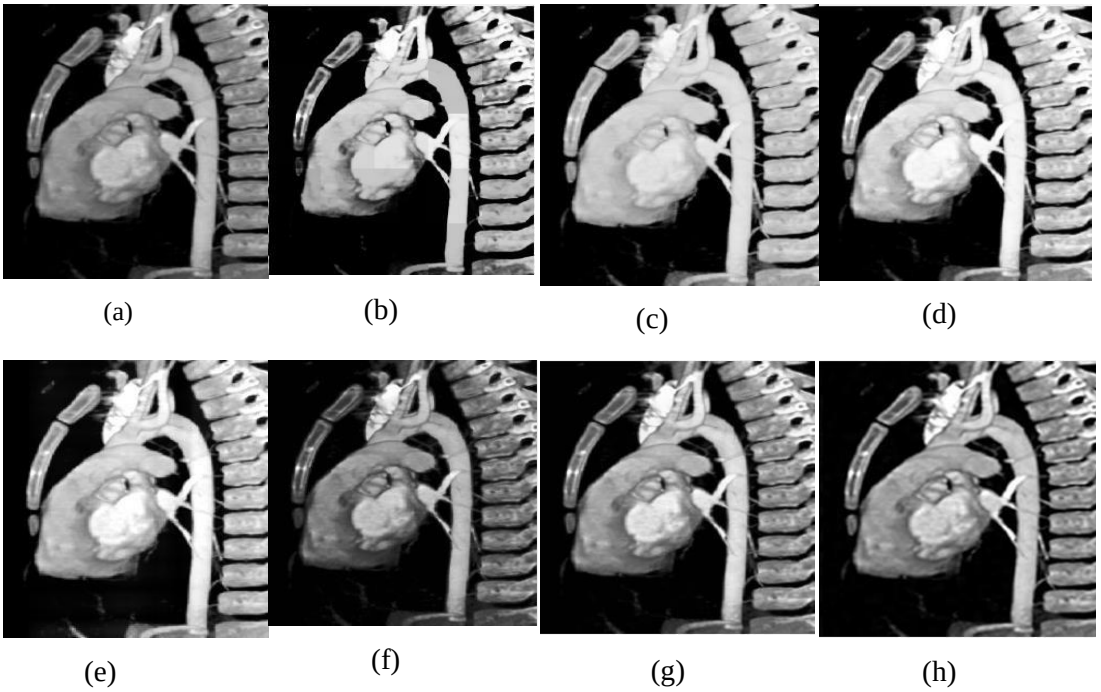

Figure 4.14: Experiment outcomes of the 'CT-7' Image (a) Original image, (b) S-curve, (c) AGC-DWT, (d) AGC-WHD, (e) GAGC-DWT, (f) EBCHE, (g) TCHE-DWT, (h) Proposed scheme

4.4.2. Quantitative (Objective) Assessment

The effectiveness of the proposed approach, which was defended in the previous section using the criteria laid out in the performance matrices section, may be measured quantitatively. Tables 4.1–4.5 provide optimal values for each metric, denoted by bold font.

Table 4.1 lists the entropy values for commonly used improvement methods. Using entropy, we may evaluate how much detail is present in a picture. The information contained in an image with a high entropy value is plentiful. Maximum entropy is sought after in contrast enhancement methods for the purpose of enhancing the finer details in a diagnostic image and enabling a precise diagnosis. Over-enhancement results in low entropy values for the S-curve methodology; for example, adrenal, gastrointestinal, and pancreas CT images only have entropy values of 5.40, 5.62, and 5.93, respectively. To illustrate, the entropy generated by the suggested method is 7.15 for the liver CT picture, 7.31 for the spleen CT image, and 7.10 for the pancreatic CT image, all of which are much higher than the entropy generated by the existing approaches. TCHE-DWT, on the other hand, produces the second highest values of 7.12, 7.26, and 7.05 for CT scans of the liver, spleen, and pancreas, respectively.

Therefore, it is superior to other existing contrast-enhancing technologies in that the original information content is preserved.

Table 4.1: Assessment of entropy outcomes

Image Name / Methods	Original	S-curve	AGC-DWT	AGC-WHD	GAGC-DWT	EBCHE	TCHE-DWT	Proposed scheme
CT-1	7.08	6.30	7.08	6.71	7.07	7.00	7.12	**7.15**
CT-2	7.37	6.81	7.47	7.08	7.38	7.27	7.45	**7.48**
CT-3	6.05	5.40	6.08	5.77	6.22	5.92	6.05	**6.33**
CT-4	6.32	6.05	6.15	6.13	**7.01**	6.19	6.51	6.59
CT-5	7.28	6.58	7.43	7.07	7.27	7.16	7.40	**7.50**
CT-6	6.30	5.62	6.29	5.91	6.67	6.17	6.32	**6.68**
CT-7	7.31	**7.62**	7.48	7.10	7.38	7.21	7.46	7.49
CT-8	7.00	6.77	7.09	6.79	7.19	6.87	7.26	**7.31**

Table 4.2 shows that compared to previous methods, the proposed method has a higher PSNR. In order to maximise PSNR, the suggested method minimises noise in the final image. This increases the likelihood of obtaining an artifact-free final product. All of the test CT scans improved in PSNR with the suggested method, from 26.04 for the stomach to 28.37 for the spleen and 26.81 for the small bowel and 27.13 for the pancreas. For comparison, EBCHE's second-best results for the stomach, spleen, small bowel, and pancreatic CT scans were 26,01, 26,60, and 26,86, respectively. The contrast of an image is enhanced when the PSNR is high. Image quality is improved and contrast is amplified because to the proposed method's high PSNR value.

Table 4.2: Assessment of PSNR outcomes

Image Name / Methods	S-curve	AGC-DWT	AGC-WHD	GAGC-DWT	EBCHE	TCHE-DWT	Proposed Scheme
CT-1	15.83	16.74	16.59	18.87	27.08	24.20	**27.13**
CT-2	15.90	16.69	14.87	16.67	**30.58**	24.45	27.10
CT-3	18.82	14.38	15.63	15.60	23.30	23.26	**30.56**
CT-4	18.93	15.96	15.89	15.85	23.94	25.89	**27.83**
CT-5	18.26	15.24	13.90	16.41	23.79	27.04	**27.88**
CT-6	18.47	14.65	14.84	17.34	23.01	24.67	**27.12**
CT-7	17.17	14.64	12.69	15.43	26.01	25.61	**26.04**
CT-8	16.99	13.64	13.77	16.53	26.60	26.40	**28.37**

Table 4.3 shows that the suggested method produces a higher CII value than the state-of-the-art enhancement techniques, 1.84, 1.46, and 1.60, respectively, for CT images of the kidney, adrenal gland, and heart. The proposed method enhances contrast while conserving important information in the CT image. Additionally, the CII of 1.34, 1.06, and 1.01 for renal, adrenal, and cardiac imaging, respectively, is higher for the S-curve method than for any other contrast-enhancement technique. Increases in CII show that the suggested method improves diagnostic value by increasing image contrast, structural data, and fine features in the final CT picture.

Table 4.3: Assessment of CII outcomes

Image Name / Methods	S-curve	AGC-DWT	AGC-WHD	GAGC-DWT	EBCHE	TCHE-DWT	Proposed scheme
CT-1	1.61	0.85	1.31	1.03	**2.10**	1.32	1.62
CT-2	1.34	0.79	1.34	1.30	1.24	1.14	**1.84**
CT-3	1.06	0.99	1.04	0.89	0.76	0.92	**1.46**
CT-4	1.01	0.95	1.04	0.78	1.03	0.92	**1.60**
CT-5	**1.92**	0.97	1.13	1.17	0.93	0.89	1.27
CT-6	1.20	0.93	1.04	0.97	0.99	0.95	**1.53**
CT-7	1.05	0.78	1.45	1.70	1.78	1.32	**1.80**
CT-8	1.67	0.90	1.12	0.96	1.15	1.10	**1.74**

Compared to the other methods, the suggested method yields an EME value that falls somewhere in the middle, as shown in Table 4.4. The proposed method, which employs a moderate EME value of 24.21 or 23.27 for liver and kidney CT images, promises to generate an output free of undesirable artefacts while producing a picture with a suitable level of enhancement. It is observed that the proposed method yields an EME value that falls somewhere in the middle of the spectrum when compared to other accessible contrast enhancement solutions. Over-enhancement occurs at extremely high EME values, which have been demonstrated to be unsuitable for medical analysis (for example, 38.57 and 41.70 for the liver and kidney using the S- curve approach). Since the EME is so low, no discernible improvement in obscured image details is made (for instance, 12.83 and 13.29 for liver and kidney using the AGC-DWT approach). The proposed method's EME values are moderate, falling within the allowable range for such performance metrics as mean and standard deviation.

Table 4.4: Assessment of EME outcomes

Image Name / Methods	S-curve	AGC-DWT	AGC-WHD	GAGC-DWT	EBCHE	TCHE-DWT	Proposed scheme
CT-1	38.57	12.83	17.84	18.89	27.41	24.39	**24.21**
CT-2	41.70	13.29	17.80	18.99	25.31	23.48	**23.27**
CT-3	22.19	5.21	7.32	20.65	40.64	34.34	**8.59**
CT-4	35.77	8.78	11.14	25.80	43.33	41.78	**18.86**
CT-5	39.78	13.33	16.99	19.42	21.91	22.56	**22.93**
CT-6	48.51	9.23	11.24	28.18	55.17	27.74	**11.32**
CT-7	52.50	18.58	25.18	23.44	33.93	26.88	**27.18**
CT-8	54.07	18.27	23.79	23.69	36.73	26.52	**21.32**

Table 4.5 displays the average value of 200 CT image-based measurements for both the proposed and existing methods. The suggested method outperforms the TCHE-DWT, GAGC-DWT, AGC-DWT, EBCHE, AGC-WHD, and S-curve contrast enhancement algorithms, with a maximum average Entropy of 7.15 versus 7.10, 7.09, 6.96, 6.86, 6.70, and 6.52. Non-contrast CT images enhanced using the suggested technique have an average maximum PSNR of 27.78 dB, which is an improvement over the maximum PSNRs of 26.81 dB and 25.81 dB achieved using the EBCHE and TCHE-DWT methods, respectively. The proposed strategy had better results according to the CII assessment parameter. In addition, the proposed method had an average CII of about 1.67, while the AGC-DWT method only managed 0.90. The proposed method's EME value of 17.52 is about in the middle of the range when compared to previous contrast enhancement techniques.

Table 4.5: Average measures values for 200 CT images

Methods/Measures	Entropy	PSNR	CII	EME	MC	WC
S-curve	6.52	16.52	1.42	38.29	0.36	0.29
AGC-DWT	6.96	15.88	0.90	12.14	0.28	0.21
AGC-WHD	6.70	14.50	1.26	16.14	0.34	0.26
GAGC-DWT	7.09	16.67	1.29	18.25	0.32	0.24
EBCHE	6.86	26.81	1.54	33.37	0.40	0.28
TCHE-DWT	7.10	25.81	1.30	25.17	0.37	0.26
Proposed scheme	**7.15**	**27.78**	**1.67**	**17.52**	**0.42**	**0.32**

Over-enhancement is indicated by extremely high EME values, such as 38.29 for the S-curve, 33.37 for the EBCHE, and 25.17 for the TCHE-DWT. On the other hand, extremely low EME values for AGC-DWT, AGC-WHD, and GAGC-DWT (12.14, 16.14, and 18.25, respectively) show that few, if any, of the picture's concealed details were improved.

Measurements in Michelson contrast (MC) and Weber contrast (WC), as shown in Eqs. (24)-(26), are also gathered to assess the performance of the proposed method alongside entropy, EME, PSNR, and CII (25). A greater WC and MC value indicates a more noticeable difference. The proposed method yields the highest average Michelson and Weber contrast ratios of any compared enhancement strategy, at 0.42 and 0.32, respectively. In this way, the suggested technique improves its accuracy in enhancing contrast while preserving fine characteristics. The results show that the proposed method, enhanced by the proposed indices, can successfully process a wide range of CT medical images.

4.5.Summary

Using a DT-CWT technique and flexible morphology for effective high-frequency sub-bands denoising and low-frequency sub-bands enhancement, this work introduces a new method for enhancing non-contrast CT images. For the purpose of quantitatively and qualitatively assessing the effectiveness of the suggested approach, experiments were performed on a variety of CT scan pictures. Moreover, investigations on CT image datasets demonstrate unambiguously that the suggested methodology excels in improving and maintaining fine information free of noise, as compared to other standard enhancement strategies. All previously obscured details are now readily apparent, and the proposed algorithm preserves image brightness while increasing contrast and decreasing noise levels in CT scans. When compared to state-of-the-art enhancement techniques, the suggested methodology performs better on measures of signal-to-noise ratio, entropy, a contrast improvement index, and enhancement metrics. The proposed method is well-suited for improving CT images and could be utilised to aid in the accurate diagnosis of disease by pathologists and doctors.

CHAPTER 5

RETINEX-CENTERED CONTRAST ENHANCEMENT METHOD FOR HISTOPATHOLOGY IMAGES WITH WEIGHTED CLAHE

5.1. Introduction

Histopathological images have been found to have poor visibility in pathology testing due to a lack of brightness and contrast. Improving their quality while still retaining their inherent traits is essential for initial identification and further research. In this study, a unique method is introduced for enhancing the contrast of colour histopathology images using the principles of retina theory and local contrast modification. To begin, the V channel is extracted from the input image using the HSV color space [54]. Next, a novel technique known as multiscale retinex with adaptive weighting (MSRAW) is introduced, which is applied to the V channel. The MSRAW method combines the outputs of multiple single-scale retinexes (SSRs) in a way that adaptively determines the weights for each SSR scale based on the strength and weakness of their corresponding outputs from the value channel image. Subsequently, the L*a*b* color space [70] is employed to obtain the luminosity channel. Contrast Limited Adaptive Histogram Equalisation (CLAHE) is a widely-used technique in image processing that enhances local contrast while avoiding over-amplification of noise. Here, the novel weighted contrast limited adaptive histogram equalisation (WCLAHE) technique is utilized by merging the two CLAHE outputs corresponding to the larger and lower clip limits. The primary objective of the WCLAHE technique is to enhance local histopathological details effectively. Through this multi-step process, proposed method enhances the contrast of color histopathology images, ensuring improved visibility of crucial histopathological details for accurate diagnosis and further research.

This study compares the provided technique both aesthetically and numerically with other pre-existing algorithms. The suggested method surpasses all other conventional ways and generates higher-quality histopathology images, which is notably helpful for diagnosis, as evidenced by visual and quantitative findings on a variety of test images.

Although the contrast enhancement methods described in Chapter 2 are helpful in a variety of contexts, their results are frequently unsuitable for medical images because of the presence of multiple defects, colour degradation, noise amplification, under or

over enhancement, brightness degradation, and information distortion. To improve contrast in histology images without introducing colour distortion or over-enhancing, the current work developed a unique contrast enhancement strategy for colour histopathology images based on retinex theory and local contrast modification.

The following are the key contributions of this proposed method:

- Adaptive weighting for the multiscale retinex is used in the MSRAW approach, which is recommended to improve the overall contrast of histopathology pictures.
- Through combining the results of the two CLAHE processes, the WCLAHE approach was suggested in the paper to enhance the specificity of local histology.
- To improve contrast both globally and locally, the proposed technique combines MSRAW and WCLAHE.

5.2. Proposed Retinex-Centered Contrast Enhancement Method for Histopathology Images with Weighted CLAHE

The proposed method [125] consists of two successive actions: To improve the contrast of histopathology pictures as a whole, the MSRAW technique is suggested, whereas WCLAHE is used to extract localised details. MSRAW initially processes only the V channel in the HSV colour model [54], therefore no colour correction is necessary. The approach aimed to integrate many SSR-result photos in such a way that the weight corresponding to each SSR scale is determined adaptively from the content of the value channel, taking into account the strengths and weaknesses of each. The goal of the method was to aggregate the results of multiple SSRs such that the relative importance of the various SSR outputs could be determined adaptively from the content of the value channel. Then, the luminosity channel of the L*a*b* colour model [70] is used to improve local image quality by enhancing local contrast; this new WCLAHE method enhanced the local details in histopathology by fusing the CLAHE outputs corresponding to the large and lower clip limits, avoiding over enhancement, noise amplification, and colour distortion. These two methods considerably improve low contrast histopathology photos by increasing overall contrast while maintaining mean brightness, maintaining a realistic appearance, and optimising entropy. The block diagram of our suggested approach is shown in Fig.5.1.

5.2.1. Retinex Theory

The essential idea behind retinex is that the input picture S is a pixel-by-pixel combination of the input image's reflectance element R and its illumination element L, which may be written in the form below. [72]:

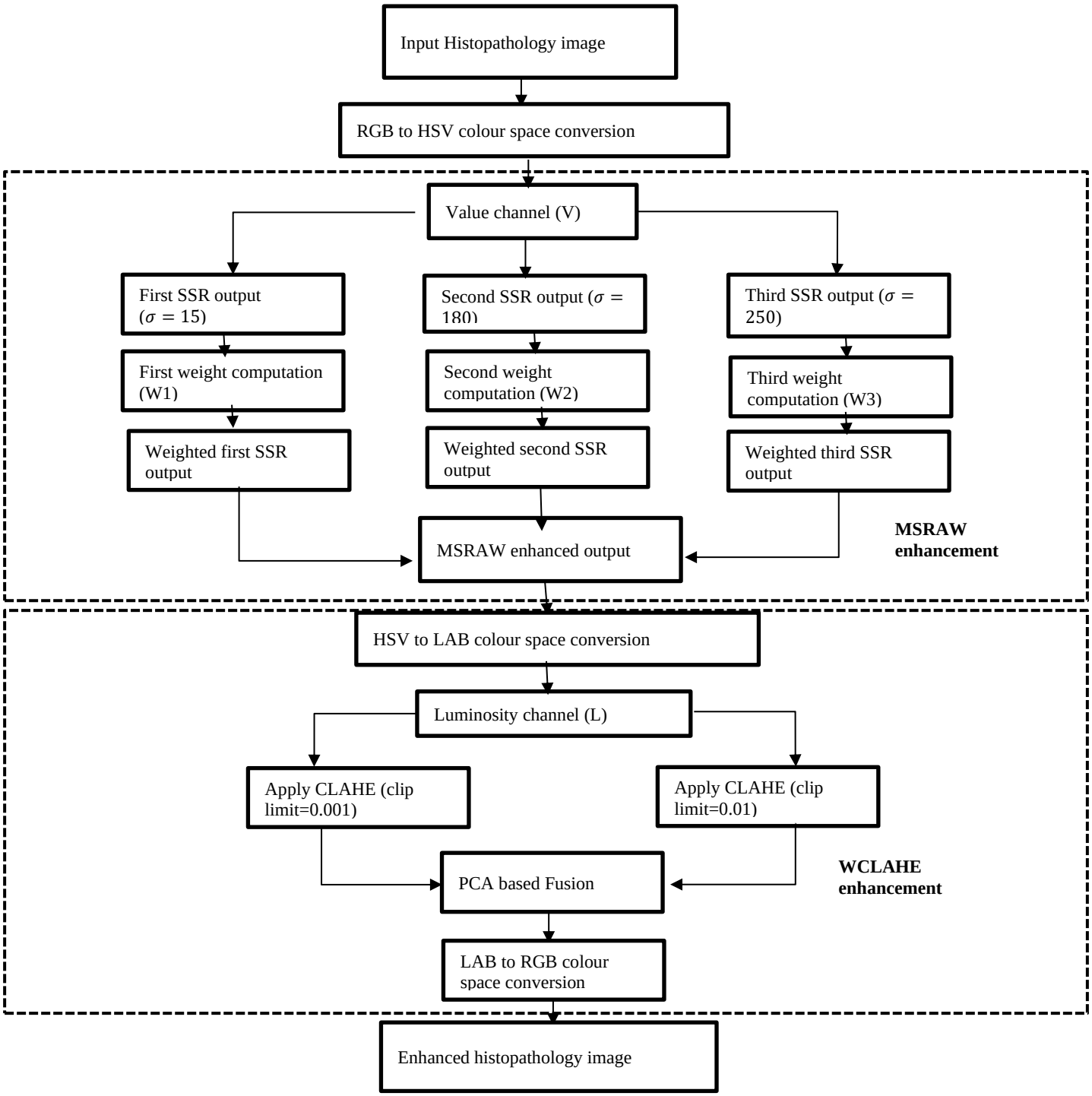

Figure 5.1: Block diagram of proposed retinex-centered contrast enhancement method for histopathology images with weighted CLAHE

$$S(x,y) = R(x,y) * L(x,y) \tag{5.1}$$

According to the retinex theory, the colour of an object's reflection is entirely dependent on the colour of the light shining on the object. Retinex-based picture improvement relies on acquiring the reflectance component R by removing the light component L. The SSR can be calculated using the following formula:

$$r_i(x,y) = \log R_i(x,y) = \log S_i(x,y) - \log L_i(x,y) \tag{5.2}$$

where i denotes the R, G, and B color channels. The lighting component $L(x,y)$ is approximated using a surround function $F(x,y)$ in the following manner: where i indicates the color components R, G, and B. The illumination element $L(x,y)$ is calculated by utilizing a surround function $F(x,y)$ as:

$$L_i(x,y) = F(x,y) * S_i(x,y) \tag{5.3}$$

where * signifies an operator for convolution. $F(x,y)$ is expressed as follows using a Gaussian filter:

$$F(x,y) = K\ exp\left(-\frac{x^2+y^2}{2\sigma^2}\right) \tag{5.4}$$

Where K is a constraint factor and it confines that

$$\int\int F(x,y)\,dxdy = 1 \tag{5.5}$$

Based on [4], the standard deviation parameter determines the trade-off between colour accuracy and dynamic range compression. The Multiscale retinex (MSR) technique, which integrates the findings of multiple SSRs, was proposed to achieve this equilibrium. The mathematical expression for MSR is:

$$r_{MSR_i} = \sum_{n=1}^{N} w_n[\log S_i(x,y) - \log(F_n(x,y) * S_i(x,y)] \tag{5.6}$$

where N denotes the number of scales and w_n denotes the weighting factor associated with each scale. Three different image scales are employed: large, medium, and small, and obtain $F_n(x, y)$ as follows:

$$F_n(x, y) = K_n \exp\left(-\frac{x^2 + y^2}{2{\sigma_n}^2}\right) \tag{5.7}$$

In order to achieve harmony in several dimensions, MSR uses a number of different zoom levels, each of which produces some degree of colour distortion. Jobson et al. [34] proposed multi-scale retinex with colour restoration (MSRCR) to improve upon MSR's already impressive colour performance. MSRCR makes use of the following colour recovery function:

$$r_{MSRCR_i} = c_i(x, y) r_{MSR_i}(x, y) \tag{5.8}$$

Where c_i (x, y) is the colour restoration function for the R, G, and B channels, respectively.

Figures 5.2 illustrates of MSR-based image enhancement applied to histopathology pictures. Histopathology image obtained from one of the databases, shown here as Fig. 5.2(a). Figures 5.2(b), 5.2(c), and 5.2(d) depict the SSR outputs for = 15, 180, and 250, respectively, while Figure 5.2(a) displays the result of the enhancement based on MSR (e). To improve image contrast, a small-scale SSR output reduces colour saturation, over-enhances bright portions (as shown by the black circles in Fig. 5.2(b), and introduces artefacts, as shown in Fig. 5.2. On the other hand, as seen by the black circle in Fig. 5.2, increasing the scale has the opposite effect, maintaining the colour tone rendering but amplifying the noise in the dark areas (d). To reach a satisfactory compromise, a retinex of intermediate scale is typically used, as depicted in Fig. 5.2(c). However, it is still a challenge to find the optimal scale, which can vary from image to image. MSR is an enhanced form of SSR that combines the positive aspects of small-, medium-, and large-scale retinex to achieve tonal stability and a decrease in dynamic range. To obtain acceptable picture augmentation and colour tone rendition [8, 9], a combination of three different scales (n = 15, 80, and 250) with equal weighting (wn = 1/3) is suitable for most photos (see Fig. 5.2(e)). However, MSR provides an artificial

image in which the overall brightness is diminished and amplifies the noise contained within a large dark patch. The results of these tests indicate that histopathological images with complex backgrounds, high grey scale image intensities, and dark sections do not benefit from the use of multiscale retinex.

Histopathological images with complex backgrounds, high grey-scale image intensities, or dark patches are not good candidates for retinex.

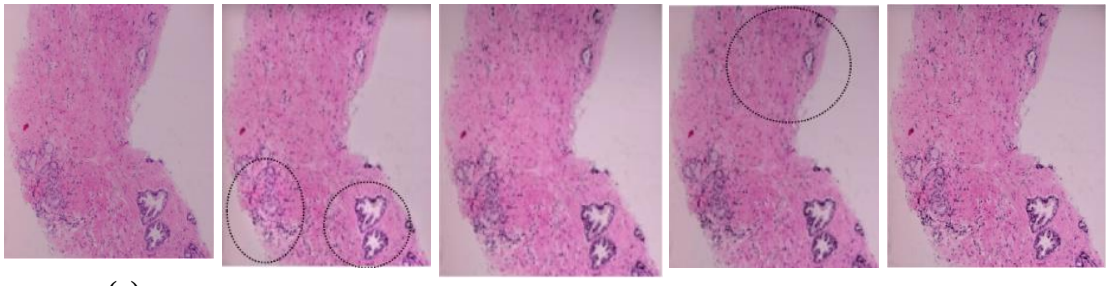

(a) (b) (c) (d) (e)

Figure: 5.2 (a) Original test histopathology image (b) SSR output ($\sigma = 15$) (c) SSR output ($\sigma = 80$) (d)SSR output ($\sigma = 250$) (e) MSR output

5.2.2. Proposed MSRAW Method

The goal of this piece is to introduce an MSRAW technique for improving the contrast of histopathology images. MSRAW aimed to improve upon conventional MSR by combining the outputs of several SSRs in such a way that the weight assigned to each SSR scale is decided adaptively from the data in the input image according to the relative merits of the SSRs' contributions. To avoid the requirement for colour correcting, the proposed MSRAW only processes the HSV colour space's V channel at the outset [14]. The following is an expression of the proposed MSRAW method:

$$r(x,y) = \sum_{n=1}^{N} W_n[\log V(x,y) - \log(F_n(x,y) * V(x,y)] \tag{5.9}$$

The brightness values of all pixels in a picture are represented by three sigmoid functions, which are defined as adaptive weight functions for each SSR output in this approach. These three adaptive weights W1, W2, and W3 are shown in Fig. 5.3 for the SSR outputs 15, 180, and 250 respectively. As can be seen in Fig. 5.3, the Sigmoid midpoints (80, 100, and 150) are uniformly spread across the brightness range [0, 255],

representing the low-gray class, the medium-gray class, and the bright-high grey level class, respectively. Here is how the sigmoid-based adaptive weight functions are formulated for each SSR output:

$$w_n(x,y) = C_1 + \left(-\alpha/1 + \exp\left(-\beta * \frac{(S_n(x,y) - M)^{C_3}}{C_2} \right) \right) \tag{5.10}$$

and

$$S_n(x,y) = \log V(x,y) - \log(F_n(x,y) * V(x,y), \quad n = 1,2,3 \tag{5.11}$$

Where α is the maximum value of the resulting weight function curve, and where the maximum value of the resulting sigmoid function increases as α increases. The parameter β defines the steepness of the weight function curve. For instance, a low β value of causes the weight function curve to approach a straight line, whereas a β high value causes the curve to get steeper.

The parameter M defines where in the brightness range 0–255 the weight function curve's midpoint lies. Smaller values of M imply a lower midpoint, while bigger values indicate a maximum midpoint. Furthermore, the variables C1, C2, and C3 are used to determine weight functions, where C1 is an additive parameter that helps further define the maximum value of the curve as a sigmoid curve. For even more nuanced control over the degree of steepness of the curve, C2 can be employed. The C3 can be used to generate a sigmoid function that can be utilised as a bandpass curve by setting both ends of the curve to 0. When these variables are adjusted, new sigmoid functions are generated.

The parameter α are set to 1, M and C are both set to 80, and the values for C1, C2, and C3 are set to 1, 10, and 1 respectively to produce the initial weight function (w1) matching to the SSR output with the scale 15. The parameters, M, C1, C2, and C3 are set to 2, 1, 100, 2, 350, and 2, respectively, for the second weight function (w2) that corresponds to the SSR output with a scale of 180. For the third weight computation (w3), we use the following values for, M, C1, C2, and C3: -1, 0.8, 150, 0, 10, and 1. The weight function curves displayed in Fig.5.3 are computed using the fixed parameter values chosen based on experimental observation in order to selectively crop the images for SSR processing to include just the necessary pixels.

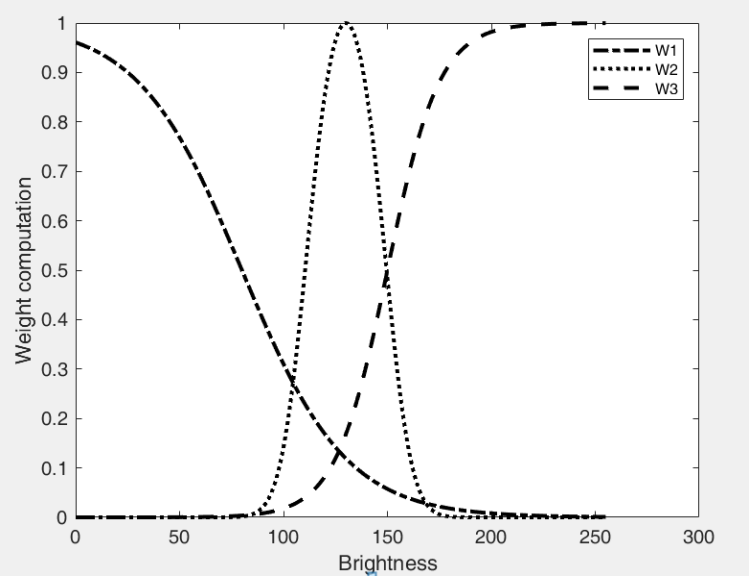

Figure. 5.3 illustrates three adaptive weights with scales of 15, 180, and 250 for each of the SSR outputs

Since problems like over-enhancement in bright areas are common in histopathological pictures, the first adaptive weight function (w1), which corresponds to the SSR output with scale 15, is designed to prioritise low grey levels. The third adaptive weight (w3), which is associated with the scale value of 250, is intended to give the least amount of importance to low-frequency grey levels. This is done to prevent noise enhancement in the dark grey areas. To better bring out finer features in histopathology images, the second weight (w2) associated with scale 180 is meant to add a substantial weight to the mid-grey level. The following notation can be used to express these three weight functions after they have been further normalised for use in Eq.5.12:

$$W_n(x,y) = \frac{w_n}{\sum_{n=0}^{3} w_n} \tag{5.12}$$

The weight maps depicted in Fig. 5.4 represent the relative importance of each grayscale value in the image depicted in Fig. 5.2 (a). It's clear that the input value image's grayscale will determine the weight assigned to each pixel. It's also interesting to note that the weight map for small scale SSR (W1) assigns greater importance to darker shades of grey. In contrast, the largest weights for grey levels may be found in the brightest regions (W3) of the scaled spatial sensitivity map, and the smallest weights can be found in the finest details (W2) of the scaled spatial sensitivity map.

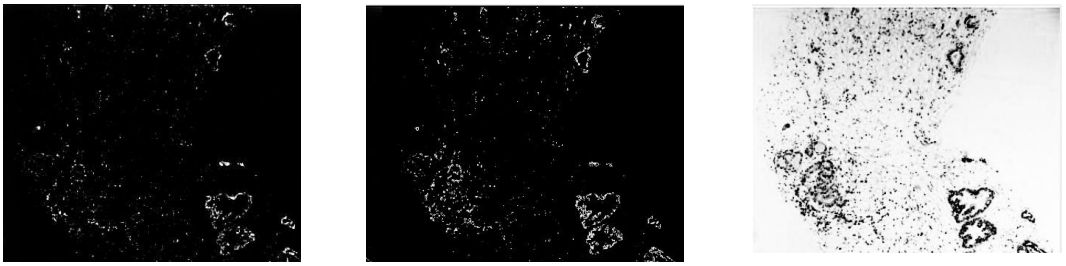

(a) (b) (c)

Figure: 5.4 Weight maps associated with the SSR output images are shown (a) W1 (b) W2 (c) W3

5.2.3. **Proposed WCLAHE Method**

In histopathology photos, the WCLAHE technique is used to highlight local material in order to improve both local and global contrast. The CLAHE works to increase local contrast by dividing the input image into smaller sections (called tiles) and then equalising the histogram inside each tile. At a fixed clip limit value, the local enhancement produced by conventional CLAHE [46] is always subpar. As can be shown in Fig. 5.5, it provides unsatisfactory results in medical picture enhancement because to its low local enhancement at low clip limits and excessive enhancement and colour distortion as the clip limit increases. Experimental studies of a wide variety of clinical images form the basis for clip limitations in medical image enhancement algorithms [16,19-33, 22,25].

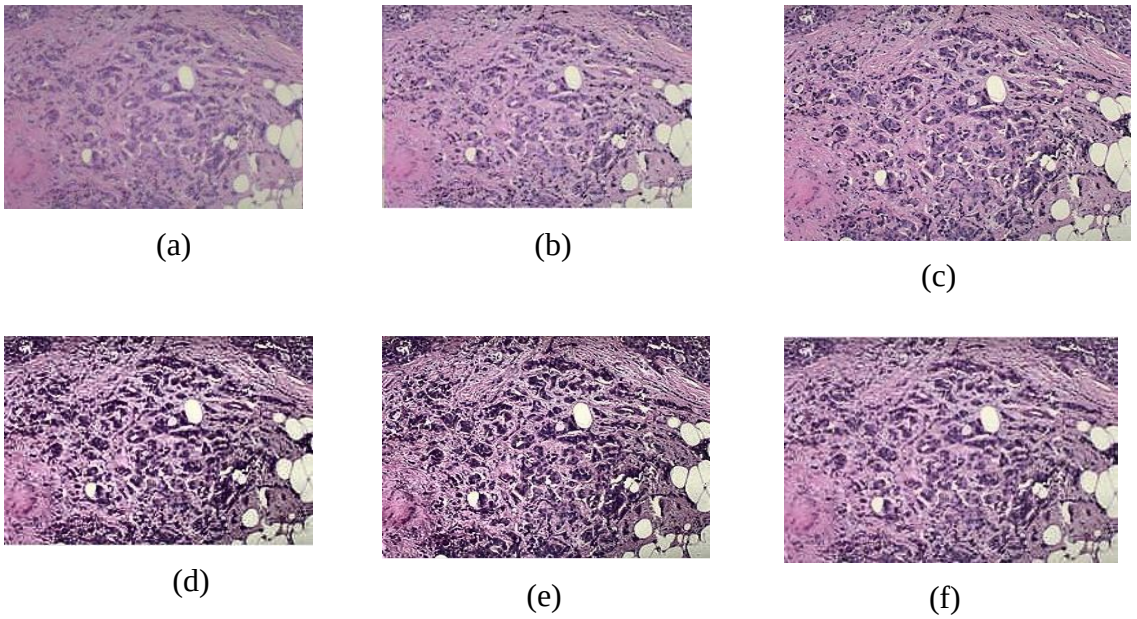

(a) (b) (c)

(d) (e) (f)

Figure: 5.5 (a) Original test histopathology image (b) CLAHE output image (clip

limit=0.001) (c) CLAHE output image (clip limit=0.01) (d) CLAHE output image (clip limit=0.1) (e) CLAHE output image (clip limit=0.3) (f) WCLAHE enhanced image

As can be seen in Fig. 5.5(b), Fig. 5.5(c), Fig. 5.5(d), and Fig. 5.5(e), the experimental results of this study show that the CLAHE approach provides inadequate local enhancement at low clip limits and generates over-enhancement in bright areas with an increase in clip limit, resulting in complete distortion of small details in high-pixel areas and colour distortion (e). When using a large clip limit, which CLAHE does, the output histopathological images gain noise, but the contrast is improved. Histopathological pictures generated using the CLAHE method, as a result, display an increase in noise, a distortion of the bright areas, a decrease in the overall brightness, and an alteration in colour.

As can be shown in Fig. 5.5 (f), by combining the CLAHE outputs corresponding to the large and lower clip limits, one can effectively govern over enhancement, mean brightness preservation, and noise, leading to better natural local enhanced histopathology images. Therefore, histopathology pictures benefit from a weighted CLAHE technique applied to boost local contrast. Using the free CLAHE toolbox in MATLAB, two outputs with clip limits of 0.01 and 0.001 are generated, and method set the number of tiles to 8.

Extensive testing with a large number of histopathological images led to the establishment of these two fixed clip limit values. A clipping threshold of 0.001 is being considered since it has been found to be optimal with respect to colour distortion and excessive enhancement, and going any lower produces an image that is indistinguishable from the original. Due to the fact that extending the clip limit past the value of 0.1 causes widespread colour and information distortion, this value has been settled upon as the maximum allowable clip limit.

In order to perform CLAHE on the luminance channel and prevent colour distortion in colour histopathology photos, the resulting MSRAW image is first transformed into L*a*b* colour space [54]. Using an image fusion method to mix the necessary data from several sub-pictures is an effective way to integrate the distinguishing characteristics of images. Multiresolution approaches, such as the wavelet transform and Laplacian pyramid breakdown, may produce satisfactory results in picture fusion [114], but they are computationally demanding and susceptible to noise interference. The weighting factors for combining the two CLAHE luminance channel outputs were

calculated using the Principal Component Analysis (PCA) in the proposed WCLAHE algorithm. Finding the principle components of input images and the weights of the source images to be fused based on principal components requires computing the feature vectors of the source images and the related feature values [115]. The PCA method is depicted in Fig. 5.6. As there are two different images serving as sources, the outputs of the C1 and C2 luminance channels of CLAHE are each represented by an n-dimensional vector denoted by the symbol Xp, where p is either 1 or 2. Here is how the image-combining process goes::

***Step:1*:** Using the source images, create matrix X.

$$X = \begin{bmatrix} x_{11} & \cdots & x_{21} \\ \vdots & \ddots & \vdots \\ x_{1n} & \cdots & x_{2n} \end{bmatrix} = [x_1, x_2] \tag{5.13}$$

***Step:2*:** Calculate the X data matrix's covariance matrix C.

$$C = \begin{bmatrix} \sigma_{11}^2 & \sigma_{12}^2 \\ \sigma_{21}^2 & \sigma_{22}^2 \end{bmatrix} \tag{5.14}$$

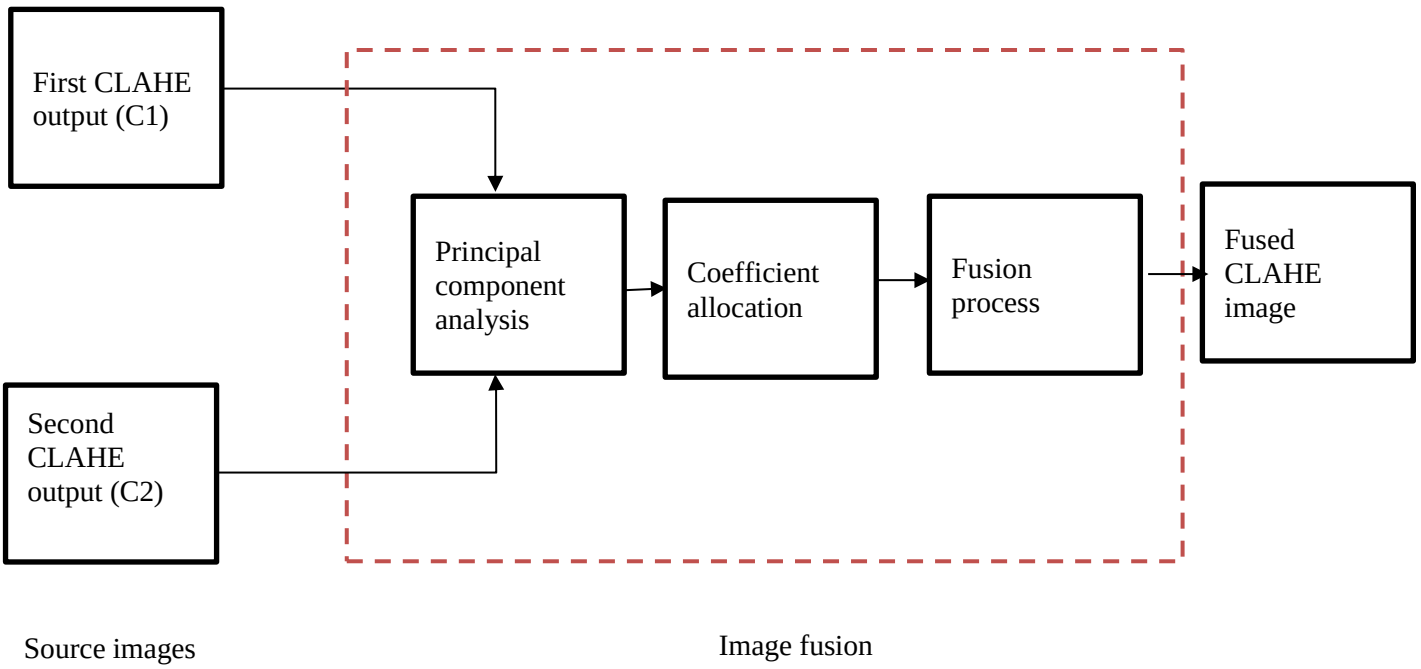

Figure. 5.6 PCA based image fusion process

σ_{ij}^2 is the image's covariance, which meets the following conditions:

$$\sigma_{ij}^2 = \frac{1}{n}\sum_{i=1}^{n}\left(x_{i,l} - \overline{x_i}\right)\left(x_{j,l} - \overline{x_j}\right) \quad (5.15)$$

$\overline{x_i}$ is the i th source image's average grayscale value.

Step:3 Construct the eigenvalue equation $|\lambda \mathrm{I} - \mathrm{C}| = 0$ and compute the eigenvalue (λ_1, λ_2) and feature vector (ξ_1, ξ_2) of the covariance matrix C, where ξ is a two-dimensional vector $\begin{bmatrix}\xi_1 \\ \xi_2\end{bmatrix}$

Step:4 Choose a higher eigenvalue.

$$p = \arg\max(\lambda_p) \qquad p = 1 \; or \; 2 \quad (5.16)$$

Step:5 Utilizing the feature vector associated with the largest eigenvalue, calculate the weight coefficient.

$$W1 = \frac{\xi_{i1}}{\xi_{i1} + \xi_{i2}} \quad (5.17)$$

and

$$W2 = \frac{\xi_{i2}}{\xi_{i1} + \xi_{i2}} \quad (5.18)$$

Step:6 Fuse the two CLAHE luminance resultant images and find the merged enhanced luminance channel as follow

$$F = W_1 C_1 + W_2 C_2 \quad (5.19)$$

Where $C_1$and C_2 are the two CLAHE luminance channel outputs.

Step:7 To obtain the final enhanced histopathology image, the fused enhanced luminance channel is transferred back to RGB space.

Fig 5.7 shows the intermediate steps of the proposed algorithm as part of the overall process for illustrating detailed steps involved in the process. The detailed steps for implementation of proposed algorithm are provided in Algorithm 1.

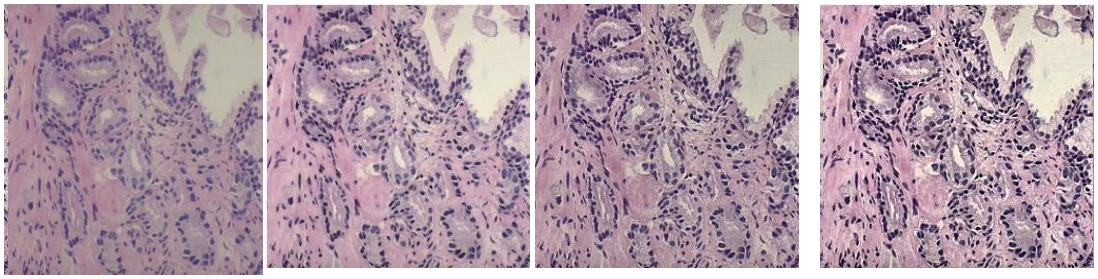

(a) (b) (c) (d)

Figure 5.7**:** Middle phases of the proposed method (a) Input images, (b) luminosity enhanced image, (c)contrast enhancement on original image, (d) contrast enhancement on luminosity enhanced image (5.6(b))

Algorithm 1:

Input: Input RGB color histopathology image J , clip limits(CL_1=0.001, CL_2=0.01)

, Output: Enhanced image I_{out}

1: Color space conversion: V ← RGB to HSV (J)

2: For each pixel calculate

3: $S_n(x,y) = log\, V(x,y) - log(F_n(x,y) * V(x,y), \quad n = 1,2,3$

4: $w_n(x,y) = C_1 + \left(-\alpha/1 + \exp\left(-\beta * \frac{(S_n(x,y)-M)^{C_3}}{C_2}\right)\right)$

5: Normalization: $W_n = \frac{w_n}{\sum_{n=0}^{3} w_n}$

6. $r(x,y) = \sum_{n=1}^{N} W_n[\log V(x,y) - \log(F_n(x,y) * V(x,y)]$

6: end

7: Color space conversion: I ← HSV to RGB (r)

8: Color space conversion: L← RGB to LAB (I)

9: Compute I $_1$*← CLAHE (L,* CL_1*)*

10: Compute I $_2$*← CLAHE (L,* CL_2*)*

11: w $_n$*←PCA based Weight computation*

12: Normalization: $W_n = \frac{w_n}{\sum_{n=0}^{3} w_n}$

13: Fusion: $Y = \sum_{n=1}^{2} W_n * I_n$

14: Color space conversion: Iout ← LAB to RGB (Y)

5.3.Datasets

Different histopathological photos obtained from various open-source databases are used to evaluate and validate the suggested approach. The first available dataset is housed at the University of California, Santa Barbara's Center for Bio-Image Informatics (https://bioimage.ucsb.edu/research/bio-segmentation). This data set is part

of a larger bio segmentation benchmark collection maintained by the University of California, Santa Barbara. Images of breast cancer tissues stained with hematoxylin and eosin (H&E) in RGB colour space. The University of Washington's Department of Laboratory Medicine and Pathology provides access to a second dataset of histopathology photos (https://dlmp.uw.edu/resources/education-gallery). Hundreds of histopathology photos from a wide range of patients are included in this dataset. Hundreds of histopathology slides representing a wide range of patient cases and anatomical sites are available in the HAPS histology picture database (http://hapshistology.wikifoundry.com). Histopathology slides on a wide range of topics are available from the Pathology Department at the UC San Diego School of Medicine (https://meded.ucsd.edu/hist-img-bank). Histopathological images of a group of breast cancer biopsy frames stained with H&E may be found in the MITOS-ATYPIA grand challenge benchmark dataset (https://mitos-atypia-14.grand-challenge.org/Dataset). Publicly accessible and developed with pedagogical ends in mind, each of these datasets is available to anyone who wants to use it. These archives are kept in JPEG format and are all resized to 256x256 pixels before processing.

5.4.Results and Discussions

Here, we conduct a series of tests on a dataset of 150 test histopathology photos culled from different sources to estimate the effectiveness and viability of the suggested method. Eight test histopathology photos are considered initially for both subjective and objective assessment, with the average of performance characteristics from a larger sample size of 150 images used for the final objective evaluation. The proposed technique is evaluated in contrast to six other approaches: RBLA [75], IAGCM [66], AGC-WHD [65], EBCHE [50], HCMBE [86], and TCHE-DWT [51]. All optimization techniques are verified on a Windows 10 desktop with an Intel Core i5 CPU and 8 GB of RAM to determine how well they perform. Our tests use 15, 80, and 250 on the small, medium, and big scales, respectively. There is subjectivity and objectivity to these comparisons. A single 3.1 GHz machine is used for both testing.

5.4.1. Qualitative (Subjective) Assessment

A visual understanding of a condition is the subject's evaluation of that condition. The purpose of presenting output visuals to a subject is to provoke an emotional response. A person's visual perception allows for a thorough assessment of image artefacts, detail

degradation, odd appearance, colour deformation, and excessive augmentation. This article performs visual quality assessment, an important way for measuring the efficacy of various image contrast enhancement strategies.

Visual comparisons of the proposed way with known contrast-enhancing techniques for a number of test histopathology images are provided in Figs. 5.7-5.14. The visual results of suggested and existing approaches applied to the initial histopathological image "Img1" are shown in Fig. 5.7. Overly brightened areas and excessively brilliant photos, as seen in Fig. 5.7c and 5.7d, are the outcome of the image enhancement approaches (IAGCM and AGC-WHD), which wash out essential characteristics and render them invisible. Figure 5.7f demonstrates how the HCMBE method artificially colours the image by distorting its small elements. Figure 5.7b and 5.7e show the enhanced images produced by the RBLA and EBCHE method, but with unchecked contrast in most locations. TCHE-DWT yields images with only a slight boost in local contrast, as can be seen in Fig. 5.7g. As can be seen in Fig. 5.7h, local characteristics are correctly accentuated, and contrast was appropriately increased without compromising the image's colour or information.

Images with increased contrast are shown in Fig. 5.8. These images are based on the 'img2' image. As can be observed in Fig. 5.8c, most of the output image became darker and lost detail since the IAGCM approach did not increase the contrast enough.

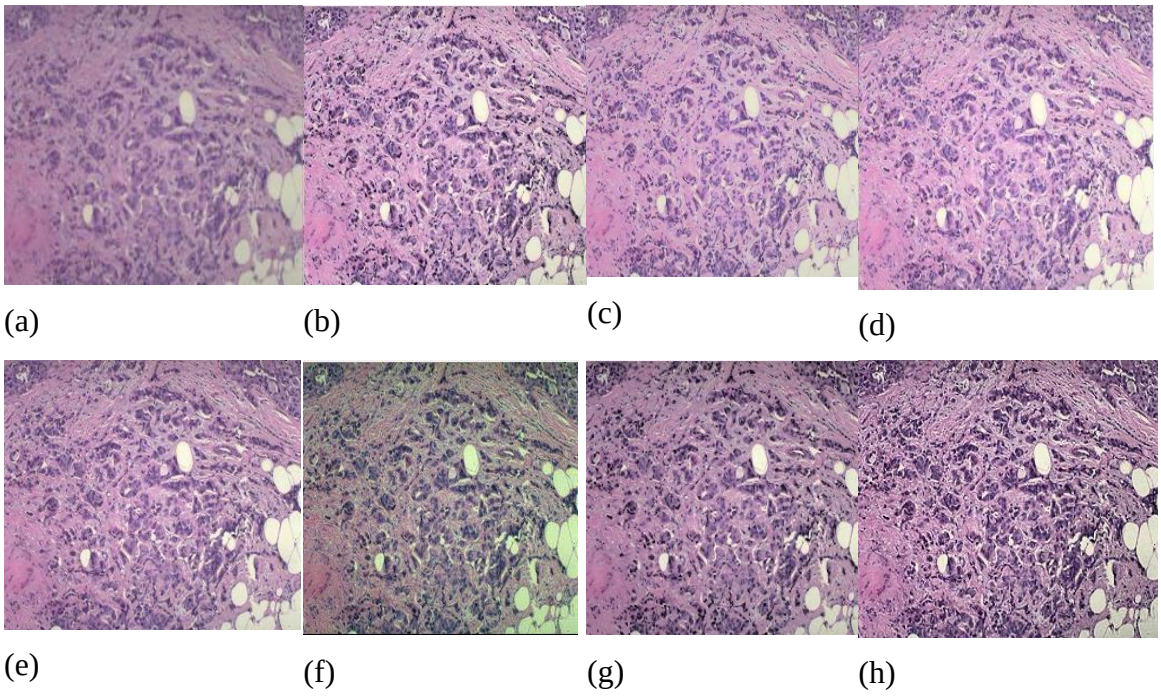

Figure: 5.8 Experiment outcomes of the ‘Img1’ (a) Original image, (b) RBLA, (c)

IAGCM, (d) AGC-WHD, (e) EBCHE, (f) HCMBE, (g) TCHE-DWT, (h) Proposed scheme

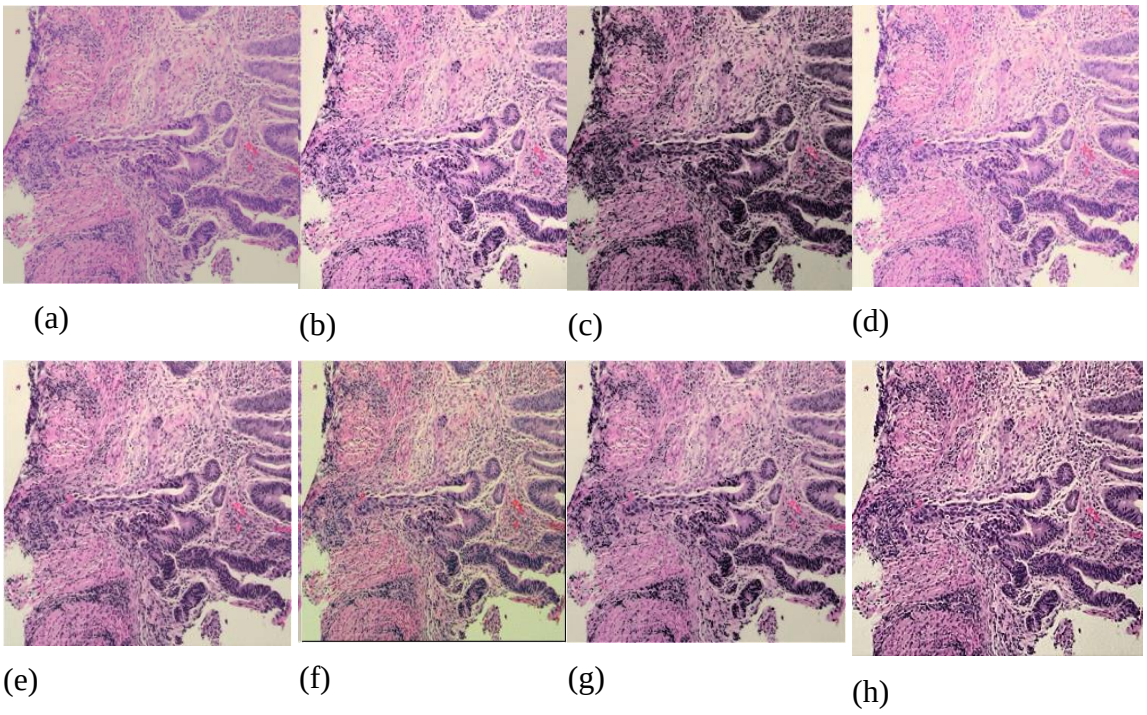

Figure: 5.9 Experiment outcomes of the ‘Img2’ (a) Original image, (b) RBLA, (c) IAGCM, (d) AGC-WHD, (e) EBCHE, (f) HCMBE, (g) TCHE-DWT, (h) Proposed scheme

Inadequate texture features and considerable augmentation, especially in bright regions of Fig. 5.8b and 5.8d, were produced using the RBLA and AGC-WHD method. In Fig. 5.8e and 5.8g, we see that while the EBCHE and TCHE- DWT systems kept the overall mean brightness stable, they were unable to highlight the local texture information in the image.

Figure 5.8f shows that the output images from the HCMBE system have adequate contrast improvement but severe colour distortion. Figure 5.8h demonstrates that the proposed approach can produce visually good contrast-enhanced histopathology output, allowing the user to regulate the enhancement rate and better see minute but crucial details.

Figure 5.9 displays the original "Img3" image with its contrast-enhanced variations, one acquired with the proposed procedure and the others with six more traditional methods. Figure 5.9c shows that the IAGCM method yielded darker findings in some regions, indicating data sparsity. Figures 5.9e and 5.9g show that the EBCHE and TCHE-DWT methods little alter the contrast, therefore the resulting images are faithful to the

originals. Important features of the handled image are lost, despite the fact that the RBLA and AGC-WHD (Fig. 5.9b and 5.9d) succeeded in improving contrast while keeping brightness adequate. In Fig. 5.9f, HCMBE's decreased visibility of fine details and frequent brightness deterioration were both the result of an incorrect exposure value setting. Figure 5.9h demonstrates that the suggested method has the potential to provide histopathology images that are both visually appealing and technically superior, with improved mean brightness retention and enhanced visibility of minute details.

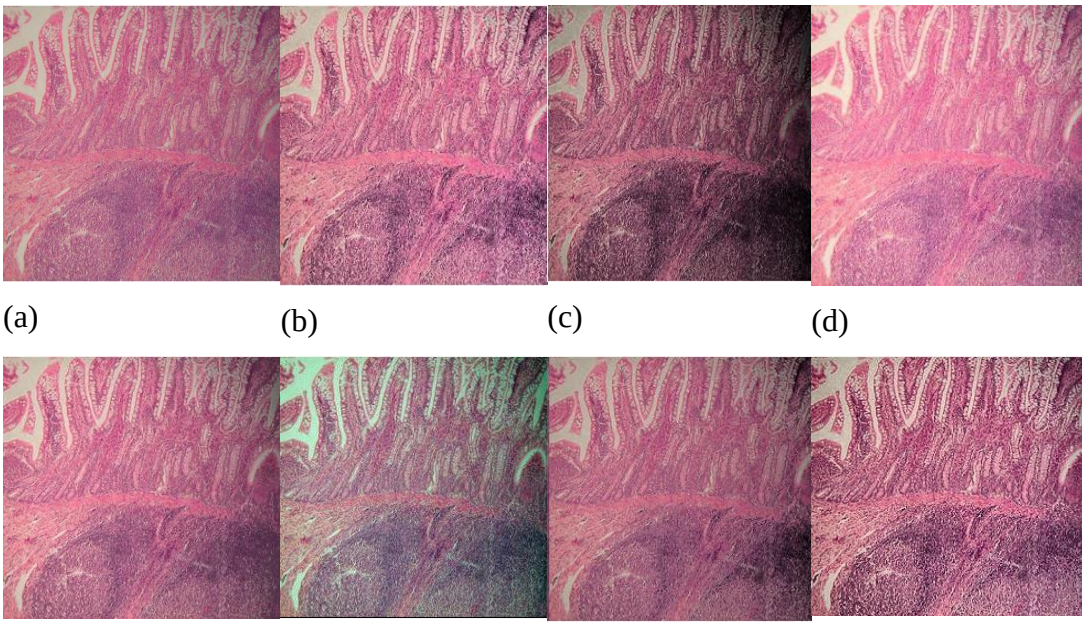

(a) (b) (c) (d)

(e) (f) (g) (h)

Figure: 5.10 Experiment outcomes of the ‘Img3’ (a) Original image, (b) RBLA, (c) IAGCM, (d) AGC-WHD, (e) EBCHE, (f) HCMBE, (g) TCHE-DWT, (h) Proposed scheme

The enhancements made to the image "img4" using both the suggested and the standard methods are shown in Fig. 5.10. When compared to the original img4 image (Fig. 5.10c, 5.10d, and 5.10e), the IAGCM, AGC-WHD, and EBCHE methods produced significantly better results in terms of reducing visual intensity disparities between different items in the final histopathology image. This leads to subpar final photos being produced by these techniques. In Fig. 5.10g, we can see that the TCHE-DWT method yields images with somewhat higher contrast.

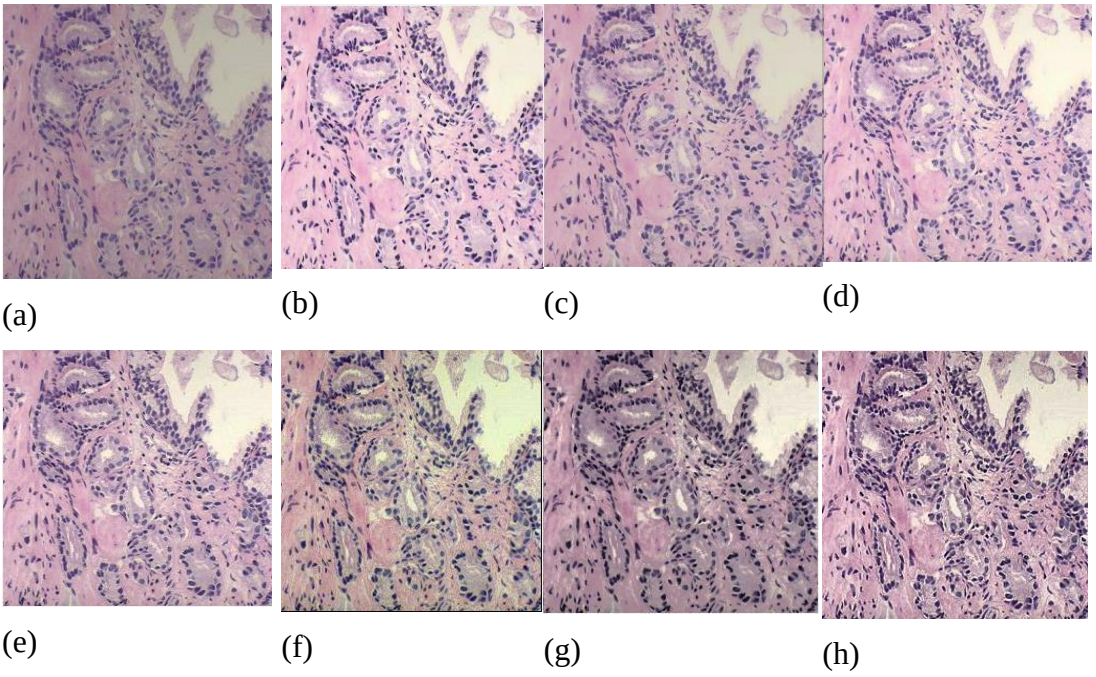

(a) (b) (c) (d)

(e) (f) (g) (h)

Figure: 5.11 Experiment outcomes of the ‘Img4’ (a) Original image, (b) RBLA, (c) IAGCM, (d) AGC-WHD, (e) EBCHE, (f) HCMBE, (g) TCHE-DWT, (h) Proposed scheme

False colours formed in the final product because HCMBE was unable to properly boost contrast. Fig. 5.10b, when interpreted visually, shows that the RBLA method results in an over-enhanced output image in most places. When compared to the other six methods currently in use, the suggested algorithm performs better in terms of improving contrast, preserving brightness, and maintaining a natural appearance. As may be seen in Fig. 5.10h, as a result, most items blend into the scenery.

A comparison of the suggested method and six alternative methods for improving contrast is displayed in Fig. 5.11. Figures 5.11b and 5.11d show that the RBLA and AGC-WHD method artificially enhanced the histopathology pictures, obscuring subtle details. Under enhancement of the image, as seen in Fig. 5.11g, occurred despite the TCHE-DWT strategy's intention to increase contrast. As can be observed in Fig. 5.11f, the HCMBE method's attempt to improve contrast has instead led to the destruction of the colours within the histopathological image, making it harder to identify features. An undesirable side effect of this method is amplified background noise. Figure 5.11c and 5.11e indicate that the IAGCM and EBCHE methods both resulted in higher contrast in the images, but neither maintained the mean brightness nor provided any local enhancement. Figure 5.11h demonstrates once again that the proposed approach

yields superior visual results for the 'Img5' histopathology image. Moreover, as can be seen in Fig. 5.11h, the various little but significant details contained within the picture areas were accurately improved, allowing for an efficient visual comparison.

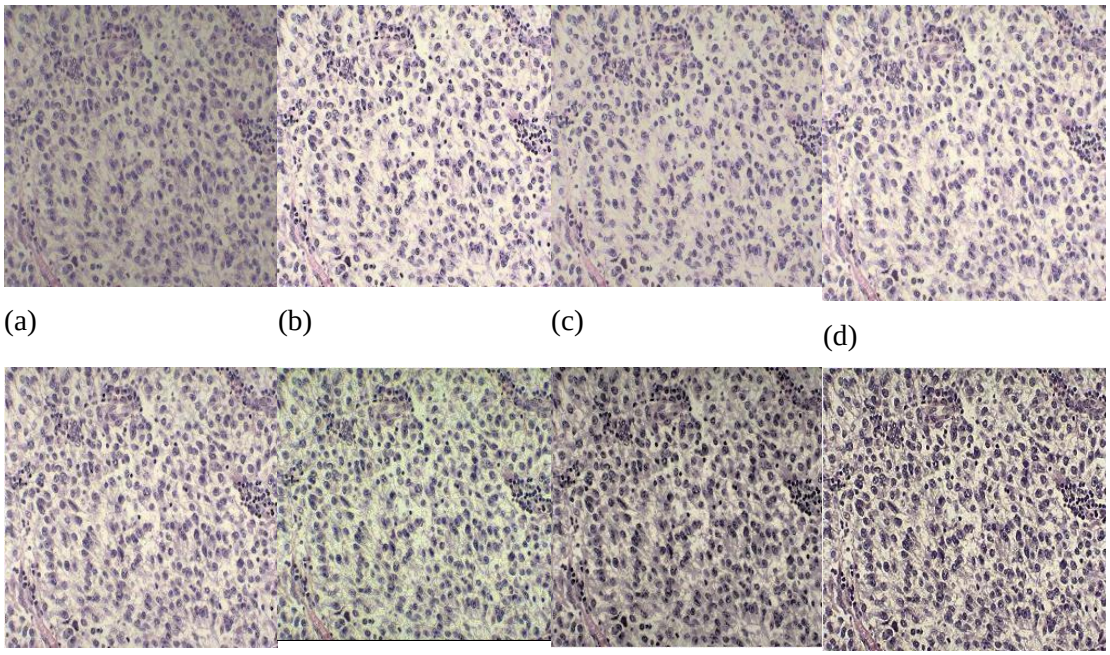

(a) (b) (c) (d)

(e) (f) (g) (h)

Figure: 5.12 Experiment outcomes of the ‘Img5’ (a) Original image, (b) RBLA, (c) IAGCM, (d) AGC-WHD, (e) EBCHE, (f) HCMBE, (g) TCHE-DWT, (h) Proposed scheme

Figures 5.12–5.14 demonstrate the improved quality of images img6, img7, and img8. By visually comparing the outcomes of the three experiments, we conclude that the proposed enhancement procedure is the best method for boosting the contrast of histopathology images without introducing defects like colour distortion, brightness degradation damage, noise enhancement, and an unnatural appearance. Over- and under-enhancement, undesired defects, colour distortion, brightness decline damage, noise augmentation, and an unnatural appearance are all problems that are introduced by other methods. The recommended framework successfully improves the overall contrast of the histopathological picture without generating distracting artefacts, as shown by a visual evaluation of all three findings. Moreover, it preserves the average intensity and fine detail of the image, which aids in accurate diagnosis.

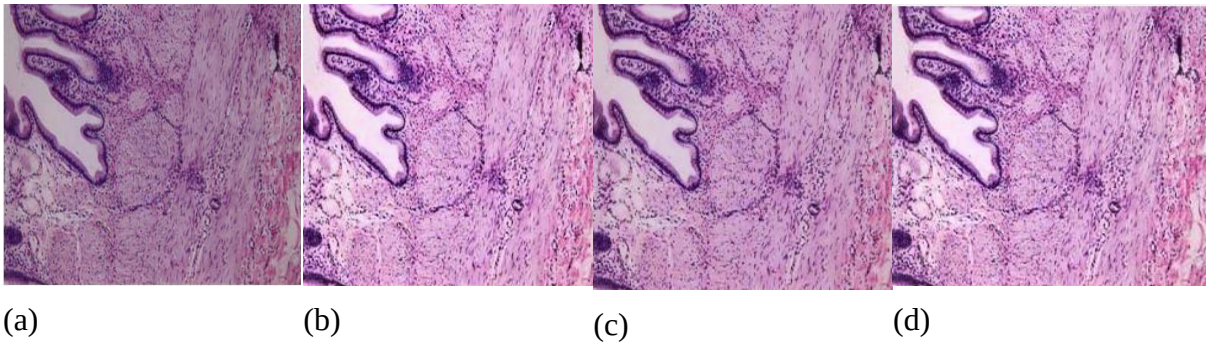

(a) (b) (c) (d)

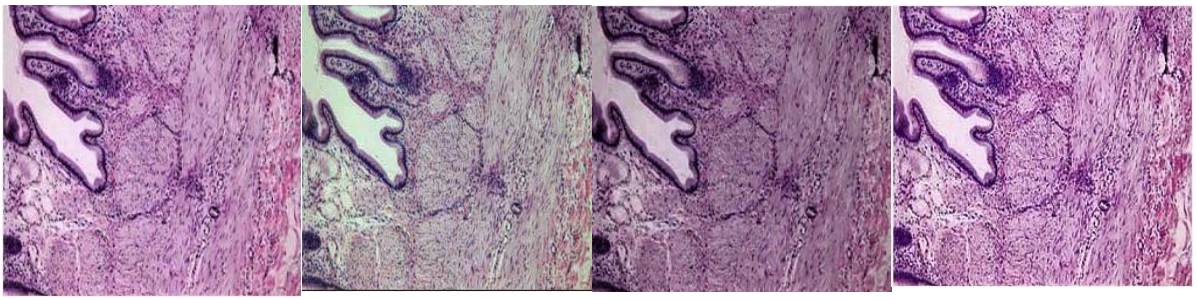

(e) (f) (g) (h)

Figure: 5.13 Experiment outcomes of the 'Img6' (a) Original image, (b) RBLA, (c) IAGCM, (d) AGC-WHD, (e) EBCHE, (f) HCMBE, (g) TCHE-DWT, (h) Proposed scheme

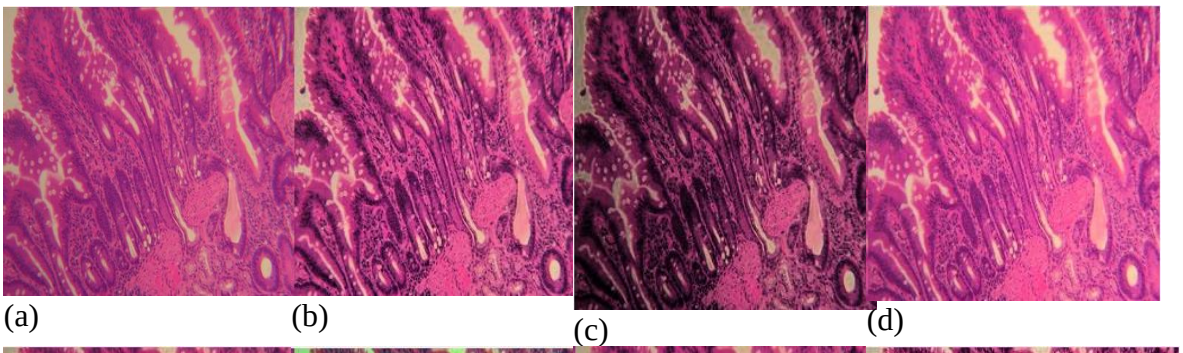

(a) (b) (c) (d)

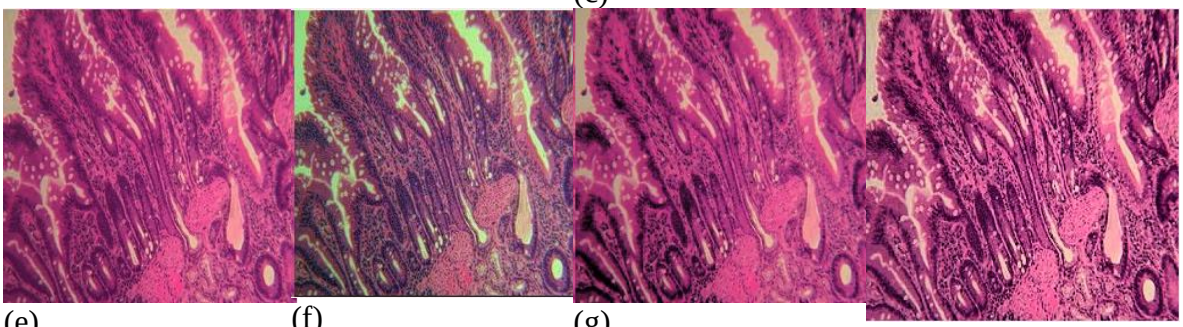

(e) (f) (g) (h)

Figure: 5.14 Experiment outcomes of the 'Img7' (a) Original image, (b) RBLA, (c) IAGCM, (d) AGC-WHD, (e) EBCHE, (f) HCMBE, (g) TCHE-DWT, (h) Proposed scheme

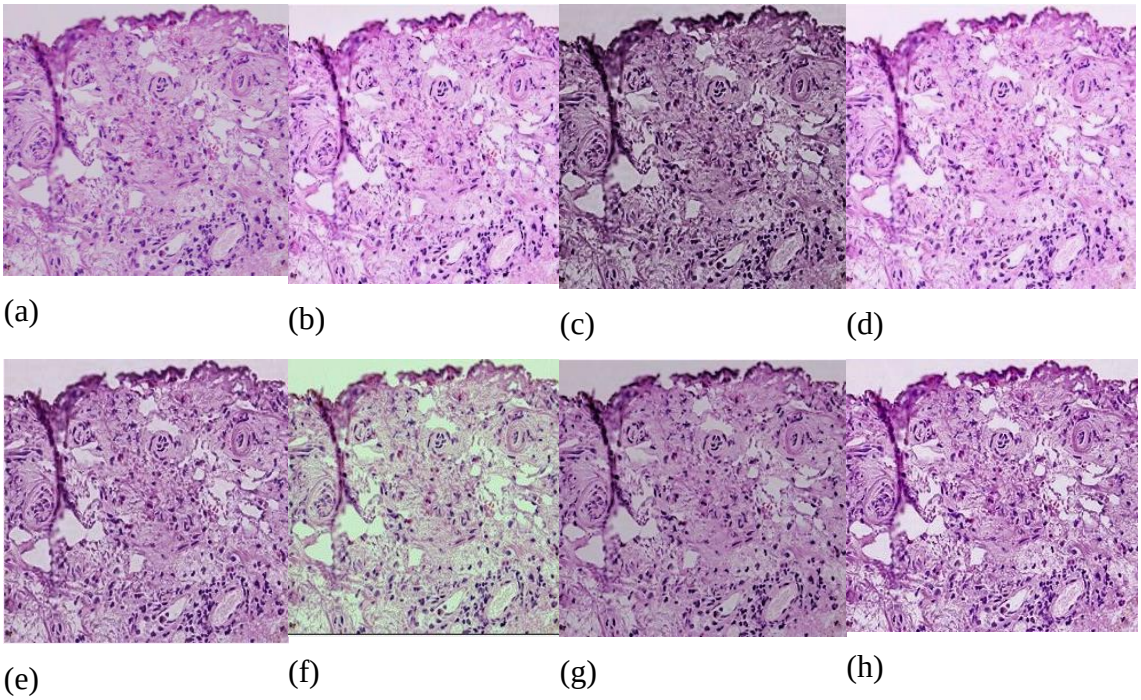

(a) (b) (c) (d)

(e) (f) (g) (h)

Figure: 5.15 Experiment outcomes of the 'Img8' (a) Original image, (b) RBLA, (c) IAGCM, (d) AGC- WHD, (e) EBCHE, (f) HCMBE, (g) TCHE-DWT, (h) Proposed scheme.

5.4.2. Quantitative (Objective) Assessment

Six metrics, including entropy, EPI, CII, WC, MC, and UIQI, are used to assess the effectiveness of both new and established approaches. Values in bold in Tables 5.1–5.5 represent the most optimal evaluation metrics for improving images.

The entropy values of the various ways of enhancement are shown in Table 5.1. Image information is quantified using a measure called entropy. Many details can be extracted from an image with a high entropy. In order to accurately analyse a diagnostic image, it is essential to use contrast enhancement techniques to achieve the maximum possible entropy value, highlighting the finer details.

Due to information loss during over or under augmentation, the IAGCM approach produces low entropy values. It is demonstrated that the proposed method generates considerably more entropy than competing approaches for all test histopathology images. As a result, unlike alternative contrast enhancement techniques, the original data is not lost.

Table 5.1 Assessment of entropy outcomes

Image Name / Methods	Original	RBLA	IAGCM	AGC-WHD	HCMBE	EBCHE	TCHE-DWT	Proposedscheme
Img1	6.82	7,41	6.98	7.19	7.24	7.20	7.41	**7.76**
Img2	6.92	7.36	7.49	7.10	7.40	7.27	7.49	**7.77**
Img3	7.21	7.47	7.47	7.40	7.40	7.34	7.44	**7.68**
Img4	7.57	7.78	7.41	7.70	7.60	7.42	7.78	**7.86**
Img5	6.57	7.16	6.75	7.11	7.11	7.27	7.44	**7.72**
Img6	6.55	7.02	6.76	7.02	7.02	7.26	7.35	**7.56**
Img7	7.05	7.09	7.50	7.08	7.08	7.13	7.17	**7.56**
Img8	7.02	7.41	7.13	7.44	7.50	7.24	7.39	**7.70**

Table 5.2 shows that compared to the other approaches, the suggested scheme has the highest EPI. The highest EPI value suggests a high degree of edge retention in the improved output image, suggesting the possibility of creating an image free of undesirable artefacts with the proposed technique. The EPI value of the proposed technique is greater than that of any other common contrast improvement technique

Table 5.2 Assessment of EPI outcomes

Image Name / Methods	RBLA	IAGCM	AGC-WHD	HCMBE	EBCHE	TCHE-DWT	Proposed scheme
Img1	0.99	0.94	0.99	0.99	0.96	0.96	**1.01**
Img2	0.98	1	0.98	0.99	0.97	0.94	**1.05**
Img3	1	1	0.97	0.98	0.98	0.95	**1.02**
Img4	0.97	0.99	0.97	0.98	0.98	0.94	**1**
Img5	0.98	0.94	0.99	0.99	0.96	0.96	**1**
Img6	0.98	0.95	**1**	**1**	0.94	0.96	**1**
Img7	0.97	0.99	0.97	0.98	0.98	0.94	**1**
Img8	0.98	0.95	0.99	**1**	0.97	0.96	**1**

If you want your image to have the best possible contrast and edge preservation, set the EPI value as high as you can. When applied to this scenario, the high EPI value of the suggested approach produces an image with superior edge retention and enhanced contrast. Evaluation of Post-Enhancement Edge Retention using EPI. When improving medical images, it is very important to do so without distorting the edges of the image. When EPI is close to 1, edge retention in the augmented image is at its finest. Looking

at Table 5.3, it is clear that the CII value produced by the suggested method is greater than that of previously-existing enhancement methods. The proposed technique enhances contrast across the board while preserving crucial histopathological image characteristics. It is demonstrated that the proposed strategy has a greater CII value than any of the previously mentioned contrast-improving methods. The diagnostic value of the final CT image is increased as a result of the suggested method's enhancement of image contrast, local data, and fine features.

Table 5.3 Assessment of CII outcomes

Image Name / Methods	RBLA	IAGCM	AGC-WHD	HCMBE	EBCHE	TCHE-DWT	Proposed scheme
Img1	1.55	1.05	1.20	1.18	1.23	1.23	**1.82**
Img2	1.40	1.66	1.24	1.26	1.26	1.28	**1.72**
Img3	1.44	1.64	1.78	1.92	1.96	1.70	**2.02**
Img4	1.12	1.01	1	1.01	1.01	1.01	**1.37**
Img5	1.45	1.08	1.53	1.53	1.53	1.53	**1.80**
Img6	1.50	1,08	1.36	1.34	1.37	1.37	**1.83**
Img7	1.03	1.09	1.01	1.01	1.01	1.01	**1.11**
Img8	1.09	1.02	1.03	1.03	1.03	1.07	**1.24**

Table 5.4 shows that when compared to other methods currently in use, the UIQI of the suggested method is significantly higher. Superior image quality in terms of correlation, brightness, and contrast is achieved using the proposed method with a maximum UIQI score. as a result, the capacity to generate an image devoid of distracting artefacts. IAGCM scores low on the Universal Health and Quality of Life Index. This could be because the IAGCM method's enhancement findings lack chrominance information. We find that the proposed strategy outperforms the state-of-the-art in contrast improvement in terms of UIQI. Image quality is enhanced when the UIQI score is high. Improved visual contrast is one effect of the suggested framework's high UIQI score.

Table 5.4 Assessment of UIQI outcomes

Image Name / Methods	RBLA	IAGCM	AGC-WHD	HCMBE	EBCHE	TCHE-DWT	Proposed scheme
Img1	0.97	0.97	0.95	**0.99**	**0.99**	0.97	**0.99**
Img2	0.98	0.86	0.97	**0.99**	0.97	0.98	**0.99**
Img3	0.98	0.81	0.96	**0.99**	0.94	0.92	**0.99**
Img4	0.98	0.78	0.97	0.99	0.97	0.90	**0.99**
Img5	0.92	0.96	0.92	0.95	**0.99**	0.98	**0.99**
Img6	0.91	0.96	0.92	0.96	0.94	0.98	**0.99**
Img7	0.98	0.93	0.97	**0.99**	0.97	**0.99**	**0.99**
Img8	0.91	0.96	0.92	0.96	0.98	**0.99**	**0.99**

Table 5.5 provides a summary of the mean values for proposed and existing approaches based on an analysis of 150 histopathology pictures. As was previously said, averaging entropy, CII, EPI, and UIQI yields better results than other methods. The performance of the proposed process is assessed using Michelson and Weber contrast measurements in addition to the entropy, CII, EPI, and UIQI metrics, as detailed in Eqs. (24)-(26). (25). A higher WC and MC value means there is more of a distinction between the two. The proposed method achieves the highest contrast ratio of any comparable enhancement technique, with an average Michelson and Weber contrast ratio of 0.97 and 0.96, respectively. That's why the proposed strategy works better at increasing contrast and preserving tiny details than previous approaches. The outcomes reveal that the suggested method, with the help of the extra metrics, is reliable and efficient in dealing with various histopathological medical pictures.

Table 5.5 Average measures values for 150 Histopathology images

Methods/Measures	Entropy	CII	EPI	UIQI	MC	WC
RBLA	7.18	1.42	0.98	0.97	0.93	0.86
IAGCM	7.26	1.66	1	0.91	0.95	0.90
AGC-WHD	7	1.57	0.98	0.97	0.55	0.53
HCMBE	7.27	1.69	1.01	0.96	0.96	0.91
EBCHE	7.14	1.76	0.97	0.97	0.90	0.85
TCHE-DWT	7.24	1.82	0.95	0.97	0.93	0.90
Proposed scheme	**7.53**	**2.03**	**1.04**	**0.98**	**0.97**	**0.96**

5.5. Summary

Based on retinex theory and local contrast modification, this study introduces a novel approach to improving colour histopathology images. To improve the contrast of a colour histopathology picture in the HSV colour model, we first provide an unique multiscale retinex with adaptive weighting, and then we use a new weighted CLAHE methodology to the brightness component of the image to boost the local details. Histopathology images have been used in tests to gauge the success of the proposed technique quantitatively and qualitatively. Furthermore, investigations employing histopathology image databases show that the proposed methodology significantly exceeds existing standard enhancement strategies in terms of overall contrast improvement and fine detail preservation. The suggested method produces natural histopathological images with intact brightness and improved contrast, free of any visible image artefacts. On measures such as edge preservation index, entropy, a universal quality index, and enhancement metrics, the suggested system outperforms the state-of-the-art. Histopathology images can be amended using the proposed method, which can then be used to aid in the diagnostic process. In spite of the fact that the majority of the image enhancement methodologies defined in Chapter 2 are effective across a wide range of application domains, their effects on diagnostic images are frequently unacceptable and unsatisfactory for fundus images due to issues such as image artefacts, colour falsification, noise amplification, over enhancement, mean brightness deterioration, and detail distortion. The following is a brief summary of the benefits of the suggested algorithm.

CHAPTER 6
A HYBRID METHOD FOR IMPROVING THE LUMINOSITY AND CONTRAST OF COLOR RETINAL IMAGES USING THE JND MODEL AND MULTIPLE LAYERS OF CLAHE

6.1. Introduction

Imaging of the retina has been shown to detect some common eye and heart problems. However, low-quality retinal fundus medical images are ineffective for diagnosis, especially in computerised image analysis systems, because of non-uniform or inadequate lighting and low contrast. Retinal fundus colour photographs have low brightness and contrast, however this section proposes an effective strategy for enhancing these images. An HSV [20] colour model is first applied to the input colour retinal fundus image, which disentangles the luminance channel (V) from the other colour elements hue (H) and saturation (S). Then, a novel JND-based adaptive gamma correction algorithm is used on the luminosity channel (V) to enhance the brightness of fundus images. After that, a novel contrast enhancement method using multiple layers of CLAHE is used to boost the luminance contrast in the L*a*b* colorspace [20]. While maintaining the average brightness, maintaining an original appearance, and optimising entropy, these two methods significantly boost the total luminance and contrast in retinal images. The effectiveness of the suggested technique is evaluated experimentally on a wide variety of fundus images. The suggested methodology outperforms state-of-the-art enhancement methods in terms of edge preservation index, entropy, enhancement measure, contrast ratio, and enhancement metrics, as shown by a comprehensive objective evaluation. In order to help ophthalmologists better examine for retinal problems and provide more precise computerised image analysis for medical diagnosis, this retinal fundus image enhancement approach can be used.

While the majority of the previously defined image enhancement methodologies in Chapter 2 are effective for a variety of application domains, the results are often unsatisfactory and unacceptable for fundus images due to image artefacts, colour falsification, noise amplification, over enhancement, mean brightness deterioration, and detail distortion. The following is a brief overview of the benefits of the suggested algorithm.:

- Increase the brightness of retinal fundus images with a novel adaptive gamma

correction technique connected to the just visible difference concept.

- A unique contrast enhancement method using several layers of CLAHE is proposed for suitably boosting the contrast of fundus pictures.
- The average brightness is maintained, the images retain their natural look, and entropy is maximised for input retinal fundus images while these two approaches dramatically boost luminance and contrast.

6.2. Proposed Technique for Improving the Luminosity and Contrast of Color Retinal Images using the JND Model and Multiple Layers OF CLAHE

The suggested method [126] consists of two stages: first, brightness is increased to better illuminate the entire retinal fundus image, and then, contrast is increased to gather information at a more granular level inside the retinal fundus image. The block diagram of the suggested design is shown in Fig. 6.1.

6.2.1. JND-based Adaptive Gamma Correction Method for Luminosity Improvement

Improving the luminance impact of retinal fundus images is critical because poor or inconsistent lighting obscures the visual insight of these images, making aberrant characteristics inaccessible. Inappropriate gamma value settings for big pixel intensities cause distortion in high grey level regions when using existing gamma correction based luminous enhancement algorithms for retinal pictures based on [54-55,70]. The optic disc, macula, exudates, blood vessels, and other lesions are all completely obscured by these methods, and the mean brightness of the original image is degraded as a side effect. Using the just noticeable difference (JND) paradigm [24], this research introduces a unique adaptive gamma correction technique for improving the brightness of retinal fundus images. The calculated adaptive gamma values from the JND model are significantly lower in the low grey level region and gradually increase in the moderate and high grey level regions, protecting the moderate and high grey level regions from undesired distortion and maintaining the average brightness of the input retinal picture.

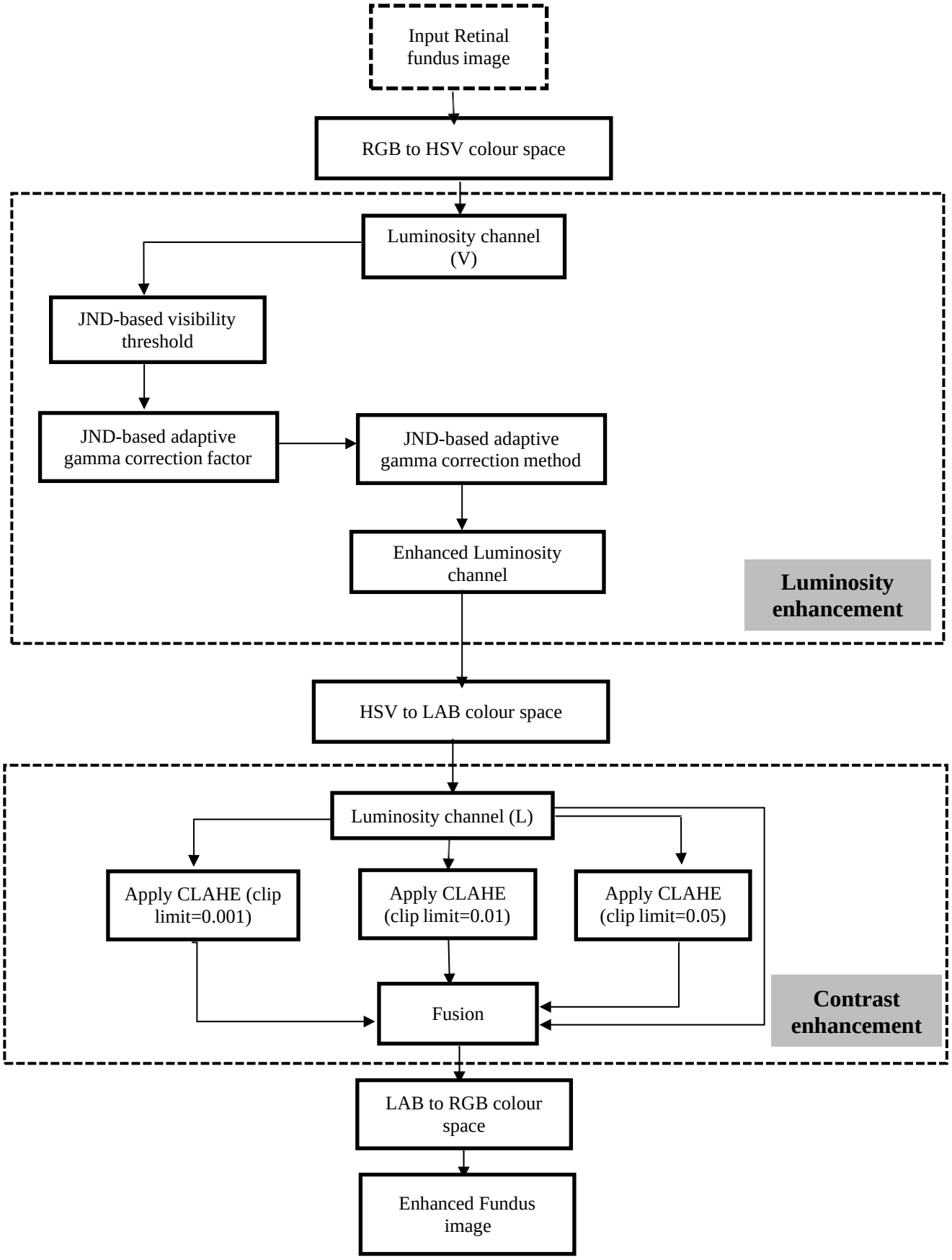

Figure 6.1: Bock Diagram of the proposed method for improving the luminosity

and contrast of color retinal images using the JND model and multiple layers of CLAHE

HSV colour model [54] is first applied to the input colour fundus image, which separates the brightness component (V) from the two colour elements (H) and (S). The H and S components are omitted since they do not contribute to brightness. To enhance the brightness of the fundus image, a new JND-based adaptive gamma correction approach is implemented, and its formula is as follows:

$$V_{out}(x,y) = V(x,y)^{\gamma_{jnd}(x,y)} \tag{6.1}$$

Where V_{out} denotes the output gamma-corrected normalized luminosity image, V denotes the input normalized luminosity image, and γ_{jnd} denotes the JND-based adaptive gamma correction factor.

6.2.2. The JND-based Adaptive Gamma Correction Factor

The JND threshold in HVS is highly dependent on the subject's ability to adjust to changing levels of illumination. The HVS is more sensitive to areas of high grey level than low grey level, and the visibility threshold is highly correlated with the average luminance. In this section, we apply the luminosity JND paradigm to determine the gamma values necessary to brighten the retinal fundus image. The JND threshold luminosity is related to the background luminosity as shown below.

$$T_l(x,y) = \begin{cases} 17\left(1 - \sqrt{\frac{I(x,y)}{127}}\right) + 3 & if\ I(x,y) \le 127 \\ \frac{3}{128}(I(x,y) - 127) + 3 & otherwise \end{cases} \tag{6.2}$$

where T_l is the visibility threshold and $I(x,y)$ is the local mean background luminosity of the input image of pixel located at (x,y). The input V luminosity image is used as a background luminosity for the computation of $T_l(x,y)$. To adaptively control the luminance of the retinal fundus image, the gamma values will be set pixel by pixel to establish the demarcation between areas of low and high grey levels. Notably, a lower γ_{jnd} in Eq. (6.1) results in the greatest modification of pixel values, resulting in a more gamma-corrected output. As a result, γ_{jnd} is adjusted to fluctuate inversely with

background luminance to provide lower γ_{jnd} values for darker areas and slightly higher γ_{jnd} values for medium and higher grey level areas. The γ_{jnd} is mathematically derived from the visibility threshold and is represented as

$$\gamma_{jnd}(x,y) = K + \frac{(1-I_M)}{(1+exp\{10*[T_l(x,y)-I_M]\})} \quad (6.3)$$

Where I_M denotes the overall median intensity value of the input luminosity channel and K denotes the parameter used to adjust the maximum value of γ_{jnd}, which is set to 0 in the proposed technique. Figure 6.2(b) depicts the correlation between γ_{jnd} and ambient light. The gamma correction method for adaptively changing the pixels as provided by Eq. (6.1) includes a JND-based adaptive gamma factor. To prevent over-enhancement in the mid- and high-grey levels after gamma correction, a big f γ_{jnd} is generated to softly control the illumination in these regions. On the other hand, a little f γ_{jnd} is generated to adjust the brightness, especially in shadowy regions, so that features are brought out appropriately in the mid-tone range of grayscale. Finally, the enhanced fundus image is created by combining the improved luminosity channel Vout with the remaining two-color components.

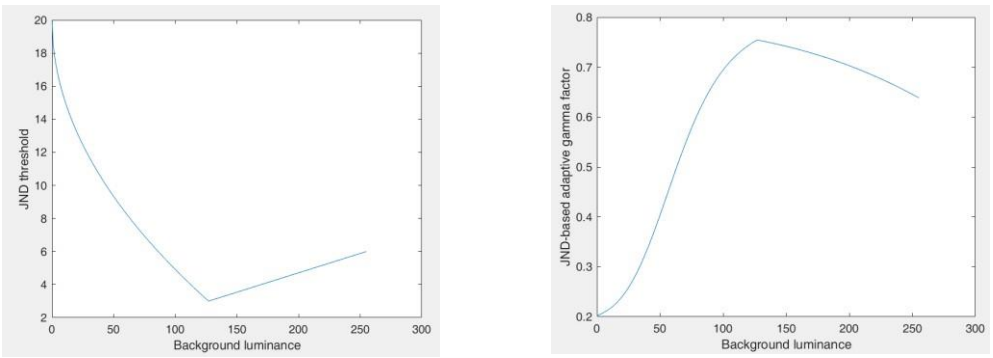

(a) (b)

Figure 6.2: Connection between the luminosity JND threshold and the JND-based gamma factor γ_{jnd} (a) Luminosity JND threshold. (b) γ

6.2.3. Contrast enhancement using multiple layers of CLAHE

In particular, for retinal images with low or irregular illumination, the luminosity augmentation mentioned above may help correct the global luminance. In order to make the important details in the fundus picture stand out against the background, we need to

increase the contrast between the two. Contrast in fundus pictures is typically enhanced using the conventional CLAHE approach [54-55,70]. The algorithm works by separating the input image into many small, non-overlapping units called tiles, cutting the histogram of each tile to the set clip limit, and finally equalising the histogram of each tile to get the final output image. Clip limit, which is defined as a value between 0 and 1, and the publicly accessible MATLAB code are used to implement CLAHE. In spite of its widespread use, traditional CLAHE always results in subpar local enhancement at a given clip limit value when applied to fundus images to improve contrast. Even at the lowest clip limitations, it just marginally improves contrast. On the other hand, as shown in Fig. 3, information distortion and colour falsification occur as a result of the clip bound increasing, which causes high local contrast enhancement and excessive enhancement in particular locations. Also, the high clip constraint used by CLAHE to boost contrast also amplifies noise, reduces average brightness, and negates some of the beneficial effects of the uneven illumination correction applied to the fundus images. The clip limit in most modern medical image enhancement methods [54-55,70] is determined by experimental analysis of a large collection of clinical images, making these methods notoriously difficult to implement. As part of this work, this section developed a novel method of applying stacked CLAHE to improve the contrast of fundus images. There are three phases to the proposed contrast enhancement method: local enhancement, weight computation, and merging.

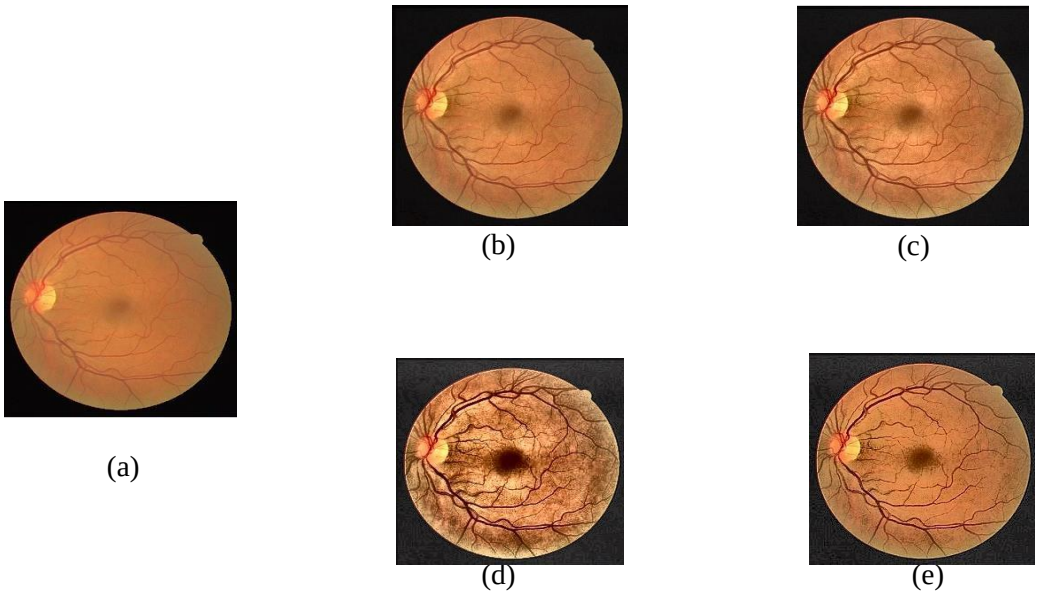

(a) (b) (c) (d) (e)

Figure 6.3**:** (a) The initial sample retinal picture (b) The CLAHE image using a small clip limit (c) The CLAHE image using a medium clip limit (d) The CLAHE image using a high clip limit (e) proposed approach improved image

6.2.3.1. Local enhancement

Since raising contrast in the luminosity component (L) of the L*a*b* colour system enhances details more effectively than increasing contrast in HSV space [16], the suggested method makes use of the L*a*b* colour system [20] for contrast enhancement. In order to correct for colour shifts, the input retinal image (I) with its enhanced luminance colour is first translated to the L*a*b* colour scheme so that CLAHE may be applied to the luminosity component (L). With lower, medium, and maximum clip limits of 0.001, 0.01 and 0.05, respectively, the luminosity channel (L) will be run through CLAHE three times. All three variations use an 8x8 grid of tiles. Images produced by CLAHE with clip limits of 0.001, 0.01, and 0.05 are shown in Fig. 6.3. The following are inferences made about the effect of clip limit on the outcome of CLAHE based on the original retinal image shown in Fig.6.3(a):

- As seen in Fig. 6.3(b), the low clip limit (0.001) produces an improved fundus image with moderate contrast improvement while preserving the overall brightness.
- As can be observed in Fig. 6.3(c), a fundus image output with a medium clip limit (0.01) has sufficient contrast improvement but loses natural brightness in some locations.
- As demonstrated in Fig. 6.3(d), fundus images created with the high clip limit (0.05) suffer from extreme contrast augmentation, colour and information distortion, and over enhancement, especially in the high grey level region, and lose all of their original mean brightness.

6.2.3.2. Weight computation

The above theory informs the proposed method, which fuses the three CLAHE enhanced luminosity channels corresponding to low, medium, and high clip limits to produce a high contrast-enhanced, artifact-free, and mean-brightness-preserving output fundus image with natural-looking illumination. To begin, the [0, 255] range is now supported for all brightness channels. Following this, the luminance values of all pixels in each channel were used to generate four Gaussian models, which were then used to extract the desired features and sidestep the drawbacks of the aforementioned CLAHE outputs. The median values of these four Gaussian distributions represent the four distinct classes of grayscale image pixels: very high, somewhat high, moderately low,

and very low. (un, n = 0, 1, 2, 3) evenly distributed across the luminance range [0, 255] and analytically adjusted to 224, 160, 96, and 32. Each class's standard deviation (σn, n = 0, 1, 2, 3) is specified as 32. That is, $\sigma 0 = \sigma 1 = \sigma 2 = \sigma 3 = 32$. Thus, gaussian model-based weight functions associated with each of these CLAHE enhanced luminosity channel s are determined as follows for a given pixel value $Ln(x, y)$.

$$w_n(x,y) = e^{-\frac{(L_n(x,y)-u_n)^2}{2{\sigma_n}^2}} \quad ,n = 0,1,2,3 \tag{6.4}$$

Where L0 is the luminosity channel of the original colour retinal image, L1, L2, and L3 are the three CLAHE-enhanced luminosity channels for low, medium, and high clip limits of 0.001, 0.01, and 0.05, respectively. It's worth noting that w1 represents a CLAHE output with a very tiny clip limit (0.001), $w_2$represents a CLAHE output with a medium clip limit (0.01), and w_3 represents a CLAHE output with a very big clip limit (0.05). The luminosity channel L of the input fundus image is combined with each CLAHE enhanced luminosity channel to get the final enhanced output fundus image, which is then given the weight function w_0 in the interest of generating a genuine retinal output picture.

Using these weight values, we then standardise the weights associated with the luminosity channels of the input retinal image and the luminosity channels of each CLAHE-resulted image:

$$W_n(x,y) = \frac{w_n(x,y)}{\sum_{n=0}^{3} w_n(x,y)} \quad ,n = 0,1,2,3 \tag{6.5}$$

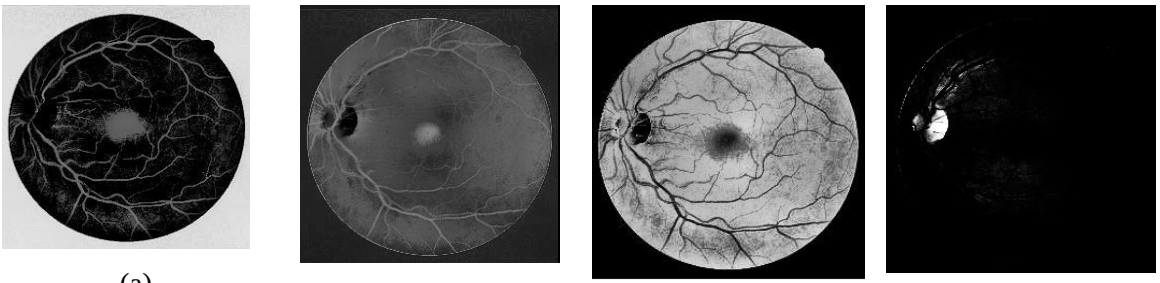

(a) (b) (c) (d)

Figure 6.4: Weight maps related to the CLAHE resultant luminosity channels and the input retinalluminosity channel (a) w_3 (b) w_2 (c)w_1 (d) w_0

Weight maps, presented in Fig.6.4, display the associated weight values for each pixel in the image given in Fig.6.3(a). In this example, we see that the pixel value from the original image can give each intensity value its own set of weights. It is also clear from Fig. 6.4(a) and (b) that the highest weights in the weight map corresponding to the high-clip limit (0.05) CLAHE output are assigned to pixels with the lowest grey levels, while the largest weights in the weight map corresponding to the medium-clip limit (0.01) CLAHE output are assigned to pixels with medium-low grey levels. Selecting high-contrast features like blood vessels in the low and medium-low grey level regions was a priority, therefore these weight maps were selected. At the same time, pixels that produce colour and information distortion and over enhancement were also avoided, especially in the high grey level zone. Large weight values will be assigned to pixels with medium-high grey levels in the weight map corresponding to the low-clip limit (0.001) CLAHE output. To produce the natural enhanced retinal fundus image with maximum mean brightness preservation, we must first obtain the input fundus image with maximum weight values for pixels in big high grey level areas (see Fig. 6.4(c) and Fig. 6.4(d)).

6.2.3.3. Merging

To integrate the positive aspects of the various CLAHE results and prevent their shortcomings, these CLAHE enhanced luminance channels are fused in this step. Eq. (6) fuses the three CLAHE output luminance channels from the preceding step and the original image luminance channel L to obtain the improved output luminance channel L_e, which is then merged with other two-color components to obtain the improved output retinal fundus image specified in Fig. 6.3(e)

$$L_e = W_0 * L + W_1 * L_1 + W_2 * L_2 + W_3 * L_3 \qquad (6.6)$$

where, W_0, W_1, W_2 and, W_3 are the weighting factors. L_1, L_2, L_3 denote the three CLAHE enhanced luminosity channels for lower, medium, and upper clip limits of 0.001, 0.01, and 0.05, respectively.

Fig 6.5 shows the intermediate steps of the proposed algorithm as part of the overall process for illustrating detailed steps involved in the process. The detailed steps for implementation of proposed algorithm are provided in Algorithm 1.

Algorithm 1:

Input: Input RGB color retinal image J , clip limits CL_n *, and parameters* u_n, σ_n *for computing weights for n=0,1,2,3Output: Enhanced image* I_{out}

1: Color space conversion: V ← RGB to HSV (J)

2: For each pixel

3: Compute JND threshold: $T_l(x, y) \leftarrow V(x, y)$

4: Compute JND-based gamma factor: $\gamma_{jnd}(x, y) \leftarrow T_l(x, y)$

5: Apply novel JND-based adaptive gamma correction method: $V_{out}(x, y) \leftarrow V(x, y)^{\gamma jnd(x,y)}$

6: end

7: Color space conversion: I ← HSV to RGB (V_{out}*)8: Color space conversion: L← RGB to LAB (I)*

9: $I_0 \leftarrow L$

10: Compute $I_n \leftarrow$ *CLAHE (L,* CL_n*)*

11: $w_n \leftarrow$ *Weight computation* (I_n, u_n, σ_n)

12: Normalization: $W_n = \frac{w_n}{\sum_{n=0}^{3} w_n}$

13: Fusion: $L = \sum_{n=0}^{3} W_n * I_n$

14: $Y = W_0 * I_0 + L$

15: Color space conversion: Iout ← LAB to RGB (Y)

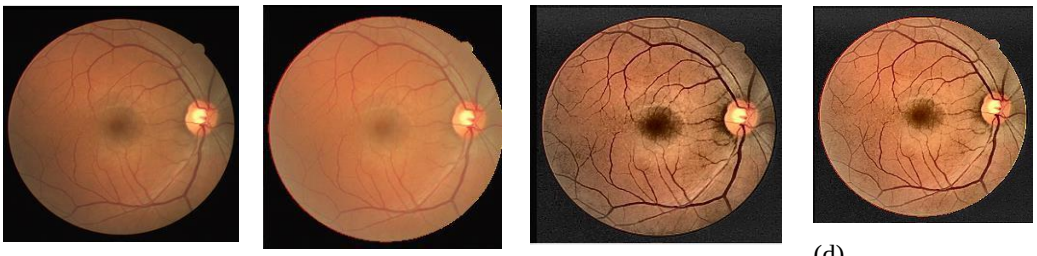

(a) (b) (c) (d)

Figure 6.5**:** Middle phases of the proposed method (a) Input images, (b) luminosity enhanced image, (c)contrast enhancement on original image, (d) contrast enhancement on luminosity enhanced image (5(b))

6.3. Datasets

The proposed algorithm's performance is compared to six existing techniques using 300 test retinal fundus images from the STARE dataset (https://cecas.clemson.edu/ahoover/stare/),DIARETDBI(https://www.it.lut.fi/project/imageret/diaretdb1/) dataset, DRIVE dataset (https://drive.grand-challenge.org/), and the HRF image database (https://www5.cs.fau.de/research/data/fundus-images/). These databases are maintained in the jpg file format and are scaled to the identical size of 256*256 prior to analysis.

6.4. Results and Discussions

There are both subjective and objective comparisons made between the suggested approach and the other five well-known methodologies. The same mechanism with an Intel Core i5 processor running at 3.1 GHz and 8 GB of RAM is used for both testing.

6.4.1. Subjective (Qualitative) judgment

In Figs. 6.6-6.13, we visually compare the proposed process to state-of-the-art contrast-enhancement strategies for a variety of test retinal fundus pictures. On the initial fundus image, labelled "Ret1," Fig. 6.6 displays the visual results of both the proposed and existing approaches. Figure 6.6d demonstrates how the technique proposed by Gupta et al. [22] leads to overly light regions and very bright output, distorts crucial characteristics like the optic disc, and renders them unnoticeable. Figures 6.6c, 6.6e, and 6.6g show that the enhanced images produced by AGC-WHD, EBCHE, and TCHE-DWT do not improve contrast; as a result, important details are not brought to the fore. Instead, these methods have a major brightness degradation problem. With the current approach, as seen in Fig. 6.6f, the resulting fundus image is fuzzy and over-enhanced, making it difficult to make out the image's underlying structures. Zhou et al. [19] enhanced the luminance of the final fundus image, Fig. 6.6b shows, without significantly increasing the contrast or mean brightness of the original image. Fig. 6.6h demonstrates the potential for the proposed method to produce visually appealing retinal pictures with better mean brightness retention and considerably improved visibility of features and structures in the output fundus image.

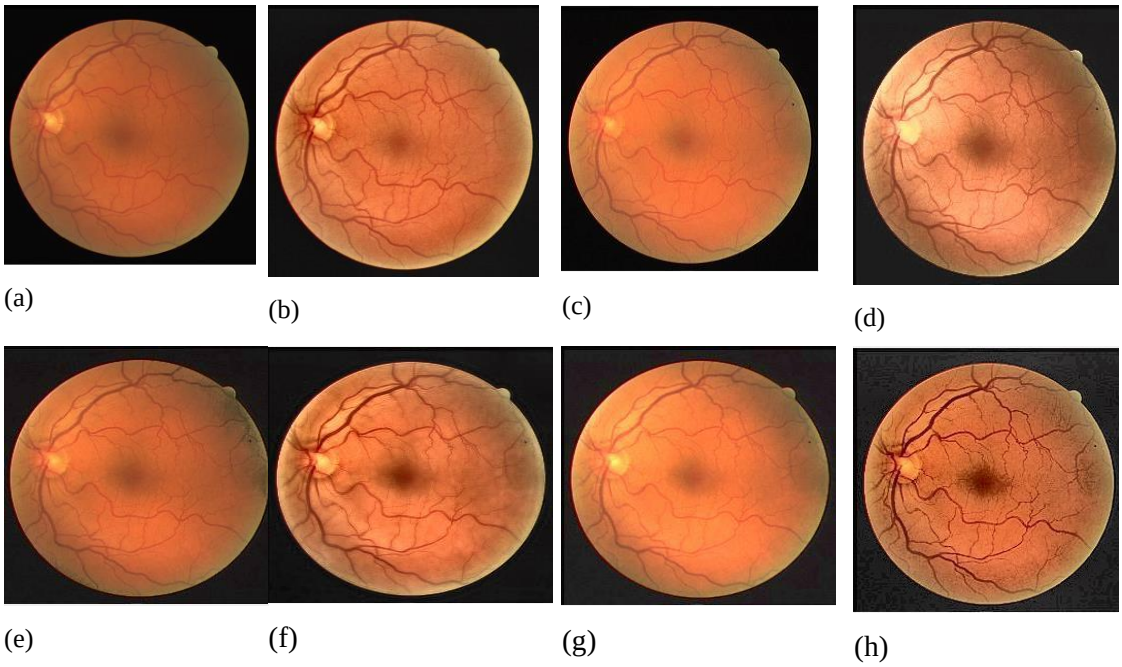

Figure 6.6: Experimentation outputs of the Ret-1 dataset (a) input image, (b) Zhou et al. [54], (c) AGC-WHD image, (d) Gupta et al. [55], (e) EBCHE image, (f) Palanisamy et al. [70], (g) TCHE-DWT image, (h) Proposed system

Images of "Ret2" with increased contrast are seen in Figure 6.7. Figure 6.7e demonstrates how the EBCHE method failed to adequately increase the contrast, leading to a darkening of most of the output picture and a loss of information. Figure 6.7b and 6.7f show that the Zhou et al. [19] and Palanisamy et al. [24] methods over enhanced the light regions near the vascular structure and the fovea. Even though the average brightness was preserved by both the AGC-WHD and TCHE-DWT systems (Fig. 6.7c and 6.7g), local details were lost in the process. In Fig. 6.7b, we can see that the Gupta et al. [22] method yields excessive improvement, especially in the extremes of brightness and darkness. As can be seen in Fig. 6.7h, the proposed method is able to provide aesthetically pleasing contrast-enhanced fundus images, while also allowing the rate of enhancement in bright areas to be controlled and the visibility of small vital details information to be improved.

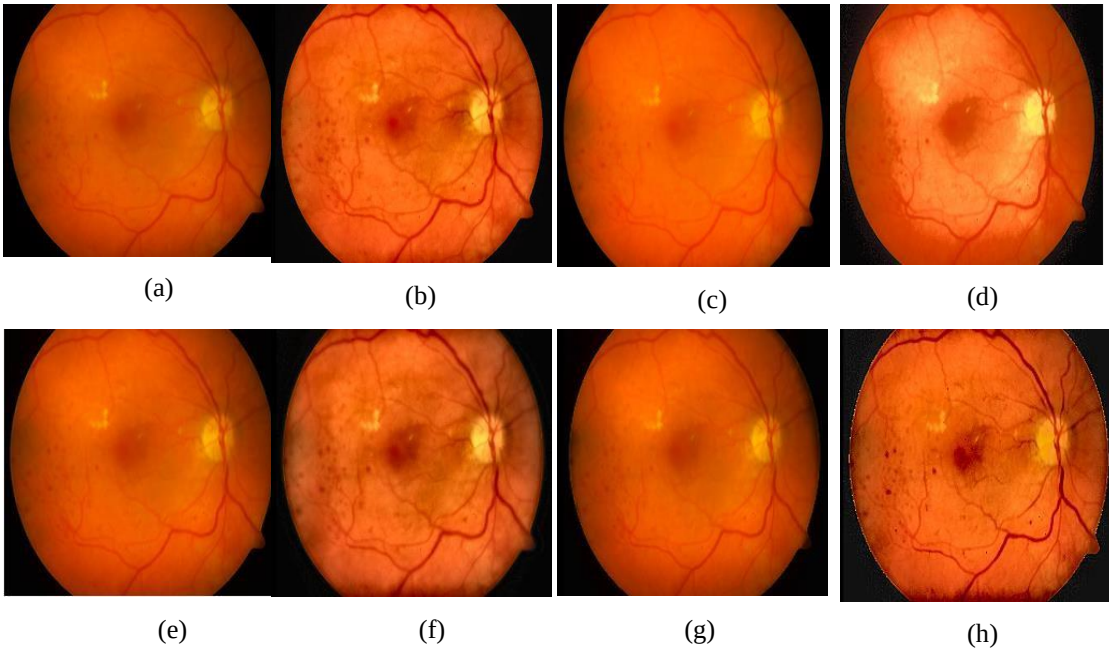

Figure 6.7: Experimentation outputs of the Ret-2 dataset (a) input image, (b) Zhou et al. [54], (c) AGC- WHD image, (d) Gupta et al. [55], (e) EBCHE image, (f) Palanisamy et al. [70], (g) TCHE-DWT image, (h) Proposed system

In Fig. 6.8, we see the original 'Ret3' image next to its contrast-enhanced counterparts that were created using the suggested method and six other more traditional methods. Figure 6.8d demonstrates that the approach proposed by Gupta et al. [22] produced bright images that appeared washed out in some spots, suggesting that information was absent there. Figures 6.8c and 6.8g demonstrate that the AGC-WHD and TCHE-DWT techniques often degraded the original image's brightness and lowered the perceptual visibility of minor details. Critical components of the processed image, such as blood vessels, are not effectively highlighted from the background despite the fact that Zhou et al. [19] and Palanisamy et al. [24] (Fig. 6.8b and 6.8f) succeeded in boosting contrast while keeping an acceptable level of brightness. For this reason, the contrast of the output images is unaffected by EBCHE (see Fig. 6.8e).

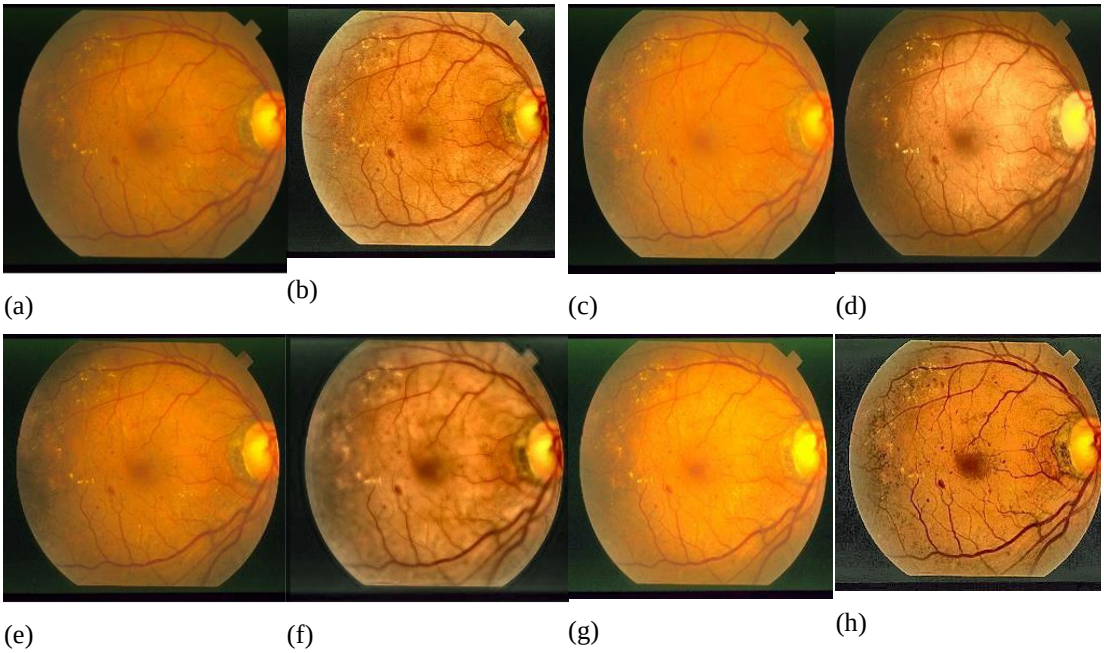

Figure 6.8: Experimentation outputs of the Ret-3 dataset (a) input image, (b) Zhou et al. [54], (c) AGC-WHD image, (d) Gupta et al. [55], (e) EBCHE image, (f) Palanisamy et al. [70], (g) TCHE-DWT image, (h) Proposed system

As shown in Fig.6. 8h, the suggested method improves the contrast of vascular structures like blood vessels, allowing the ophthalmologist to make a more precise diagnosis. The results of both the proposed and the standard enhancement approaches for the image "Ret4" are displayed in Fig. 6.9. Visual intensity differences between objects in the output fundus images were diminished by the AGC-WHD, Gupta et al. [22], and TCHE-DWT approaches (Fig. 6.9c, 6.9d, and 6.9g), all of which degraded the mean brightness of the original Ret4 image. This means that the final images created using these methods are subpar. Figure 6.9e shows how the EBCHE technique produces slightly more contrasty images. In Fig. 6.9b, we can see that the output image from the approach developed by Zhou et al. [19] features over-enhanced regions in the vast majority of cases. Figure 6.9f shows that the improved result achieved by Palanisamy et al. [24] is severely blurry and over-enhanced, destroying fine details and structures in the original image. The suggested algorithm surpasses the previous six methods by increasing contrast, keeping brightness, and keeping a natural appearance. Figure 6.9h shows that as a result, the majority of objects, including the optic disc, macula, and vascular structures, stand out clearly.

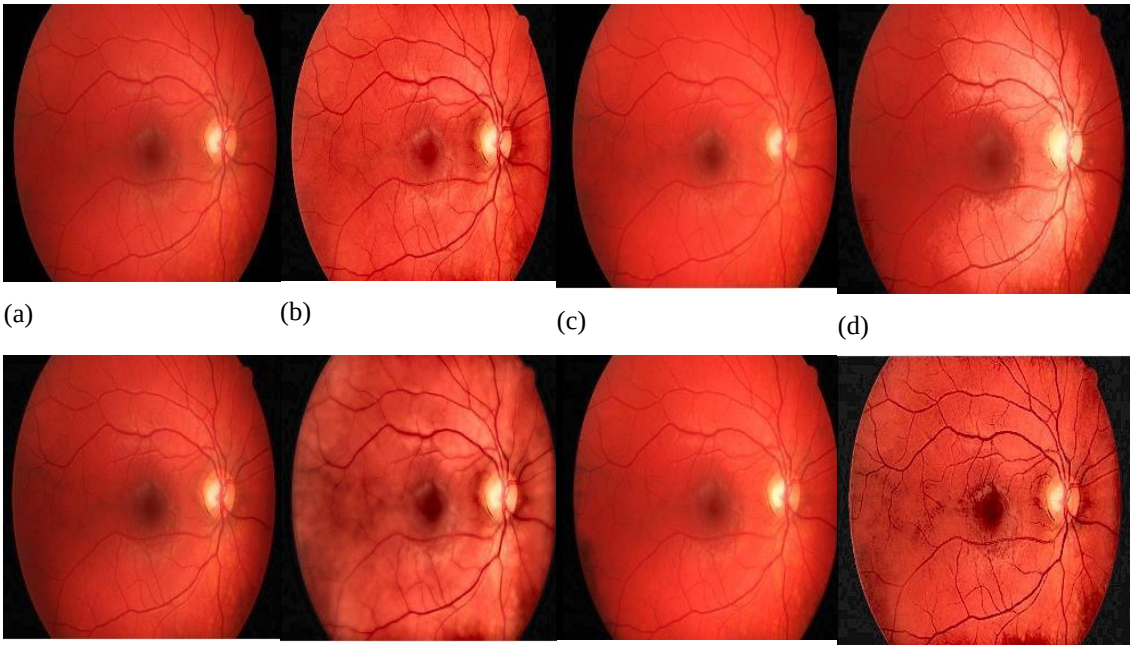

(a) (b) (c) (d)

(e) (f) (g) (h)

Figure 6.9: Experimentation outputs of the Ret-4 dataset (a) input image, (b) Zhou et al. [54], (c) AGC- WHD image, (d) Gupta et al. [55], (e) EBCHE image, (f) Palanisamy et al. [70], (g) TCHE-DWT image, (h) Proposed system

In Fig. 6.10, we see the 'Ret-5' image alongside the contrast-enhanced results obtained using the proposed and six other existing methods. Figures 6.10c and 6.10g demonstrate that the AGC-WHD and TCHE-DWT methods produced over-enhanced fundus pictures, which obscured secondary details. As can be seen in Fig. 10g, the image's fine details were lost because the contrast was boosted too much using the TCHE-DWT method. Figures 6.10(d) and (f) illustrate that while the Zhou et al. [19] and Palanisamy et al. [24] approaches increased the contrast of the images, they did not preserve the average brightness. Their resulting images look the same as they did before they were processed using the EBCHE method (see Fig. 10e), thanks to the low contrast loss that occurs during the process. The visual interpretation in Fig. 6.10d shows that the Gupta et al. [22] method yields a low-quality image with certain parts over-exposed. The 'Ret5' fundus image is significantly enhanced visually using the proposed method. As can be seen in Fig. 6.10h, the correct enhancement of the picture sections allowed for an accurate visual comparison of the various small but crucial data included within them.

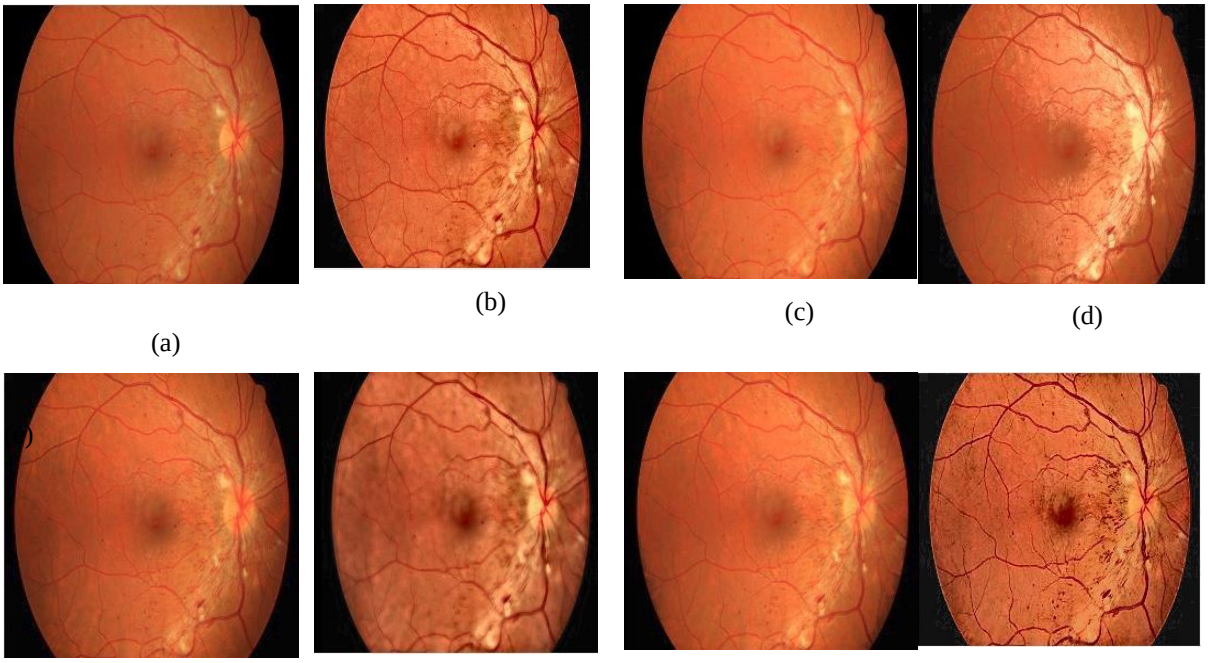

Figure 6.10: Experimentation outputs of the Ret-5 dataset (a) input image, (b) Zhou et al. [54], (c) AGC- WHD image, (d) Gupta et al. [55], (e) EBCHE image, (f) Palanisamy et al. [70], (g) TCHE-DWT image, (h) Proposed system

Figures 6.11 through 6.13 display the improved images of Rets 6, 7, and 8. Visual inspection of the results of all four experiments indicates that the proposed enhancement strategy is superior for boosting the contrast of fundus images without introducing unpleasant deficiencies like over enhancement, information distortion, brightness degradation damage, and noise enhancement, which are all present in other existing techniques. The resulting augmented retinal images show that not only are blood vessels more visible, but so are the optical disc and macula, while bright areas are protected from being over enhanced. Ophthalmologists may benefit from the proposed method since it helps preserve the naturalness of retinal images by preserving the original mean brightness while boosting key features.

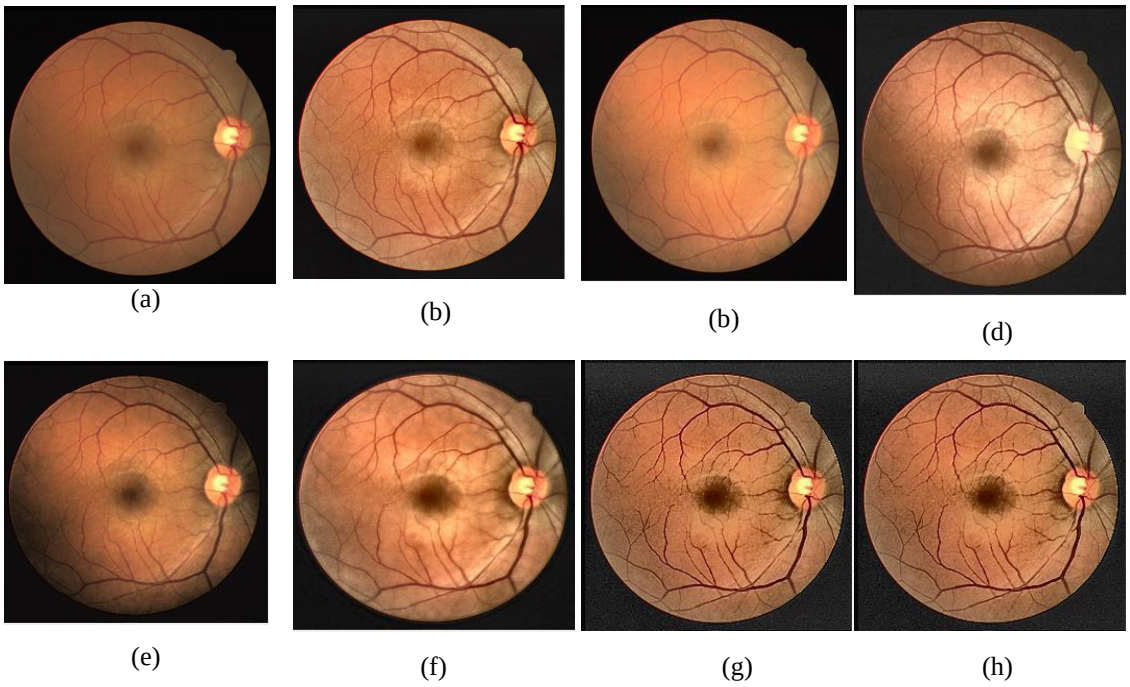

Figure 6.11: Experimentation outputs of the Ret-6 dataset (a) input image, (b) Zhou et al. [54], (c) AGC- WHD image, (d) Gupta et al. [55], (e) EBCHE image, (f) Palanisamy et al. [70], (g) TCHE-DWT image, (h) Proposed system

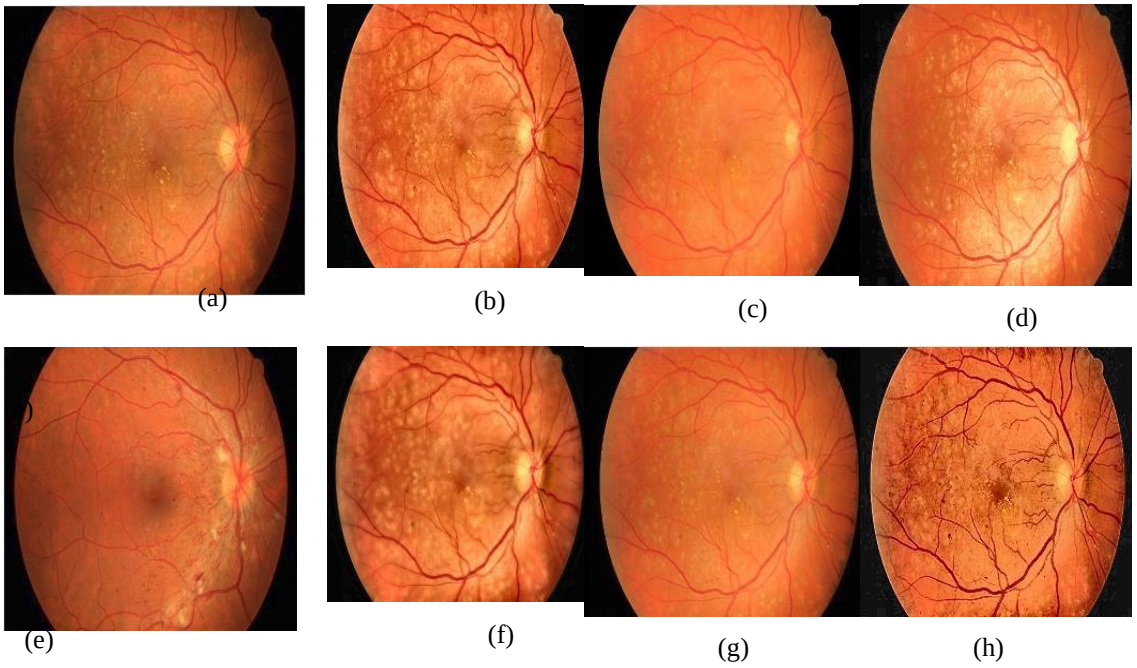

Figure 6.12: Experimentation outputs of the Ret-7 dataset (a) input image, (b) Zhou et al. [54], (c) AGC- WHD image, (d) Gupta et al. [55], (e) EBCHE image, (f) Palanisamy et al. [70], (g) TCHE-DWT image, (h) Proposed system

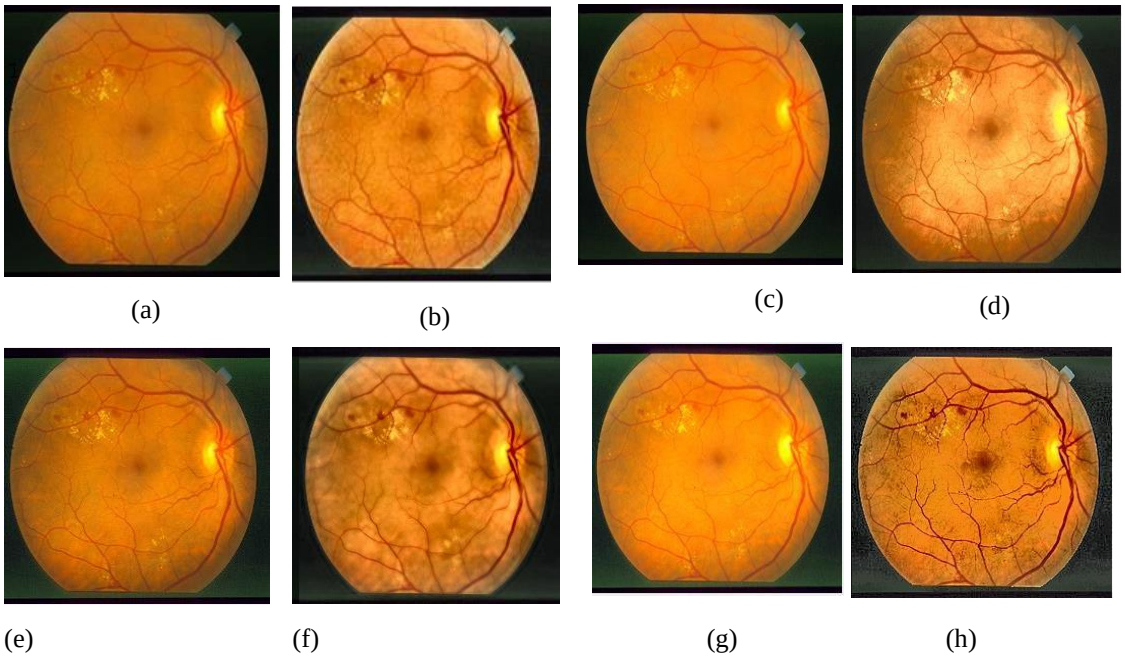

Figure 6.13: Experimentation outputs of the Ret-8 dataset (a) input image, (b) Zhou et al. [54], (c) AGC- WHD image, (d) Gupta et al. [55], (e) EBCHE image, (f) Palanisamy et al. [70], (g) TCHE-DWT image, (h) Proposed system

6.4.2. Objective (Quantitative) judgement

Six metrics, including entropy, EPI, CII, WC, MC, and EME, are used to assess the effectiveness of both new and established approaches. Bold values in Tables 6.1–6.5 denote the most effective metrics for judging image quality improvements.

Table 6.1 displays the entropy values for the various improvement methods. The entropy of an image is a measure of how much information it contains. An image with a high entropy has a lot of data packed into a small area. Obtaining the maximum entropy value is essential for accurately analyzing a retinal image since it highlights the tiniest of details. The information lost during excessive or insufficient amplification contributes to the poor entropy values of the AGC-WHD method. For all of the used test fundus images, it is demonstrated that the suggested scheme generates significantly more entropy than comparable earlier strategies. Therefore, unlike any other contrast enhancement method, the original information is retained accurately.

Table 6.1 Assessment of entropy outcomes

Image Name / Methods	Original	Zhou et al. [19]	AGC-WHD [21]	Gupta et al.[22]	EBCHE[26]	Palanisamyet al. [24]	TCHE-DWT [29]	Proposed scheme
Ret1	6.72	7.34	6.94	7.22	6.96	7.43	7.46	**7.66**
Ret2	6.54	7.30	6.82	6.99	6.73	7.45	7.24	**7.60**
Ret3	6.67	7.32	6.84	7	6.86	7.40	7.09	**7.59**
Ret4	7.29	7.58	7.32	7.40	7.39	7.60	7.17	**7.62**
Ret5	7.14	7.36	7.14	7.42	7.41	7.51	7.19	**7.56**
Ret6	7.25	7.23	7.18	7.16	7.33	7.43	7.15	**7.48**
Ret7	7.02	6.99	6.93	7.11	7.10	7.22	7.01	**7.28**
Ret8	7.24	7.31	7.03	7.24	7.23	7.44	7.38	**7.51**

Table 6.2 shows that compared to other common approaches, the suggested method has the largest EPI. Indicating the feasibility of creating an image devoid of undesired artefacts, the highest EPI value produced by the suggested method implies a high degree of edge retention in the output image after enhancement. The proposed method outperforms all previously published contrast enhancement techniques in terms of the EPI value. The best contrast and edge preservation can be found in retinal images with a high EPI value. Specifically, the suggested method yields a retinal image with optimal edge retention and increased contrast because of its high EPI value. The Edge Preservation Index (EPI) measures how well an enhanced image retains its edges. When improving medical images, it is crucial to do so without causing any loss of detail in the image's edges. As EPI gets closer to 1 or crosses that threshold, the enhanced image's edge preservation is at its peak.

Table 6.2 Assessment of EPI outcomes

Image Name / Methods	Zhou et al.[19]	AGC-WHD [21]	Gupta et al.[22]	EBCHE[26]	Palanisamyet al. [24]	TCHE-DWT [29]	Proposedscheme
Ret1	0.95	0.95	0.93	0.94	0.80	0.94	**1**
Ret2	0.89	0.97	0.92	0.95	0.71	0.91	0.96
Ret3	0.92	0.96	0.91	0.92	0.76	0.78	**0.98**
Ret4	0.95	0.92	0.92	0.97	0.72	0.77	**1**
Ret5	0.92	0.92	0.86	0.95	0.86	0.79	**0.97**
Ret6	0.89	0.89	0.79	0.94	0.80	0.76	**0.95**
Ret7	0.90	0.91	0.78	0.93	0.77	0.81	**0.97**
Ret8	0.90	0.90	0.77	0.96	0.76	0.95	**1**

Table 6.3 shows that the proposed method yields a higher CII value compared to more

traditional methods of improvement. The proposed method preserves as many important features of the retinal fundus picture as feasible while still maximising contrast. It is shown that the CII value of the suggested method is higher than that of any of the previously described contrast-enhancement procedures. The diagnostic value of the output fundus picture is expected to rise as a result of the suggested method's enhancement of local data and fine features, as indicated by an increased CII value.

Table 6.3 Assessment of CII outcomes

Image Name / Methods	Zhou et al.[19]	AGC-WHD [21]	Gupta et al. [22]	EBCHE[26]	Palanisamyet al. [24]	TCHE-DWT [29]	Proposed scheme
Ret1	0.88	1.02	0.84	0.96	0.85	0.92	**2.05**
Ret2	1.02	1.05	1.01	1.12	1.16	0.97	**2.51**
Ret3	0.86	1.05	0.84	0.96	0.82	0.94	**1.48**
Ret4	1.01	1.02	0.92	1.04	0.96	0.99	**1.89**
Ret5	1	1.05	0.91	0.99	1.05	1	**1.85**
Ret6	0.92	1.03	0.88	0.96	0.98	1.01	**1.71**
Ret7	0.67	1	0.70	0.70	0.70	0.99	0.91
Ret8	0.85	1	0.95	0.83	0.79	0.85	**1.34**

In addition, as shown in Table 6.4, the suggested framework provided the most accurate assessments of EME quality. The proposed method yields the greatest results for EME compared to other existing approaches. Results like these prove that the proposed method can significantly improve image quality in areas like uniformity and contrast. It is possible to evaluate a picture's level of detail with EME. A high EME score is indicative of a high level of detail in the associated image. The proposed method is demonstrated to have a higher EME value than any of the existing contrast enhancement methods. To see how much an image's quality can be enhanced with EME, look for a value of EME that's relatively high.

Table 6.4: Assessment of EME outcomes

Image Name / Methods	Zhou et al.[19]	AGC-WHD [21]	Gupta et al.[22]	EBCHE[26]	Palanisamyet al. [24]	TCHE-DWT[29]	Proposed scheme
Ret1	13.31	12.32	10.89	10.81	5.47	9.55	**22.28**
Ret2	14.04	10.95	10.33	14.90	5.76	9.12	**18.88**
Ret3	12.35	12.10	9.96	9.66	5.35	8.72	**18.08**
Ret4	12.75	11.35	10.30	10.58	5	9.47	**16.44**
Ret5	10.58	9.54	7.10	8.02	4.95	7.63	**14.28**
Ret6	10.16	10.11	7.70	8.42	4.89	8.56	**15.56**
Ret7	9.53	9.53	8.53	7.49	5.14	210	**14.07**
Ret8	9.38	9.38	7.98	9.39	4.83	1.18	**14.75**

Table 6.5 displays the mean scores obtained from 300 retinal fundus pictures using several proposed and existing methods. Compared to other methods, the average values of entropy, EPI, EME, and CII produce better results. When both the WC and MC are raised, the contrast between objects is made more apparent. A Michelson contrast ratio of 0.46 and a Weber contrast ratio of 0.45 are achieved on average using the proposed method, which is considered to be the highest of any comparable enhancement technique. This means that the proposed method is robust and effective at dealing with various retinal fundus pictures, and that the proposed strategy boosts contrast while keeping fine characteristics.

Table 6.5 Average measures values for 300 Retinal fundus images

Methods/Measures	Entropy	EME	EPI	CII	MC	WC
Zhou et al. [19]	7.17	10.56	0.88	0.97	0.21	0.26
AGC-WHD [21]	6.83	8.50	0.92	1.02	0.27	0.24
Gupta et al. [22]	7.05	10.66	0.84	0.90	0.19	0.37
EBCHE [26]	6.88	8.85	0.93	0.96	0.37	0.27
Palanisamy et al. [24]	7.12	11.24	0.67	0.90	0.29	0.22
TCHE-DWT [29]	6.85	7.73	0.85	0.97	0.31	0.27
Proposed scheme	**7.29**	**14.71**	**0.95**	**1.23**	**0.46**	**0.45**

6.5.Summary

The goal of this chapter is to present an effective method for enhancing colour retinal fundus images through adjustments to brightness and contrast. First, a novel JND-based adaptive gamma correction method is used to boost the colour retinal image's

brightness, and then several layers of CLAHE are applied in the L*a*b* colour mode to boost the image's contrast. The quality and efficiency of the proposed technique are measured through a series of experiments using test retinal pictures. Experiments conducted on databases of retinal images further illustrate the dominance of the suggested method over the status quo of enhancing techniques. With the suggested method, we can get high-contrast, anatomically accurate photographs of the fundus that look completely natural. In comparison to the best existing enhancement techniques, the suggested approach performs better in terms of edge preservation index, entropy, a measure of enhancement, and enhancement metrics. The proposed scheme can be utilised to improve colour retinal images, which in turn can aid in the proper diagnosis of disease by ophthalmologists and other medical professionals.

CHAPTER 7
CONCLUSION AND FUTURE SCOPE

7.1. Conclusion

Medical image enhancement plays a crucial role in improving diagnostic images for illness diagnosis, disease monitoring, and treatment planning. However, existing image enhancement methods often fall short when applied to medical images, as they may introduce various defects, color distortion, noise amplification, and information distortion. This dissertation addressed these shortcomings by proposing a range of medical image enhancement algorithms tailored to CT scans, digital histopathology images, and retinal fundus images.

In Chapter 3, a unique approach to enhancing low-quality CT scans is proposed. First, the original CT image is enhanced with the OMT approach, and then the DWT method is used to divide both the enhanced and original CT images into four chunks. The SVD approach is used on the LL sub-band output alone to boost contrast while maintaining picture brightness, while the EM technique is used to denoise the original CT image's HH sub-band. Comparing the proposed strategy to six existing enhancement methods, it clearly fares better. The testing outcomes showed that the suggested method effectively improved CT pictures without altering their original characteristics. When compared to other approaches like S-curve, AGC-DWT, AGC-WHD, GAGC-DWT, EBCHE, and TCHE-DWT, the enhanced pictures produced by the suggested method have better EME, CII, Michelson contrast ratio, Weber contrast ratio, PSNR, and entropy. The proposed technique is useful for improving CT scans and could be utilised to aid in the accurate diagnosis made by pathologists or doctors.

In Chapter 4, a novel method is introduced for efficiently improving non-contrast CT images, using DT-CWT methodology and flexible morphology for effective high-frequency sub-bands denoising and low-frequency sub-bands enhancement. For the purpose of quantitatively and qualitatively assessing the effectiveness of the suggested approach, experiments were performed on a variety of CT scan pictures. Moreover, investigations on CT image datasets demonstrate unambiguously that the suggested methodology excels in improving and maintaining fine information free of noise, as compared to other standard enhancement strategies. With the proposed approach, CT images retain their brightness while boasting improved contrast and reduced noise, making previously obscured details readily apparent. The proposed way is well-suited

for improving CT images and may be utilised to aid pathologists and doctors in making an accurate diagnosis.

In Chapter 5, a new technique for improving colour histopathology photos using retinex theory and local contrast modification is presented. To improve the contrast of a colour histopathology picture in the HSV colour model, it first provides a unique multiscale retinex with adaptive weighting, and then we use a new weighted CLAHE methodology to the brightness component of the image to boost the local details. Histopathology images have been used in tests to gauge the success of the suggested technique quantitatively and qualitatively. Furthermore, investigations using histopathology image databases demonstrate conclusively that the proposed methodology outperforms existing standard enhancement strategies with respect to overall contrast improvement and fine detail preservation. The suggested method produces natural histopathological images with intact brightness and improved contrast, free of any visible image artefacts. The proposed technology is well-suited to the improvement of histopathology images and could be used to aid pathologists or doctors in establishing precise diagnosis.

In Chapter 6, a technique for enhancing colour retinal fundus images with better brightness and contrast is presented. First, a novel JND-based adaptive gamma correction method is used to boost the colour retinal image's brightness, and then several layers of CLAHE are applied in the L*a*b* colour mode to boost the image's contrast. The suggested method is tested experimentally with reference test retinal pictures, and its results are analysed using both qualitative and quantitative metrics. Experiments conducted on databases of retinal images further illustrate the superiority of the advised method over the status quo of enhancing techniques. The suggested method yields enhanced contrast images of the fundus that look completely natural. The proposed process can be utilised to improve colour retinal images, which in turn can aid in the proper diagnosis of disease by ophthalmologists and other medical professionals.

In conclusion, this thesis has presented a comprehensive exploration of novel image enhancement methods tailored for bio-medical images. By addressing the shortcomings of existing techniques, current study have made significant contributions to the research community in the field of medical imaging. The proposed approach for enhancing low-quality CT scans, utilizing optimized morphology transform (OMT) and the Discrete Wavelet Transform (DWT), demonstrated substantial improvements in contrast and image clarity without compromising original features. Additionally, the introduction of

the Dual-Tree Complex Wavelet Transform (DT-CWT) combined with adaptive morphology significantly enhanced non-contrast CT images by effectively preserving fine details and reducing noise. In the context of histopathology images, a novel technique based on retina theory and local contrast modification introduced the multiscale retinex with adaptive weighting (MSRAW) and the weighted contrast limited adaptive histogram equalization (WCLAHE) methodologies. This approach offered natural and visually appealing histopathological images with improved contrast, essential for accurate diagnoses. Lastly, current work addressed the challenge of enhancing color retinal fundus images through JND-based adaptive gamma correction and multiple layers of CLAHE. The method produced contrast-enhanced fundus images that appeared entirely natural, aiding ophthalmologists and medical professionals in precise disease diagnosis.

Collectively, these contributions provide advanced and effective solutions to the critical task of enhancing bio-medical images, ultimately contributing to more accurate and reliable medical diagnoses and treatment planning. These novel image enhancement methods have the potential to significantly impact the research community and medical field, opening up new possibilities for improving patient care and medical decision-making.

7.2. Future Scope of Work

Based on the current work in this thesis, the subsequent next steps are proposed:

1. Image classification and segmentation have seen substantial advancements with the emergence of deep learning techniques. Convolutional Neural Networks (CNNs) [87]and other deep architectures have demonstrated impressive performance in tasks like organ segmentation and disease classification in medical images. The proposed image enhancement methods can serve as pre-processing steps for image classification and segmentation tasks. High-quality, enhanced images can lead to more accurate and reliable results in subsequent computer-assisted diagnostic procedures. Future work can explore how the enhanced images impact the performance of deep learning-based classification and segmentation algorithms in the medical domain.

2. Deep learning has revolutionized various fields, including medical imaging. Generative Adversarial Networks (GANs) [122] and attention mechanisms are

some of the state-of-the-art architectures that have shown promising results in image generation and enhancement tasks. Integrating deep learning approaches into medical image enhancement can lead to more adaptive and context-aware enhancement techniques. The proposed MSRAW and WCLAHE methods can potentially benefit from the inclusion of attention mechanisms to focus on critical regions in histopathology images or utilize GANs to generate high-quality retinal fundus images. Investigating the synergy between deep learning and the proposed methods can yield enhanced images with superior visual quality and informative content.

3. Machine learning techniques, such as Random Forests, Support Vector Machines (SVMs), and decision-based models [100], have been utilized in image enhancement tasks to handle specific challenges, like noise reduction and contrast enhancement. Exploring alternative machine learning algorithms for image enhancement can augment the current enhancement methods' capabilities. For instance, combining DT-CWT with decision-based denoising methods can address the directional selectivity limitations, providing more effective denoising for medical images. Evaluating the performance of various machine learning models on specific medical image enhancement tasks can lead to tailored approaches that align with different image characteristics and modalities.

4. Diverse and extensive medical image datasets are becoming more accessible, allowing researchers to train and validate algorithms on larger and more representative samples. The current thesis utilizes CT scans, histopathology, and retinal fundus images, but future work can benefit from including more medical image modalities, such as MRI, PET, and ultrasound. Expanding the dataset enables a comprehensive evaluation of the proposed methods' generalizability and robustness across diverse medical imaging scenarios. Furthermore, including data from different patient demographics and disease stages can improve the methods' effectiveness in real-world clinical settings.

5. Validating image enhancement methods in real clinical settings is crucial to their successful adoption in medical practice. Future work should involve close collaboration with medical professionals to conduct rigorous clinical validation of the proposed methods. Evaluating the methods on a diverse set of patient data and

comparing the results with ground truth annotations from experienced radiologists, pathologists, and ophthalmologists can demonstrate the methods' effectiveness and potential impact on patient care.

LIST OF PUBLICATIONS

1. Rao K, Bansal M, Kaur G. An optimized morphology transform based diagnostic computed tomography image enhancement using edge map. International Journal of Imaging Systems and Technology. pp. 1-18. 2022. doi:10.1002/ima.22727 SCIE (I.F.: 2.00)
2. Rao, K, Bansal, M, and Kaur G. Retinex-Centered Contrast Enhancement Method for Histopathology Images with Weighted CLAHE. Arabian Journal for Science and Engineering, pp.1-18. 2022. https://doi.org/10.1007/s13369-021-06421-w SCIE (I.F.: 2.3)
3. Rao, K, Bansal, M, and Kaur G. A hybrid method for improving the luminosity and contrast of color retinal images using the JND model and multiple layers of CLAHE. Signal, Image and Video Processing, pp. 1-11, 2022. https://doi.org/10.1007/s11760-022-02223-1 SCIE (I.F.:2.157)
4. Rao K, Bansal M, Kaur G. An effective CT medical image enhancement system based on DT-CWT and adaptable morphology, Circuits, Systems, and Signal Processing, 2022. https://doi.org/10.1007/s00034-022-02163-8. SCIE (I.F.:2.225)
5. Rao K, Bansal M, Kaur G," An optimal system for increasing the contrast resolution qualities of histopathology images in the wavelet domain.", International Journal of Imaging Systems and Technology., (Under Revision) SCIE, (I.F.:2.00)
6. Rao, K., Bansal, M. & Kaur, G. An Improved and Efficient Approach for Enhancing the Precision of Diagnostic CT Images. SN computer sciences.,. pp. 113 2023. https://doi.org/10.1007/s42979-022-01535-w
7. Rao K, Bansal M, Kaur G, "A Hybrid Approach to Image Enhancement in Digital Histopathology.", SN computer sciences., (Submitted), (Scopus)

REFERENCES

[1] Amelio, L. and Amelio, A., 2019. Classification methods in image analysis with a special focus on medical analytics. In Machine Learning Paradigms (pp. 31-69). Springer, Cham.

[2] Suetens, P., 2017. Fundamentals of medical imaging. Cambridge university press.

[3] Beutel, J., Kundel, H.L., Kim, Y., Van Metter, R.L. and Horii, S.C., 2000. Handbook of medical imaging (Vol. 3). Spie Press.

[4] Ganguly, A. and KARIM, R., 2016. Essential physics for radiology and imaging. Academic Publishers.

[5] Ivan, D., 2012. Atlas of Histopathology.

[6] Glass, L.R.D. and Freitag, S.K., 2016. Orbital inflammation: Corticosteroids first. survey of ophthalmology, 61(5), pp.670-673.

[7] Power, S.P., Moloney, F., Twomey, M., James, K., O'Connor, O.J. and Maher, M.M., 2016. Computed tomography and patient risk: facts, perceptions and uncertainties. World journal of radiology, 8(12), p.902.

[8] Mendonça, P.R., Lamb, P. and Sahani, D.V., 2013. A flexible method for multi-material decomposition of dual-energy CT images. IEEE transactions on medical imaging, 33(1), pp.99-116.

[9] Inkoom, S., Togobo, J., Emi-Reynolds, G., Oddoye, A., Ntiri, T.O. and Gyekye, P.K., 2012. Retrospective patient dose analysis of Ghana's first direct digital radiography system. Health physics, 103(2), pp.133-137.

[10] Zohair, A.A., Shamil, A.A. and Sulong, G., 2015. Latest methods of image enhancement and restoration for computed tomography: a concise review. Applied Medical Informatics, 36(1), pp.1-12.

[11] Song, Q., Bai, J., Han, D., Bhatia, S., Sun, W., Rockey, W., Bayouth, J.E., Buatti, J.M. and Wu, X., 2013. Optimal co-segmentation of tumor in PET-CT images with context information. IEEE transactions on medical imaging, 32(9), pp.1685-1697.

[12] Diwakar, M. and Kumar, M., 2018. A review on CT image noise and its denoising. Biomedical Signal Processing and Control, 42, pp.73-88.

[13] Bhadauria, H.S. and Dewal, M.L., 2011, March. Performance evaluation of curvelet and wavelet based denoising methods on brain computed tomography images. In 2011 International Conference on Emerging Trends in Electrical and Computer Technology (pp. 666-670). IEEE.

[14] Bhadauria, H.S., Dewal, M.L. and Anand, R.S., 2011, February. Comparative analysis of curvelet based techniques for denoising of computed tomography images. In 2011 International Conference on Devices and Communications (ICDeCom) (pp. 1-5). IEEE.

[15] Attivissimo, F., Cavone, G., Lanzolla, A.M.L. and Spadavecchia, M., 2010. A technique to improve the image quality in computer tomography. IEEE Transactions on Instrumentation and Measurement, 59(5), pp.1251-1257.

[16] Gurcan, M.N., Boucheron, L.E., Can, A., Madabhushi, A., Rajpoot, N.M. and Yener, B., 2009. Histopathological image analysis: A review. IEEE reviews in biomedical engineering, 2, pp.147-171.

[17] Jordan, T., Williams, D., Criswell, S. and Wang, Y., 2019. Comparison of bleaching protocols utilizing hematoxylin and eosin stain and immunohistochemical proliferation marker MCM3 in pigmented melanomas. Journal of Histotechnology, 42(4), pp.177-182.

[18] https://www.labce.com/routine_h_and_e_staining.aspx.

[19] Moles Lopez, X., D'Andrea, E., Barbot, P., Bridoux, A.S., Rorive, S., Salmon, I., Debeir, O. and Decaestecker, C., 2013. An automated blur detection method for histological whole slide imaging. PloS one, 8(12), p.e82710.

[20] Rubin, R., Strayer, D.S. and Rubin, E. eds., 2008. Rubin's pathology: clinicopathologic foundations of medicine. Lippincott Williams & Wilkins.

[21] Gurcan, M.N., Boucheron, L.E., Can, A., Madabhushi, A., Rajpoot, N.M. and Yener, B., 2009. Histopathological image analysis: A review. IEEE reviews in biomedical engineering, 2, pp.147-171.

[22] Pan, L., Feng, Z. and Peng, S., 2022. A review of machine learning approaches, challenges and prospects for computational tumor pathology. arXiv preprint arXiv:2206.01728.

[23] Su, H., Xing, F., Kong, X., Xie, Y., Zhang, S. and Yang, L., 2015, October. Robust cell detection and segmentation in histopathological images using sparse reconstruction and stacked denoising autoencoders. In International

Conference on Medical Image Computing and Computer-Assisted Intervention (pp. 383-390). Springer, Cham.

[24] Abràmoff, M.D., Garvin, M.K. and Sonka, M., 2010. Retinal imaging and image analysis. IEEE reviews in biomedical engineering, 3, pp.169-208.

[25] Hani, T. Soomro, I. Faye, N. Kamel, "Retinal Imaging and Image Analysis". Optical Imaging for Biomedical and Clinical Applications, pp.291-358, 2017.

[26] Abràmoff, M.D., Garvin, M.K. and Sonka, M., 2010. Retinal imaging and image analysis. IEEE reviews in biomedical engineering, 3, pp.169-208.

[27] Paulus, J., Meier, J., Bock, R., Hornegger, J. and Michelson, G., 2010. Automated quality assessment of retinal fundus photos. International journal of computer assisted radiology and surgery, 5(6), pp.557-564.

[28] Sevik, U., Kose, C., Berber, T. and Erdol, H., 2014. Identification of suitable fundus images using automated quality assessment methods. Journal of biomedical optics, 19(4), p.046006.

[29] Mookiah, M.R.K., Acharya, U.R., Chua, C.K., Lim, C.M., Ng, E.Y.K. and Laude, A., 2013. Computer-aided diagnosis of diabetic retinopathy: A review. Computers in biology and medicine, 43(12), pp.2136-2155.

[30] Gonzalez, R.C., 2009. Digital image processing. Pearson education india.

[31] Kim, Y.T., 1997. Contrast enhancement using brightness preserving bi-histogram equalization. IEEE transactions on Consumer Electronics, 43(1), pp.1-8.

[32] Mustafa, W.A. and Kader, M.M.M.A., 2018, June. A review of histogram equalization techniques in image enhancement application. In Journal of Physics: Conference Series (Vol. 1019, No. 1, p. 012026). IOP Publishing.

[33] Chen, S.D. and Ramli, A.R., 2003. Minimum mean brightness error bi-histogram equalization in contrast enhancement. IEEE transactions on Consumer Electronics, 49(4), pp.1310-1319.

[34] Chen, S.D. and Ramli, A.R., 2003. Contrast enhancement using recursive mean-separate histogram equalization for scalable brightness preservation. IEEE Transactions on consumer Electronics, 49(4), pp.1301-1309.

[35] Sim, K.S., Tso, C.P. and Tan, Y.Y., 2007. Recursive sub-image histogram equalization applied to gray scale images. Pattern Recognition Letters, 28(10), pp.1209-1221.

[36] Jenifer, S., Parasuraman, S. and Kadirvelu, A., 2016. Contrast enhancement and brightness preserving of digital mammograms using fuzzy clipped contrast-limited adaptive histogram equalization algorithm. Applied Soft Computing, 42, pp.167-177.

[37] Ooi, C.H., Kong, N.S.P. and Ibrahim, H., 2009. Bi-histogram equalization with a plateau limit for digital image enhancement. IEEE transactions on consumer electronics, 55(4), pp.2072-2080.

[38] Wang, Q. and Ward, R.K., 2007. Fast image/video contrast enhancement based on weighted thresholded histogram equalization. IEEE transactions on Consumer Electronics, 53(2), pp.757-764.

[39] Poddar, S., Tewary, S., Sharma, D., Karar, V., Ghosh, A. and Pal, S.K., 2013. Non-parametric modified histogram equalisation for contrast enhancement. IET Image Processing, 7(7), pp.641-652.

[40] K. Rao, A. Agarwal, S. Dhall, "A Novel Hybrid Contrast Enhancement Technique". 3D Research, Vol.9, No. 3, 2018.

[41] Arici, T., Dikbas, S. and Altunbasak, Y., 2009. A histogram modification framework and its application for image contrast enhancement. IEEE Transactions on image processing, 18(9), pp.1921-1935.

[42] Abdullah-Al-Wadud, M., Kabir, M.H., Dewan, M.A.A. and Chae, O., 2007. A dynamic histogram equalization for image contrast enhancement. IEEE Transactions on Consumer Electronics, 53(2), pp.593-600.

[43] Ibrahim, H. and Kong, N.S.P., 2007. Brightness preserving dynamic histogram equalization for image contrast enhancement. IEEE Transactions on Consumer Electronics, 53(4), pp.1752-1758.

[44] Sheet, D., Garud, H., Suveer, A., Mahadevappa, M. and Chatterjee, J., 2010. Brightness preserving dynamic fuzzy histogram equalization. IEEE Transactions on Consumer Electronics, 56(4), pp.2475-2480.

[45] Zimmerman, J.B., Pizer, S.M., Staab, E.V., Perry, J.R., McCartney, W. and Brenton, B.C., 1988. An evaluation of the effectiveness of adaptive histogram equalization for contrast enhancement. IEEE Transactions on Medical Imaging, 7(4), pp.304-312.

[46] Lidong, H., Wei, Z., Jun, W. and Zebin, S., 2015. Combination of contrast limited adaptive histogram equalisation and discrete wavelet transform for image enhancement. IET Image Processing, 9(10), pp.908-915.

[47] Siddiqi, A.A., Narejo, G.B., Tariq, M. and Hashmi, A., 2019. Investigation of histogram equalization filter for CT scan image enhancement. Biomedical Engineering: Applications, Basis and Communications, 31(05), p.1950038.

[48] Saleh, M.D., Eswaran, C. and Mueen, A., 2011. An automated blood vessel segmentation algorithm using histogram equalization and automatic threshold selection. Journal of digital imaging, 24(4), pp.564-572.

[49] Bhandari, A.K., 2020. A logarithmic law based histogram modification scheme for naturalness image contrast enhancement. Journal of Ambient Intelligence and Humanized Computing, 11(4), pp.1605-1627.

[50] Subramani, B. and Veluchamy, M., 2020. A fast and effective method for enhancement of contrast resolution properties in medical images. Multimedia Tools and Applications, 79(11), pp.7837-7855.

[51] Kumar, S., Bhandari, A.K., Raj, A. and Swaraj, K., 2021. Triple clipped histogram-based medical image enhancement using spatial frequency. IEEE Transactions on NanoBioscience, 20(3), pp.278-286.

[52] Acharya, U.K. and Kumar, S., 2021. Genetic algorithm based adaptive histogram equalization (GAAHE) technique for medical image enhancement. Optik, 230, p.166273.

[53] Singh, H., Kumar, A., Balyan, L.K. and Singh, G.K., 2017, April. Dark image enhancement using optimally compressed and equalized profile based parallel gamma correction. In 2017 International Conference on Communication and Signal Processing (ICCSP) (pp. 1299-1303). IEEE.

[54] Zhou, M., Jin, K., Wang, S., Ye, J. and Qian, D., 2017. Color retinal image enhancement based on luminosity and contrast adjustment. IEEE Transactions on Biomedical engineering, 65(3), pp.521-527.

[55] Gupta, B. and Tiwari, M., 2019. Color retinal image enhancement using luminosity and quantile based contrast enhancement. Multidimensional Systems and Signal Processing, 30(4), pp.1829-1837.

[56] Al-Ameen, Z., Sulong, G., Rehman, A., Al-Dhelaan, A., Saba, T. and Al-Rodhaan, M., 2015. An innovative technique for contrast enhancement of computed tomography images using normalized gamma-corrected contrast-limited adaptive histogram equalization. EURASIP Journal on Advances in Signal Processing, 2015(1), pp.1-12.

[57] Demirel, H., Anbarjafari, G. and Jahromi, M.N.S., 2008, October. Image equalization based on singular value decomposition. In 2008 23rd International Symposium on Computer and Information Sciences (pp. 1-5). IEEE.

[58] Demirel, H. and Anbarjafari, G., 2011. Discrete wavelet transform-based satellite image resolution enhancement. IEEE transactions on geoscience and remote sensing, 49(6), pp.1997-2004.

[59] Atta, R. and Abdel-Kader, R.F., 2015. Brightness preserving based on singular value decomposition for image contrast enhancement. Optik, 126(7-8), pp.799-803.

[60] Sahnoun, M., Kallel, F., Dammak, M., Kammoun, O., Mhiri, C., Ben Mahfoudh, K. and Ben Hamida, A., 2020. Spinal cord MRI contrast enhancement using adaptive gamma correction for patient with multiple sclerosis. Signal, Image and Video Processing, 14(2), pp.377-385.

[61] Sahnoun, M., Kallel, F., Dammak, M., Kammoun, O., Mhiri, C., Ben Mahfoudh, K. and Ben Hamida, A., 2020. Spinal cord MRI contrast enhancement using adaptive gamma correction for patient with multiple sclerosis. Signal, Image and Video Processing, 14(2), pp.377-385.

[62] Kallel, F. and Hamida, A.B., 2017. A new adaptive gamma correction based algorithm using DWT-SVD for non-contrast CT image enhancement. IEEE transactions on nanobioscience, 16(8), pp.666-675.

[63] Koh, N.C.Y., Sim, K.S. and Tso, C.P., 2016, November. CT brain lesion detection through combination of recursive sub-image histogram equalization in wavelet domain and adaptive gamma correction with weighting distribution. In 2016 International Conference on Robotics, Automation and Sciences (ICORAS) (pp. 1-6). IEEE.

[64] Li, Z., Jia, Z., Yang, J. and Kasabov, N., 2020. An efficient and high quality medical CT image enhancement algorithm. International Journal of Imaging Systems and Technology, 30(4), pp.939-949.

[65] Veluchamy, M. and Subramani, B., 2019. Image contrast and color enhancement using adaptive gamma correction and histogram equalization. Optik, 183, pp.329-337.

[66] Cao, G., Huang, L., Tian, H., Huang, X., Wang, Y. and Zhi, R., 2018. Contrast enhancement of brightness-distorted images by improved adaptive gamma correction. Computers & Electrical Engineering, 66, pp.569-582.

[67] Kingsbury, N.G., 1998, August. The dual-tree complex wavelet transform: a new technique for shift invariance and directional filters. In IEEE digital signal processing workshop (Vol. 86, pp. 120-131). Citeseer.

[68] Iqbal, M.Z., Ghafoor, A., Siddiqui, A.M., Riaz, M.M. and Khalid, U., 2014. Dual-tree complex wavelet transform and SVD based medical image resolution enhancement. Signal Processing, 105, pp.430-437.

[69] Kallel, F. and Hamida, A.B., 2017. A new adaptive gamma correction based algorithm using DWT-SVD for non-contrast CT image enhancement. IEEE transactions on nanobioscience, 16(8), pp.666-675.

[70] Palanisamy, G., Shankar, N.B., Ponnusamy, P. and Gopi, V.P., 2020. A hybrid feature preservation technique based on luminosity and edge based contrast enhancement in color fundus images. Biocybernetics and Biomedical Engineering, 40(2), pp.752-763.

[71] Li, D., Zhang, L., Sun, C., Yin, T., Liu, C. and Yang, J., 2019. Robust retinal image enhancement via dual-tree complex wavelet transform and morphology-based method. IEEE Access, 7, pp.47303-47316.

[72] Al-Ameen, Z. and Sulong, G., 2015. A new algorithm for improving the low contrast of computed tomography images using tuned brightness controlled single-scale Retinex. Scanning, 37(2), pp.116-125.

[73] Vázquez, S.G., Barreira, N., Penedo, M.G., Saez, M. and Pose-Reino, A., 2010, June. Using retinex image enhancement to improve the artery/vein classification in retinal images. In International Conference Image Analysis and Recognition (pp. 50-59). Springer, Berlin, Heidelberg.

[74] Memari, N., Ramli, A.R., Bin Saripan, M.I., Mashohor, S. and Moghbel, M., 2017. Supervised retinal vessel segmentation from color fundus images based on matched filtering and AdaBoost classifier. PloS one, 12(12), p.e0188939.

[75] Fu, Q., Jung, C. and Xu, K., 2018. Retinex-based perceptual contrast enhancement in images using luminance adaptation. IEEE Access, 6, pp.61277-61286.

[76] Bai, X., Zhou, F. and Xue, B., 2012. Image enhancement using multi scale image features extracted by top-hat transform. Optics & Laser Technology, 44(2), pp.328-336.

[77] Ali, O., Muhammad, N., Jadoon, Z., Kazmi, B.M., Muzamil, N. and Mahmood, Z., 2020, January. A comparative study of automatic vessel segmentation algorithms. In 2020 3rd International Conference on Computing, Mathematics and Engineering Technologies (iCoMET) (pp. 1-6). IEEE.

[78] Liao, M., Zhao, Y.Q., Wang, X.H. and Dai, P.S., 2014. Retinal vessel enhancement based on multi-scale top-hat transformation and histogram fitting stretching. Optics & Laser Technology, 58, pp.56-62.

[79] Feng, P., Pan, Y., Wei, B., Jin, W. and Mi, D., 2007. Enhancing retinal image by the Contourlet transform. Pattern Recognition Letters, 28(4), pp.516-522.

[80] Liu, L., Jia, Z., Yang, J., Kasabov, N. and Fellow IEEE, 2015. A medical image enhancement method using adaptive thresholding in NSCT domain combined unsharp masking. International Journal of Imaging Systems and Technology, 25(3), pp.199-205.

[81] Li, L., Si, Y. and Jia, Z., 2018. Medical image enhancement based on CLAHE and unsharp masking in NSCT domain. Journal of Medical Imaging and Health Informatics, 8(3), pp.431-438.

[82] Polesel, A., Ramponi, G. and Mathews, V.J., 2000. Image enhancement via adaptive unsharp masking. IEEE transactions on image processing, 9(3), pp.505-510.

[83] Sahu, S., Singh, A.K., Ghrera, S.P. and Elhoseny, M., 2019. An approach for de-noising and contrast enhancement of retinal fundus image using CLAHE. Optics & Laser Technology, 110, pp.87-98.

[84] Saha, S.K., Xiao, D. and Kanagasingam, Y., 2018. A novel method for correcting non-uniform/poor illumination of color fundus photographs. Journal of Digital Imaging, 31(4), pp.553-561.

[85] Gandhamal, A., Talbar, S., Gajre, S., Hani, A.F.M. and Kumar, D., 2017. Local gray level S-curve transformation–a generalized contrast enhancement technique for medical images. Computers in biology and medicine, 83, pp.120-133.

[86] Katırcıoğlu, F., 2020. Colour image enhancement with brightness preservation and edge sharpening using a heat conduction matrix. IET Image Processing, 14(13), pp.3202-3214.

[87] Chi, J., Zhang, Y., Yu, X., Wang, Y. and Wu, C., 2019. Computed tomography (CT) image quality enhancement via a uniform framework integrating noise estimation and super-resolution networks. Sensors, 19(15), p.3348.

[88] Pathak, Y., Arya, K.V. and Tiwari, S., 2018. Low-dose CT image reconstruction using gain intervention-based dictionary learning. Modern Physics Letters B, 32(14), p.1850148.

[89] Anoop, V. and Bipin, P.R., 2019. Medical image enhancement by a bilateral filter using optimization technique. Journal of medical systems, 43(8), pp.1-12.

[90] Rao, B.S., 2020. Dynamic histogram equalization for contrast enhancement for digital images. Applied Soft Computing, 89, p.106114.

[91] Kandhway, P., Bhandari, A.K. and Singh, A., 2020. A novel reformed histogram equalization based medical image contrast enhancement using krill herd optimization. Biomedical Signal Processing and Control, 56, p.101677.

[92] Easley, G., Labate, D. and Lim, W.Q., 2008. Sparse directional image representations using the discrete shearlet transform. Applied and Computational Harmonic Analysis, 25(1), pp.25-46.

[93] Hou, B., Zhang, X., Bu, X. and Feng, H., 2012. SAR image despeckling based on nonsubsampled shearlet transform. IEEE Journal of selected topics in applied earth observations and remote sensing, 5(3), pp.809-823.

[94] Bai, X., Zhou, F. and Xue, B., 2011. Fusion of infrared and visual images through region extraction by using multi scale center-surround top-hat transform. Optics express, 19(9), pp.8444-8457.

[95] Wang, Y., Huang, Q. and Hu, J., 2017. Adaptive enhancement for nonuniform illumination images via nonlinear mapping. Journal of Electronic Imaging, 26(5), p.053012.

[96] Haldorsen, I.S., Espeland, A. and Larsson, E.M., 2011. Central nervous system lymphoma: characteristic findings on traditional and advanced imaging. American Journal of Neuroradiology, 32(6), pp.984-992.

[97] Koyuncu, H. and Ceylan, R., 2018. Elimination of white Gaussian noise in arterial phase CT images to bring adrenal tumours into the forefront. Computerized Medical Imaging and Graphics, 65, pp.46-57.

[98] Li, X., Shen, H., Zhang, L., Zhang, H., Yuan, Q. and Yang, G., 2014. Recovering quantitative remote sensing products contaminated by thick clouds and shadows using multitemporal dictionary learning. IEEE Transactions on Geoscience and Remote Sensing, 52(11), pp.7086-7098.

[99] Anoop, V. and Bipin, P.R., 2019. Medical image enhancement by a bilateral filter using optimization technique. Journal of medical systems, 43(8), pp.1-12.

[100] Sajadi, S.M., Alizadeh, A., Zandieh, M. and Tavan, F., 2019. Robust and stable flexible job shop scheduling with random machine breakdowns: multi-objectives genetic algorithm approach. International journal of mathematics in operational research, 14(2), pp.268-289.

[101] Deng, W., Xu, J. and Zhao, H., 2019. An improved ant colony optimization algorithm based on hybrid strategies for scheduling problem. IEEE access, 7, pp.20281-20292.

[102] Bansal JC. Particle swarm optimization. In: Bansal JC, Singh PK, Pal NR, eds. Evolutionary and Swarm Intelligence Algorithms. Springer; 2019:11-23.

[103] Shanmugavadivu, P. and Balasubramanian, K., 2014. Particle swarm optimized multi-objective histogram equalization for image enhancement. Optics & laser technology, 57, pp.243-251.

[104] Kennedy, J. and Eberhart, R., 1995, November. Particle swarm optimization. In Proceedings of ICNN'95-international conference on neural networks (Vol. 4, pp. 1942-1948). IEEE.

[105] Rezaee Jordehi, A. and Jasni, J., 2013. Parameter selection in particle swarm optimisation: a survey. Journal of Experimental & Theoretical Artificial Intelligence, 25(4), pp.527-542.

[106] Maragos, P. and Pessoa, L.F., 1999. Morphological filtering for image enhancement and detection. The Image and Video Processing Handbook,, pp.135-156.

[107] Vincent OR & Folorunso O A descriptive algorithm for Sobel image edge detection. Paper presented at: Proc. Informing Sci ence IT Education Conference (InSITE). Vol 40; 2009:97-107.

[108] Easley, G., Labate, D. and Lim, W.Q., 2008. Sparse directional image representations using the discrete shearlet transform. Applied and Computational Harmonic Analysis, 25(1), pp.25-46.

[109] Hou, B., Zhang, X., Bu, X. and Feng, H., 2012. SAR image despeckling based on nonsubsampled shearlet transform. IEEE Journal of selected topics in applied earth observations and remote sensing, 5(3), pp.809-823.

[110] Koyuncu, H. and Ceylan, R., 2018. Elimination of white Gaussian noise in arterial phase CT images to bring adrenal tumours into the forefront. Computerized Medical Imaging and Graphics, 65, pp.46-57.

[111] Bai, X., Zhou, F. and Xue, B., 2011. Fusion of infrared and visual images through region extraction by using multi scale center-surround top-hat transform. Optics express, 19(9), pp.8444-8457.

[112] Wang, Y., Huang, Q. and Hu, J., 2017. Adaptive enhancement for nonuniform illumination images via nonlinear mapping. Journal of Electronic Imaging, 26(5), p.053012.

[113] Zhou, Z., Sang, N. and Hu, X., 2014. Global brightness and local contrast adaptive enhancement for low illumination color image. Optik, 125(6), pp.1795-1799.

[114] Kaur, H., Koundal, D. and Kadyan, V., 2021. Image fusion techniques: a survey. Archives of computational methods in Engineering, 28(7), pp.4425-4447.

[115] Jha, N., Saxena, A.K., Shrivastava, A. and Manoria, M., 2017, October. A review on various image fusion algorithms. In 2017 International Conference on Recent Innovations in Signal processing and Embedded Systems (RISE) (pp. 163-167). IEEE.

[116] Bhandari, A.K., Subramani, B. and Veluchamy, M., 2022. Multi-exposure optimized contrast and brightness balance color image enhancement. Digital Signal Processing, 123, p.103406.

[117] Sathananthavathi, V. and Indumathi, G., 2021. Particle swarm optimization based retinal image enhancement. Wireless Personal Communications, 121(1), pp.543-555.

[118] Bhandari, A.K., Srinivas, K. and Maurya, S., 2022. Gamma corrected reflectance for low contrast image enhancement using guided filter. Multimedia Tools and Applications, 81(4), pp.6009-6030.

[119] Wang, P., Wang, Z., Lv, D., Zhang, C. and Wang, Y., 2021. Low illumination color image enhancement based on Gabor filtering and Retinex theory. Multimedia Tools and Applications, 80(12), pp.17705-17719.

[120] Goyal, B., Dogra, A. and Sangaiah, A.K., 2022. An effective nonlocal means image denoising framework based on non-subsampled shearlet transform. Soft Computing, pp.1-23.

[121] Lyu, Z., Chen, Y., Hou, Y. and Zhang, C., 2022. NSTBNet: Toward a nonsubsampled shearlet transform for broad convolutional neural network image denoising. Digital Signal Processing, 123, p.103407.

[122] Raj, A., Shah, N.A. and Tiwari, A.K., 2022. A novel approach for fundus image enhancement. Biomedical Signal Processing and Control, 71, p.103208.

[123] Rao K, Bansal M, Kaur G., 2022. An optimized morphology transform based diagnostic computed tomography image enhancement using edge map. International Journal of Imaging Systems and Technology. pp. 1-18.

[124] Rao K, Bansal M, Kaur G., 2022. An effective CT medical image enhancement system basedon DT-CWT and adaptable morphology, Circuits, Systems, and Signal Processing.

[125] Rao, K, Bansal, M, and Kaur G., 2022 Retinex-Centered Contrast Enhancement Method for Histopathology Images with Weighted CLAHE. Arabian Journal for Science and Engineering, pp.1-18.

[126] Rao, K, Bansal, M, and Kaur G., 2022. A hybrid method for improving the luminosity and contrast of color retinal images using the JND model and multiple layers of CLAHE. Signal, Image and Video Processing, pp. 1-11.

thesis

ORIGINALITY REPORT

15%	9%	13%	%
SIMILARITY INDEX	INTERNET SOURCES	PUBLICATIONS	STUDENT PAPERS

PRIMARY SOURCES

1	www.researchgate.net Internet Source	1%
2	link.springer.com Internet Source	1%
3	Zhijun Yao, Quan Zhou, Zhongyuan Lai, Zhiming Ren, Liming Liu. "Image Enhancement Based on Bi-Histogram Equalization with Non-Parametric Modified Technology", 2016 IEEE 22nd International Conference on Parallel and Distributed Systems (ICPADS), 2016 Publication	<1%
4	Sonu Kumar, Ashish Kumar Bhandari, Aditya Kumar, Kirti Swaraj. "Triple Clipped Histogram Based Medical Image Enhancement Using Spatial Frequency", IEEE Transactions on NanoBioscience, 2021 Publication	<1%
5	Dan Li, Jinping Sun, Hongdong Wang, Hanqin Shi, Weiwei Liu, Likai Wang. "Research on Haze Image Enhancement based on Dark	<1%